



**KTH Architecture and
the Built Environment**

UNIVERSITY OF TRENTO - Italy

**Department of Civil, Environmental
and Mechanical Engineering**



Development and application of corotational finite elements for the analysis of steel structures in fire

LUCA POSSIDENTE

Doctoral Thesis in Structural Engineering and Bridges

School of Architecture and the Built Environment

Royal Institute of Technology (KTH)

Stockholm, Sweden 2021

and

Doctoral Thesis in Civil Engineering

Department of Civil, Environmental and Mechanical Engineering

University of Trento

Trento, Italy 2021

Abstract

The ignition and the propagation of a fire inside a building may lead to global or local structural collapse, especially in steel framed structures. Indeed, steel structures are particularly vulnerable to thermal attack because of a high value of steel conductivity and of the small thickness that characterise the cross-sections. As a crucial aspect of design, fire safety requirements should be achieved either following prescriptive rules or adopting performance-based fire engineering. Despite the possibility to employ simple methods that involve member analysis under nominal fire curves, a more accurate analysis of the thermomechanical behaviour of a steel structural system is an appealing alternative, as it may lead to more economical and efficient solutions by taking into account possible favourable mechanisms. This analysis typically requires the investigation of parts of the structure or even of the whole structure. For this purpose, and in order to gain a deeper knowledge about the behaviour of structural members at elevated temperature, numerical simulation should be employed. In this thesis, thermomechanical finite elements, suited for the analyses of steel structures in fire, were developed and exploited in numerical simulation of relevant case studies.

The development of a shell and of a 3D beam thermomechanical finite element based on a corotational formulation is presented. Most of the relevant structural cases can be adequately investigated by either using one of these elements or combining them. The corotational formulation is well suited for the analyses of structures in which large displacements, but small strains occur, as in the case of steel structures in fire. The main features of the elements are described, as well as their characterization in the thermomechanical context. In this regard, the material degradation due to the temperature increase and the thermal expansion of steel were considered in the derivation of the elements. In addition, a branch-switching procedure to perform preliminary instability analyses and get important insight into the post-buckling behaviour of steel structures subjected to fire is presented.

The application of the developed numerical tools is provided in the part of the thesis devoted to the published research work. Several aspects of the buckling of steel structural elements at elevated temperature are discussed. In paper I, considerations about the influence of geometrical imperfections on the behaviour of compressed steel plates and columns at elevated temperatures are provided, as well as implications and results of the employment of the branch-switching procedure. In Paper II, the proposed 3D beam element is validated for meaningful case studies, in which torsional deformations are significant. The developed beam and shell elements are employed in an investigation of buckling resistance of compressed angular, Tee and cruciform steel profiles at elevated temperature presented in Paper III. An improved buckling curve for design is presented in this work. Furthermore, as an example of the application of Fire Safety Engineering principles, a comprehensive analysis is proposed in Paper IV. Two relevant fire scenarios are identified for the investigated building, which is modelled and analysed in the software SAFIR.

Keywords: Thermomechanical finite element, Shell element, 3D beam element, Steel structures, Buckling, Fire Safety Engineering

Sammanfattning

Utbredningen av en brand inuti en byggnad kan leda till global eller lokal strukturell kollaps, särskilt i stålramkonstruktioner. Faktum är att stålkonstruktioner är särskilt utsatta för termiska angrepp på grund av ett högt värde av stålkonduktivitet och tvärsnitten med små tjockleken. Som en viktig aspekt av konstruktionen bör brandsäkerhetskrav uppnås antingen enligt föreskrivande regler eller enligt antagande av prestationsbaserad brandteknik. Trots möjligheten att använda enkla metoder som involverar membersanalys kombinerat med nominella brandkurvor, är en mer exakt analys av det termomekaniska beteendet hos en stålkonstruktion ett tilltalande alternativ eftersom det kan leda till mer ekonomiska och effektiva lösningar genom att ta hänsyn till möjliga gynnsamma mekanismer. Denna analys kräver vanligtvis utredning av delar av strukturen eller till och med av hela strukturen. För detta ändamål och för att få en djupare kunskap om strukturelementens beteende vid förhöjd temperatur bör numerisk simulering användas. I denna avhandling utvecklades och användes termomekaniska finita element som är lämpliga för analys av stålkonstruktioner utsatta för brand. Relevanta fallstudier utfördes.

Utvecklingen av både ett termomekaniskt skal- och 3D balkelement baserade på en korotationsformulering presenteras. De flesta relevanta strukturefall kan undersökas på ett adekvat sätt genom att antingen använda något av dessa element eller kombinera dem. Korotationsformuleringen är väl lämpad för analyser av strukturer där stora förskjutningar, men små töjningar förekommer, som i fallet med stålkonstruktioner i brand. Elementens huvuddrag beskrivs, liksom deras karakterisering i termomekaniskt sammanhang. I detta avseende övervägdes materialnedbrytningen på grund av temperaturökningen och den termiska expansionen av stål vid härledningen av elementen. Dessutom presenteras en grenväxlingsprocedur för att utföra preliminära instabilitetsanalyser och få viktig insikt i efterknäckningsbeteendet hos stålkonstruktioner som utsätts för brand.

Tillämpningen av de utvecklade numeriska verktygen ges i den del av avhandlingen som ägnas åt det publicerade forskningsarbetet. Flera aspekter av knäckningen av stålkonstruktionselement vid förhöjd temperatur diskuteras. I Artikel I tillhandahålls överväganden om påverkan av geometriska imperfektioner på beteendet hos komprimerade stålplattor och kolonner vid förhöjda temperaturer, liksom implikationer och resultat av användningen av grenväxlingsprocedur. I Artikel II valideras det föreslagna 3D-balkelementet genom meningsfulla fallstudier där torsionsdeformationer är signifikanta. De utvecklade balk- och skalelementen används i en undersökning av knäckningsmotstånd hos komprimerade vinkel-, Tee- och korsformade stålprofiler vid förhöjd temperatur som presenteras i Artikel III. En förbättrad knäckningskurva för design presenteras i detta arbete. Som ett exempel på tillämpningen av principerna för brandsäkerhetsteknik presenteras en omfattande analys i Artikel IV. Två relevanta brandscenarier identifieras för den undersökta byggnaden, som modelleras och analyseras i programmet SAFIR.

Nyckelord: Termomekaniska finita element, Skalelement, 3D balkelement, Stålkonstruktioner, Knäckning, Brandskyddsteknik

Preface

The work presented in this thesis was conducted at the Department of Civil, Environmental and Mechanical Engineering of the University of Trento UNITN (Italy) and at the Department of Civil and Architectural Engineering, at KTH Royal Institute of Technology (Sweden).

I would like to express my sincere gratitude to my supervisors Professor Nicola Tondini (UNITN) and Professor Jean-Marc Battini (KTH) for their kind support and professional guidance. I feel privileged for the opportunity to work with them. Special thanks to Associate Professor John Leander for taking the time to review this thesis.

Special thanks go to my colleagues and friends at KTH and UNITN for creating a joyful and healthy work environment, made of fruitful discussions, laughs and shared professional and life experience. I am also grateful to friends and my beloved ones for being there, regardless of the distance. Friendship and love may come and go, but memories of the time spent together stay forever.

Finally, I would like to thank my parents for their love and support. All my professional accomplishments are equally shared with them.

Trento, February 2021

Luca Possidente

Publications

This thesis is based on the work presented in the following appended papers:

Paper I L. Possidente, N. Tondini, J.-M. Battini (2019). *Branch-switching procedure for post-buckling analysis of thin-walled steel members at elevated temperature*. Thin-Walled Structures 136. pp. 90-98. <https://doi.org/10.1016/j.tws.2018.12.012>.

Paper II L. Possidente, N. Tondini, J.-M. Battini (2020). *3D beam element for the analysis of torsional problems of steel structures in fire*. Journal of Structural Engineering 146(7). Article number 04020125. [https://doi.org/10.1061/\(ASCE\)ST.1943-541X.0002665](https://doi.org/10.1061/(ASCE)ST.1943-541X.0002665).

Paper III L. Possidente, N. Tondini, J.-M. Battini (2020). *Torsional and flexural-torsional buckling of compressed steel members in fire*. Journal of Constructional Steel Research 171. Article number 106130. <https://doi.org/10.1016/j.jcsr.2020.106130>.

Paper IV L. Possidente, A. Weiss, D. de Silva, S. Pustorino, E. Nigro, N. Tondini (2020). *Fire Safety Engineering principles applied on a multi-storey steel building*. Structures and Buildings. Ahead of print. <https://doi.org/10.1680/jstbu.20.00110>

Paper I, II, III and IV were implemented and written by the first author. The co-authors have provided guidance throughout the work and reviewed the drafts before submission. Alessandro Weiss and Donatella de Silva contributed to the implementation of numerical models in Paper IV.

Other relevant publications:

L. Possidente, N. Tondini, Battini J.-M. (2018). *Branch-switching procedure for buckling problems of steel elements in fire*. The 10th International Conference on Structures in Fire, Belfast, 6-8 June.

L. Possidente, N. Tondini, Battini J.-M. (2019). *A 3D beam element to study torsion of steel open sections exposed to fire*. The 7th International Conference on Structural Engineering, Mechanics and Computation, Cape Town, 2-4 September.

L. Possidente, N. Tondini, Battini J.-M. (2020). *Behaviour of axially compressed angles and built-up steel members at elevated temperature*. The 11th International Conference on Structures in Fire, Brisbane, 30 November - 3 December

L. Possidente, N. Tondini, Battini J.-M. (2021). *Numerical analysis of the torsional and flexural-torsional buckling behaviour of compressed steel members at elevated temperature*. Eurosteel 2021, Sheffield, 1-3 September, Paper accepted.

Contents

1	Introduction.....	1
1.1	Background	1
1.2	Aim and scope	1
1.3	Research contribution.....	3
1.4	Outline of the thesis.....	4
2	Corotational Shell and 3D Beam elements	7
2.1	Corotational formulation	8
2.1.1	Transformation matrices	8
2.2	Shell element	10
2.2.1	Local system.....	10
2.2.2	Local formulation	11
2.3	3D Beam element	11
2.3.1	Local system.....	12
2.3.2	Local formulation	13
2.3.3	Strain formulation	14
3	Stress integration for steel at elevated temperature.....	17
3.1	European norm provisions.....	18
3.2	2D Stress integration at elevated temperature	20
3.2.1	Modified integration scheme.....	21
3.2.2	Yield surface definition	23
4	Numerical simulation of steel structures in fire.....	25
4.1	Buckling of compressed steel plates and steel columns at elevated temperature (Paper I)	25
4.2	Steel members subject to torsion at elevated temperature (Paper II)	30
4.3	Torsional and flexural-torsional buckling of steel members in fire (Paper III)	34
4.4	Fire Safety Engineering principles applied on a multi-storey steel building (Paper IV)	40

5	Conclusions and further research	45
5.1	Conclusions	45
5.2	Further research	47
	Bibliography	51
	Paper I	59
	Paper II.....	61
	Paper III.....	63
	Paper IV	65

Chapter 1

Introduction

1.1 Background

The humankind has always feared and respected the disruptive power of fire. When human beings started to build settlements to protect themselves, they learned very soon the terrible consequences of uncontrolled fires. Nowadays, fire is still one of the most dangerous hazards when it comes to inhabited structures and should be carefully considered in the design of a building. Steel framed structures are particularly vulnerable to thermal attack. Recent events, such as the New York's World Trade Center collapse in 2001, the Plasco Building fire in Teheran in 2017 and the Wilton Paes de Almeida Building collapse in São Paulo in 2018 showed the catastrophic consequences of structural collapse of steelworks in fire, confirming that fire safety is a fundamental aspect of design of steel structures. One of two different approaches may be adopted in the design for fire safety: the prescriptive approach, following the "deemed-to-satisfy" solutions, or the performance-based approach [1]. As in common practice, following the prescriptive approach a designer might automatically accept that a steelwork needs fire protection. However, the cost of the fire protection can significantly increase the total cost of a steel structure. Instead, the understanding of the behaviour of steel structures in fire allows for a safer, more flexible and economical design [2]. This is the so-called "Performance-Based Fire Engineering approach" (PBF), which steadily relies on numerical simulation. Indeed, a comprehensive application of this approach requires the investigation of the performance of a structure in a range of relevant fire scenarios, identified among the others according to suggestions from ISO 16733-1 [3] and ISO 16732-1 [4]. Recently, several works have been focused on the application of the PBF to different structural types, in both deterministic [5]–[7] and probabilistic terms [8]–[10]. Besides, to enable an improved design, a deeper knowledge of several phenomena, such as the buckling of steel members at elevated temperature, is desirable. Reliable numerical investigations could help provide answers to still open questions. Therefore, effective numerical tools suited for the simulation of structures in fire are of utmost importance.

Several computer programmes have been proposed for the analysis of structures in fire. Some of these are specifically conceived for analyses at elevated temperature, e.g. SAFIR [11] and

VULCAN [12], [13], while others are multipurpose software, e.g. ABAQUS [14], ANSYS [15], OPENSEES [16], or DIANA [17]. All of them, are endowed with thermomechanical finite elements, which account for the effects of temperature on the mechanical behaviour. Nevertheless, an important contribution can still be given, as unsolved issues persist. For instance, the 3D beam elements implemented in SAFIR and ABAQUS do not properly account for torsional effects and for the thermal degradation of the torsional stiffness and thus, as also stated in [11] for SAFIR, such elements are not appropriate for members in which torsion is the dominant action. In the framework of the software VULCAN, a two-node element for analyses at elevated temperature with warping degrees of freedom was presented in [18], based on the element developed in [12], [13]. However, the employed formulation is well suited only for elements with a bi-symmetric section, in which the shear centre and the centroid of the section coincide and thus, is not suitable for elements with a generic cross-section.

Of course, practical matters need to find a solution as well. As mentioned above, reliable numerical investigation could help providing answers even in thoroughly investigated research subjects such as the buckling of steel members. In the design practice, the prediction of the behaviour of steel members at elevated temperature relies on the buckling curves provided in EN 1993-1-2 [19], based on the work of Franssen et al. presented in [20] and [21]. Starting from this model, several curves were proposed for other types of instability modes. For instance, in the last years, researchers have put their effort in the investigation of the lateral-torsional buckling of steel elements [22]–[28] and on how it might interact with local instabilities [29]–[31]. Recently, the major experimental and numerical findings on this topic were collected in [32], but additional works pertaining the local instabilities in fire situation can be found as well, e.g. [33], [34]. Moreover, the buckling of steel columns at elevated temperature with different cross-sections and steel types were investigated in several recent works. For instance, Kaitila [35], Feng et al. [36]–[38] and Chen et al. [39] studied the behaviour of steel channel columns in compression. Still, though many buckling phenomena very studied thoroughly, some of them were not investigated. For instance, there is a lack of knowledge about the behaviour of compressed hot-rolled and welded steel sections in fire subjected to torsional or flexural-torsional buckling. Indeed, these kind of buckling have mainly attracted the interest when the behaviour of cold-formed steel profiles at both ambient and elevated temperatures was concerned [40]–[46]. For such sections, due to the shape and the small thickness, buckling typically occurs as an interaction of local, distortional and global buckling, as showed by Dinis et al. [47] for angular, tee and cruciform cold-formed members at ambient temperature. However, despite the great interest showed about other instability phenomena at elevated temperature, there is a paucity of studies devoted to the investigation of torsional and flexural-torsional buckling in fire situation of hot-rolled and welded steel sections. Moreover, even in hot topics such as the buckling of steel elements in fire [22]–[34], methodological issues should be clarified. Among the others, the definition of an appropriate initial imperfection might not be straightforward for structural elements that buckle at elevated temperature, in particular in case of a non-uniform temperature distribution. It is a well-established practice to introduce initial imperfections in the analyses at elevated temperature based on buckling modes at ambient temperature, obtained by a linear buckling analysis. However, Maraveas et al. [48], [49] showed that even for steel plates with a uniform temperature distribution, the lowest failure load can be obtained with shapes of the initial imperfection that do not match the shapes of the buckling modes at ambient temperature. Hence, the investigation of how the choice of imperfection might affect the results of numerical analyses deserves a deeper interest.

1.2 Aim and scope

Considering the above issues, the objectives are organised in such a way that the initial theoretical development are described first, and the practical implications are discussed afterwards. The first goal is to develop efficient and reliable thermomechanical finite elements for modelling steel structures in fire. The focus is set on shell and 3D beam elements since most of the relevant structural cases, as well as important phenomena such as buckling, can be adequately investigated with these elements. Moreover, the intention is to provide finite elements that allow for improved numerical simulation. For instance, a consistent formulation for torsion in 3D beam elements for steel members with open cross-section is investigated, since elements implemented in available software, e.g. SAFIR, do not properly consider torsion. Among the different finite elements developed in the past decades, corotational finite elements exhibit features suited for the investigation of structures in fire. Indeed, the corotational formulation allows for structural analysis in which large displacements, but small strains occur, which is the typical situation of steel structures in fire.

The second objective of this work is to provide novel research on the buckling of steel members in fire. Indeed, in numerical simulation critical aspects might arise due to the introduction of temperature in the models. For instance, the initial imperfections should be individuated carefully since they determine the behaviour and the resistance of the steel members. In this respect, the investigation of buckling of steel members by means of a procedure that is free from the bias introduced with the initial imperfections is appealing. This is the case of the so-called branch-switching procedure, which applies on perfect structures and enables the numerical simulation of structural problems without the introduction of initial imperfections. Moreover, a challenging goal is to give a contribution with a design buckling curve for the resistance of steel members in fire subjected to torsional or flexural-torsional buckling. For this purpose, analyses based on finite elements that properly account for torsional effects at elevated temperature should be performed.

Last but not least, this thesis aims to suggest how thermomechanical finite elements might be employed in the application of Fire Safety Engineering (FSE) principles for a performance-based design. Indeed, a structure subjected to fire may be investigated combining fire propagation models and finite element analyses. The objective is to provide conclusions about the analysed case study that might be relevant for similar structures and may be useful for engineers.

1.3 Research contribution

The research work presented in this thesis resulted in the following contributions:

- A thermomechanical shell finite element, well suited for the analysis of steel structures in fire.
- A thermomechanical 3D beam finite element that properly accounts for torsion and warping in steel members at elevated temperatures.
- Considerations about the influence of initial imperfections on the behaviour of steel elements at elevated temperature and a branch-switching procedure to study the perfect structures, i.e. without introducing initial imperfections.

- A buckling curve for the design of compressed steel columns with angular, Tee or cruciform cross-section, subject to torsional and flexural-torsional buckling.
- An application of Fire Safety Engineering to a building based on numerical simulation.

These contributions have been presented in the four appended papers. Figure 1.1 depicts how the research objectives have been addressed in the papers.

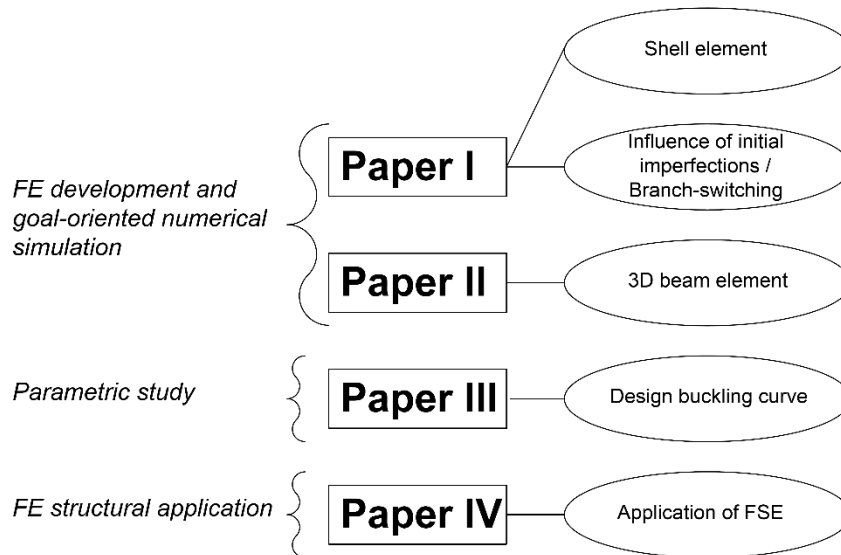


Figure 1.1 Research work organisation.

1.4 Outline of the thesis

This thesis consists of 5 Chapters. An introduction to the research work and a brief description of the developed finite elements are provided in Chapters 1-3, whilst Chapter 4 and Chapter 5 contain an extended summary of the published research work, as well as the relevant conclusions and suggestions for future research. The main text is followed by four appended papers. In detail:

Chapter 1 delineates the context and the structure of the research work. The research background and aims are introduced and the contributions of the research are presented.

In Chapter 2, the derivation of the finite elements is summarised. The corotational framework is described in brief, while more attention is given to the local formulations for the shell and the 3D beam elements.

Chapter 3 focuses on the stress integration procedure for steel at elevated temperature. Effects of temperature on the material are accounted according to the provisions of EN 1993 1-2 [19].

In Chapter 4 the research work is summarised. The chapter organisation follows the sequence of the four appended paper. In Paper I, the buckling and post-buckling behaviour of steel plates and columns at elevated temperature was studied. The influence of initial imperfections was highlighted and an alternative procedure, namely branch-switching, was proposed to

perform the analyses. Paper II is devoted to the validation and application of the developed 3D beam element. Steel members subjected to significant torsional actions at elevated temperature are investigated to assess the performance of the beam element. In Paper III, both the 3D beam element and the shell element are employed in a parametric study. The scope is the definition of design buckling curves for concentrically compressed steel member in fire, prone to torsional and flexural-torsional buckling. This is the case of mono-symmetric or built-up cross-sections, such as angles or Tee and cruciform sections, which are frequently employed in bracing systems or in truss structures. Paper IV shows an application of Fire Safety Engineering to a building. The fire development in a compartment is investigated with different approaches and software.

In Chapter 5, the main conclusions and indications for further research are discussed.

Chapter 2

Corotational Shell and 3D Beam elements

In principle, a coupled problem should be solved to investigate structures in fire, involving fully coupled heat transfer and mechanical analyses. This means, that the thermal response affects the mechanical response, and vice versa. A complete description of the problem is beyond the scope of this thesis, but more information can be found in literature [2], [50]. It is sufficient to specify that fully coupled analyses are performed rarely, since the effects of the thermal response on the mechanical one may be deemed negligible for most of the structural applications. Hence, the heat transfer and the mechanical analyses are performed sequentially. Temperatures inside the structural elements are determined first, and only afterwards a mechanical analysis is executed considering the obtained temperatures. Consequently, it is appropriate to develop thermomechanical finite elements based on elements suited for mechanical analyses, regardless from the possible requirements of heat transfer analysis.

Due to their flexibility in modelling a wide range of three-dimensional problems, shell finite elements are very popular. In the structural field, shells allow for analysing structural elements such as slabs, walls and thin plates, but also for studying the local behaviour of structural members such as steel beams and columns. Nevertheless, for the solution of large structural problems, shell elements-based analyses entail a high computational demand and 3D beam elements are instead preferred. Beam elements enable faster analyses and a simple definition of large structural models. Furthermore, in beam models classical boundary conditions, such as simply supported condition or internal hinges, can be easily defined. However, less information is provided and only the global behaviour of the structural elements can be investigated. Therefore, both finite elements are essential tools of numerical analysis of structures and depending on the investigated case study, models should be defined with shell or 3D beam elements.

The finite elements developed herein are based on a corotational formulation. The latter became very popular as it allows for an effective approach to derive non-linear finite elements [51]–[71]. Typically, steel structures in fire undergo large displacements, but small strain can still be assumed in the structural members. Hence, the corotational approach is very

convenient for the derivation of thermomechanical finite elements, as it is well-suited for analyses in which large displacements and rotations occur, but the small strains assumption is still valid. It is rather indicative that in SAFIR [11], both the shell [72] and the 3D beam elements are implemented in a corotational framework [73].

The purpose of this chapter is to present the derivation of two finite elements well-suited for thermomechanical analyses. A brief description of the corotational formulation is provided as well, to show the framework in which the shell and the 3D beam elements are embedded.

2.1 Corotational formulation

The corotational approach relies on the idea that the motion of an element can be decomposed into rigid body and pure deformational parts. The latter is captured at the level of a local reference frame, which continuously translates and rotates with the element. The transformation matrices that relate the local and the global systems allow the geometric nonlinearity induced by the large rigid-body motion to be considered. Thus, a simple geometrical linear element can be chosen as local element. However, material nonlinearity needs to be introduced at the level of the local formulation. In this paragraph is described the corotational framework in which a shell element and a 3D beam element are incorporated. Additional information can be found in [54], [56], [57], [60]. Here and in the rest of the thesis, vectors are defined by bold letters, whereas matrices are in bold capital letters.

2.1.1 Transformation matrices

The corotational framework is based on a local system which continuously translates and rotates with the element. The motion of the element from the initial to the final deformed configuration is split into two stages, consisting in a rigid body motion and a pure deformation. The relations between the quantities expressed in respect to the local and the global frame define the corotational framework. For sake of clarity, the framework of the shell element is depicted in Figure 2.1, but the considerations taken here are valid for the 3D beam element as well.

The local displacements of \mathbf{p}_l are expressed as functions of the global ones

$$\mathbf{p}_l = \mathbf{p}_l(\mathbf{p}_g) \quad (2.1)$$

Local displacements are used to compute the local internal force vector and stiffness matrix, \mathbf{f}_l and \mathbf{K}_l respectively. The global internal force vector \mathbf{f}_g and global tangent stiffness matrix \mathbf{K}_g are derived from the corresponding local quantities \mathbf{f}_l and \mathbf{K}_l . Let us assume that the displacement vectors are related by a transformation matrix \mathbf{B} such that

$$\delta \mathbf{p}_l = \mathbf{B} \delta \mathbf{p}_g \quad (2.2)$$

The virtual work V gives the following relation between the internal force vectors \mathbf{f}_l and \mathbf{f}_g associated to \mathbf{p}_l and \mathbf{p}_g respectively

$$V = \delta \mathbf{p}_g^T \mathbf{f}_g = \delta \mathbf{p}_l^T \mathbf{f}_l \quad (2.3)$$

Which, by using (2.2) gives

$$\mathbf{f}_g = \mathbf{B}^T \mathbf{f}_l \quad (2.4)$$

The tangent stiffness matrices \mathbf{K}_l and \mathbf{K}_g are defined by

$$\mathbf{K}_l = \frac{\partial \mathbf{f}_l}{\partial \mathbf{p}_l}, \quad \mathbf{K}_g = \frac{\partial \mathbf{f}_g}{\partial \mathbf{p}_g} \quad (2.5)$$

Substituting (2.4) in the second equation of (2.5) gives

$$\mathbf{K}_g = \frac{\partial (\mathbf{B}^T \mathbf{f}_l)}{\partial \mathbf{p}_g} = \mathbf{B}^T \frac{\partial \mathbf{f}_l}{\partial \mathbf{p}_g} \frac{\partial \mathbf{p}_l}{\partial \mathbf{p}_g} + \frac{\partial \mathbf{B}^T}{\partial \mathbf{p}_g} : \mathbf{f}_l \quad (2.6)$$

where the symbol “:” denotes a contraction. Finally, using (2.2) in (2.5), we obtain

$$\mathbf{K}_g = \mathbf{B}^T \mathbf{K}_l \mathbf{B} + \frac{\partial \mathbf{B}^T}{\partial \mathbf{p}_g} : \mathbf{f}_l \quad (2.7)$$

The transformation matrix \mathbf{B} is derived by three successive change of variables associated to the rotation matrices depicted in Figure 2.1. The initial configuration frame is obtained through the rotation matrix \mathbf{R}_0 . The orientation of the local frame is defined by the rigid rotation \mathbf{R}_r . The global rotation of the node i of the elements is defined by the matrix \mathbf{R}_i . $\bar{\mathbf{R}}_i$ describes the local small rotation acting on the nodes due to the pure deformation. Since there are two equivalent transformations available to define the final frame for each node, the following equations can be written

$$\mathbf{R}_r \bar{\mathbf{R}}_i = \mathbf{R}_i \mathbf{R}_0 \quad i = 1, 2, 3 \quad (2.8)$$

Due to the properties of the rotation matrices (2.8) can be rearranged as

$$\bar{\mathbf{R}}_i = \mathbf{R}_r^T \mathbf{R}_i \mathbf{R}_0 \quad i = 1, 2, 3 \quad (2.9)$$

\mathbf{B} is derived by change of variables associated to equation (2.9). A detailed description of this procedure can be found in [68] for the shell element and in [54] for the 3D beam element. Through the described transformations the global stiffness matrix \mathbf{K}_g and force vector \mathbf{f}_g are obtained from the local quantities \mathbf{f}_l and \mathbf{K}_l . Note that the corotational framework is independent from the choice of the local formulation characterised by \mathbf{f}_l and \mathbf{K}_l . This means that several existing elements can be adopted as local formulation, without compromising the structure of the general framework.

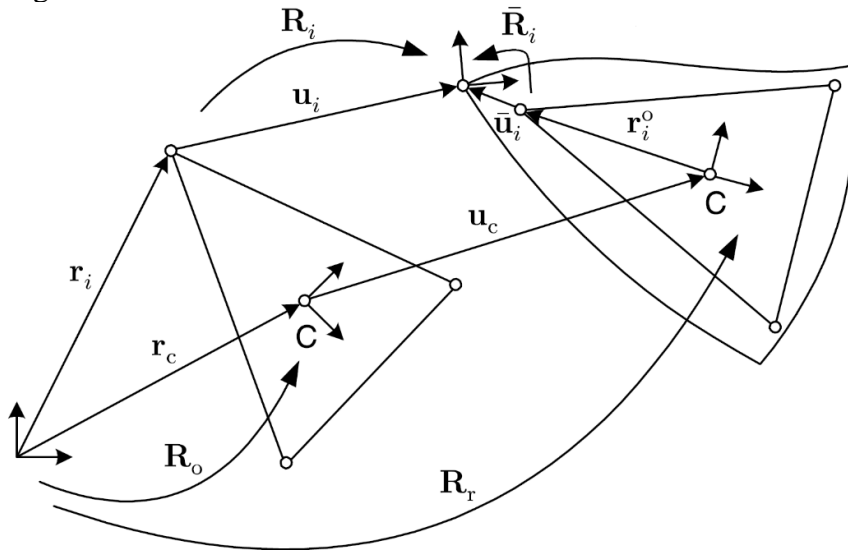


Figure 2.1 Corotational shell element framework.

2.2 Shell element

A triangular flat three-noded thin shell element is developed in the context of the corotational framework (see Figure 2.1). In thin shells the thickness is small compared with the overall dimensions and the transverse shear deformations are neglected. Since the thin-shell theory applies to most of the steel profiles, or at least to most of steelworks employed in construction, the presented element is suitable for the investigation of steel structures in fire.

The deformational displacement vector expressed in the global frame \mathbf{p}_g consists of displacements \mathbf{u}_i^g and rotations $\boldsymbol{\theta}_i^g$ expressed in global coordinates:

$$\mathbf{p}_g = [\mathbf{u}_1^{gT} \quad \boldsymbol{\theta}_1^{gT} \quad \mathbf{u}_2^{gT} \quad \boldsymbol{\theta}_2^{gT} \quad \mathbf{u}_3^{gT} \quad \boldsymbol{\theta}_3^{gT}]^T \quad (2.10)$$

$$\boldsymbol{\theta}_i^g = \log(\mathbf{R}_i) \quad (2.11)$$

The local displacement vector \mathbf{p}_l is composed by three deformational nodal displacements $\bar{\mathbf{u}}_i$ and three rotations $\bar{\boldsymbol{\vartheta}}_i$

$$\mathbf{p}_l = [\bar{\mathbf{u}}_1^T \quad \bar{\boldsymbol{\vartheta}}_1^T \quad \bar{\mathbf{u}}_2^T \quad \bar{\boldsymbol{\vartheta}}_2^T \quad \bar{\mathbf{u}}_3^T \quad \bar{\boldsymbol{\vartheta}}_3^T]^T \quad (2.12)$$

$$\bar{\mathbf{u}}_i = \mathbf{R}_r^T (\mathbf{r}_i^g + \mathbf{u}_i^g - \mathbf{r}_c^g - \mathbf{u}_c^g) - \mathbf{r}_i^0, \quad \bar{\boldsymbol{\vartheta}}_i = \log(\bar{\mathbf{R}}_i) \quad (2.13)$$

$\bar{\mathbf{u}}_i$ and $\bar{\boldsymbol{\vartheta}}_i$ are the local displacements and rotations. $\mathbf{r}_i^g, \mathbf{u}_i^g, \mathbf{r}_c^g$ and \mathbf{u}_c^g are the initial position and global displacement of node i and the centroid C (see Figure 2.1).

2.2.1 Local system

The choice of the local system is essential to the definition of the shell element. Among different frame orientations of the local system, the philosophy of minimising local nodal displacements is pursued. The described local system was first presented and compared to other formulations in [57].

The rigid rotation matrix \mathbf{R}_r is defined by the triplet $[\mathbf{e}_1 \quad \mathbf{e}_2 \quad \mathbf{e}_3]$. The first step for the definition of the local frame consists in taking \mathbf{e}_1 parallel to the side 1-2 of the element in its current configuration. The three axis vectors are then defined by

$$\mathbf{e}_1 = \frac{\mathbf{x}_{12}^g}{\|\mathbf{x}_{12}^g\|}, \quad \mathbf{e}_3 = \frac{\mathbf{x}_{12}^g \times \mathbf{x}_{13}^g}{\|\mathbf{x}_{12}^g \times \mathbf{x}_{13}^g\|}, \quad \mathbf{e}_2 = \mathbf{e}_3 \times \mathbf{e}_1, \quad \mathbf{x}_{12}^g = \mathbf{x}_2^g - \mathbf{x}_1^g \quad (2.14)$$

where \mathbf{x}_i^g is the global current position of the node i , defined by

$$\mathbf{x}_i^g = \mathbf{r}_i^g + \mathbf{u}_i^g \quad (2.15)$$

By doing that, the local coordinates system depends on the node ordering of the element. In order to obtain a formulation that does not depend on the node ordering, a small out of plane rotation is performed, such that the square of the Euclidean norm of the local nodal displacements is minimised. After some calculation, this rotation is defined by

$$\tan \theta = \frac{\sum_{i=1}^3 (y_i X_i - x_i Y_i)}{\sum_{i=1}^3 (x_i X_i + y_i Y_i)} \quad (2.16)$$

In the previous equation, (X_i, Y_i) are the local components of \mathbf{r}_i^0 and (x_i, y_i) are the local components of the vector $\mathbf{r}_i^0 + \bar{\mathbf{u}}_i$. With that choice, the vectors of the rigid rotation matrix \mathbf{R}_r are then computed by

$$\mathbf{e}_{1n} = \cos \theta \mathbf{e}_1 + \sin \theta \mathbf{e}_2, \quad \mathbf{e}_{2n} = -\sin \theta \mathbf{e}_1 + \cos \theta \mathbf{e}_2, \quad \mathbf{e}_{3n} = \mathbf{e}_3 \quad (2.17)$$

2.2.2 Local formulation

The local shell element consists in the superposition of a membrane and a plate element. Thus, the strains acting in the shell element consist of a membrane and a plate strain part

$$\boldsymbol{\varepsilon}(z, \xi_i) = [\varepsilon_x \quad \varepsilon_x \quad 2\varepsilon_{xy}]^T = \mathbf{A}(z, \xi_i)\mathbf{p}_l = \mathbf{A}_m(\xi_i)\mathbf{p}_{lm} - z\mathbf{A}_p(\xi_i)\mathbf{p}_{lp} \quad (2.18)$$

where the subscript l means local, m membrane and p plate. ξ_i is the natural area coordinate of a triangle. If no volume or surface loads act on the element, the virtual work principle gives

$$\delta \mathbf{p}_l^T \mathbf{f}_l = \int_V \delta \boldsymbol{\varepsilon}^T \boldsymbol{\sigma} dV, \quad \boldsymbol{\sigma} = [\sigma_x \quad \sigma_y \quad \tau_{xy}]^T \quad (2.19)$$

The vector $\boldsymbol{\sigma}$ describes the stresses in the element assuming a plane-stress behaviour. Indeed, since a thin shell element is developed, bending shear stresses are neglected in the plate element. Introducing (2.18) in (2.19) the expression of the local force vector and stiffness matrix are obtained

$$\mathbf{f}_l = \int_V \mathbf{A}^T(z, \xi_i)\boldsymbol{\sigma} dV, \quad \mathbf{K}_l = \int_V \mathbf{A}^T(z, \xi_i)\mathbf{C}_{ct}\mathbf{A}(z, \xi_i)dV \quad (2.20)$$

where \mathbf{C}_{ct} is the consistent elastoplastic tangent operator, defined as follows

$$\delta \boldsymbol{\sigma} = \mathbf{C}_{ct}\delta \boldsymbol{\varepsilon} \quad (2.21)$$

The definition of the matrix \mathbf{A} depends on the membrane and plate elements adopted. The choice of these elements is based on an assessment of different elements presented in [56]. In this work, an optimal ANDES membrane element [61] and a DKT (Discrete Kirchhoff Triangle) plate element [74] are employed to define the matrices \mathbf{A}_m and \mathbf{A}_p respectively. Both elements are integrated using 3 Gauss points ($\xi_i = 1/6, 1/6, 2/3$, with ξ_i =natural area coordinates of a triangle).

As the stress integration will involve the effects of elevated temperatures, the procedure to obtain the stress vector $\boldsymbol{\sigma}$ from the strain vector $\boldsymbol{\varepsilon}$ will be given in Chapter 3.

2.3 3D Beam element

A two-node ($i = 1, 2$) 3D beam element for the analysis of steel members with open cross-sections was developed. The corotational framework is depicted in Figure 2.2. The deformational displacement vector expressed in the global frame \mathbf{p}_g consists of three nodal displacements \mathbf{u}_i and three nodal rotations $\bar{\boldsymbol{\theta}}_i$ for each node, expressed in global coordinates. A further degree of freedom α_i is introduced to account for warping.

$$\mathbf{p}_g = \left[\mathbf{u}_1^{gT} \quad \boldsymbol{\theta}_1^{gT} \quad \alpha_1 \quad \mathbf{u}_2^{gT} \quad \boldsymbol{\theta}_2^{gT} \quad \alpha_2 \right]^T \quad (2.22)$$

$$\boldsymbol{\theta}_i^g = \log(\mathbf{R}_i) \quad (2.23)$$

The warping degrees of freedom remain constant during the transformations between \mathbf{p}_g and \mathbf{p}_l . Moreover, due to the particular choice of local system presented in the next paragraph, the axial elongation \bar{u} is sufficient to describe the nodal displacements in the local system. Hence, the local deformational displacement \mathbf{p}_l is defined as

$$\mathbf{p}_l = [\bar{u} \quad \bar{\boldsymbol{\vartheta}}_1^T \quad \alpha_1 \quad \bar{\boldsymbol{\vartheta}}_2^T \quad \alpha_2]^T \quad (2.24)$$

$$\bar{\boldsymbol{\vartheta}}_i = \log(\bar{\mathbf{R}}_i) \quad (2.25)$$

The axial elongation \bar{u} can be determined as the difference between the current length and the initial length of the element in the initial undeformed configuration.

$$\bar{u} = l_n - l_0, \quad l_0 = \|\mathbf{x}_2^g - \mathbf{x}_1^g\|, \quad l_n = \|\mathbf{x}_2^g + \mathbf{u}_2^g - \mathbf{x}_1^g - \mathbf{u}_1^g\| \quad (2.26)$$

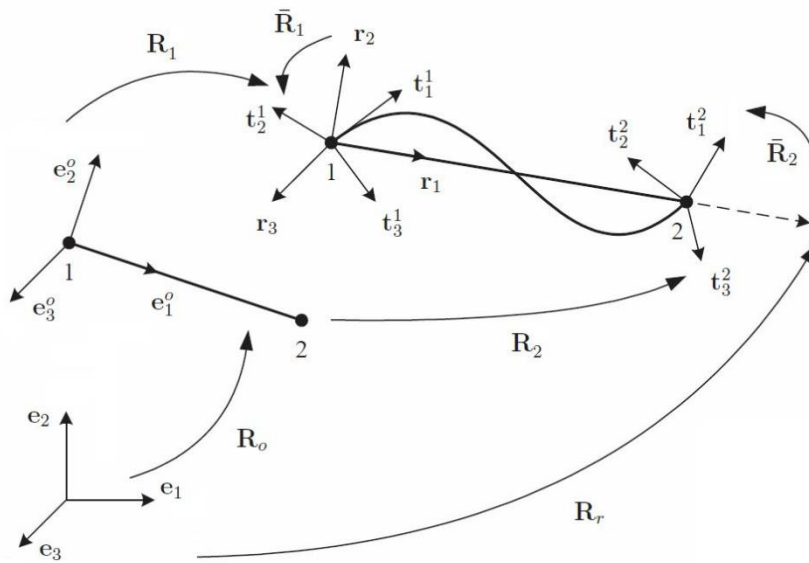


Figure 2.2 Corotational 3D beam element framework [54].

2.3.1 Local system

As depicted in Figure 2.2, the global reference system is defined by the triad of unit orthogonal vectors \mathbf{e}_j , with $j = 1, 2, 3$, while in the initial undeformed configuration the orthonormal triad \mathbf{e}_j^0 , $j = 1, 2, 3$ denotes the local system. \mathbf{t}_j^1 and \mathbf{t}_j^2 , $j = 1, 2, 3$ indicate two unit triads rigidly attached to nodes 1 and 2. The orthonormal basis vectors of the local system \mathbf{r}_j , $j = 1, 2, 3$, define the orthogonal matrix $\mathbf{R}_r = [\mathbf{r}_1 \quad \mathbf{r}_2 \quad \mathbf{r}_3]$. The first axis of the local system is determined connecting the two nodes of the element

$$\mathbf{r}_1 = \frac{\mathbf{x}_2^g + \mathbf{u}_2^g - \mathbf{x}_1^g - \mathbf{u}_1^g}{l_n} \quad (2.27)$$

Where \mathbf{x}_i^g , $i = 1, 2$ are the local nodal coordinates in the initial undeformed configuration and l_n is the current length of the beam. In order to define the remaining orthonormal vectors of \mathbf{R}_r an auxiliary vector \mathbf{q} is introduced.

$$\mathbf{q} = \frac{1}{2}(\mathbf{q}_1 + \mathbf{q}_2), \quad \mathbf{q}_i = \mathbf{R}_i \mathbf{R}_0 [0 \quad 1 \quad 0]^T, \quad i = 1, 2 \quad (2.28)$$

With \mathbf{R}_1 and \mathbf{R}_2 the orthogonal matrices associated to the orientation defined by the triads \mathbf{t}_j^1 and \mathbf{t}_j^2 respectively and $\mathbf{R}_0 = [\mathbf{e}_1^0 \quad \mathbf{e}_2^0 \quad \mathbf{e}_3^0]$ specifying the local frame orientation in the initial configuration. Once \mathbf{q} is determined, the unit vectors are obtained as follows

$$\mathbf{r}_3 = \frac{\mathbf{r}_1 \times \mathbf{q}}{\|\mathbf{r}_1 \times \mathbf{q}\|}, \quad \mathbf{r}_2 = \mathbf{r}_3 \times \mathbf{r}_1 \quad (2.29)$$

The local system specified by \mathbf{R}_r describes a rigid body motion, that is accompanied by local deformational displacements with respect to the local element axes. Hence, in the chosen local system the local translations at node 1 are zero and at node 2 the only non-zero component is the translation along \mathbf{r}_1 . This is the axial elongation \bar{u} , defined in (2.26).

2.3.2 Local formulation

Following the work done by Battini [54], the local strains $\boldsymbol{\varepsilon}$ for a 3D beam element with a generic cross-section are defined as a function of the local nodal displacement vector \mathbf{p}_l .

$$\boldsymbol{\varepsilon}(\mathbf{p}_l) = [\varepsilon_x \quad 2\varepsilon_{xy} \quad 2\varepsilon_{xz}]^T \quad (2.30)$$

Differentiation of (2.30) gives

$$\delta \boldsymbol{\varepsilon} = \mathbf{A} \delta \hat{\boldsymbol{\varepsilon}} \quad (2.31)$$

$\hat{\boldsymbol{\varepsilon}}$ is a vector composed of the displacement quantities, and their derivatives, necessary to the definition of the strain vector $\boldsymbol{\varepsilon}$. The differentiation of the vector $\hat{\boldsymbol{\varepsilon}}$ gives

$$\delta \hat{\boldsymbol{\varepsilon}} = \mathbf{G} \delta \mathbf{p}_l \quad (2.32)$$

Where \mathbf{G} is a matrix that accounts for numerical integration in the length of the beam element. Assuming that no volume or surface loads are acting on the element, the virtual work principle gives

$$\delta \mathbf{p}_l^T \mathbf{f}_l = \int_V \delta \boldsymbol{\varepsilon}^T \boldsymbol{\sigma} dV = \int_{l_0} \delta \hat{\boldsymbol{\varepsilon}}^T \hat{\boldsymbol{\sigma}} dx_1, \quad \boldsymbol{\sigma} = [\sigma_x \quad \tau_{xy} \quad \tau_{xz}]^T \quad (2.33)$$

Substituting (2.32) in the last integral of (2.33)

$$\mathbf{f}_l = \int_{l_0} \mathbf{G}^T \hat{\boldsymbol{\sigma}} dx_1 \quad (2.34)$$

$\hat{\boldsymbol{\sigma}}$ is the vector of stress resultants given by

$$\hat{\boldsymbol{\sigma}} = \int_A \mathbf{A}^T \boldsymbol{\sigma} dA \quad (2.35)$$

Differentiation of equation (2.34) gives

$$\mathbf{K}_l = \int_{l_0} \mathbf{G}^T \hat{\mathbf{D}} \mathbf{G} dx_1, \quad \delta \hat{\boldsymbol{\sigma}} = \hat{\mathbf{D}} \delta \hat{\boldsymbol{\varepsilon}} \quad (2.36)$$

The matrix $\hat{\mathbf{D}}$ is evaluated taking variations of (2.35)

$$\delta \hat{\boldsymbol{\sigma}} = \int_A [\mathbf{A}^T \delta \boldsymbol{\sigma} + \delta(\mathbf{A}^T \boldsymbol{\sigma})] dA = \int_A [\mathbf{A}^T \mathbf{C}_{ct} \mathbf{A} + \mathbf{L}] dA \delta \hat{\boldsymbol{\varepsilon}} \quad (2.37)$$

\mathbf{C}_{ct} is the consistent elastoplastic tangent operator defined by $\delta\boldsymbol{\sigma} = \mathbf{C}_{ct}\delta\boldsymbol{\varepsilon}$, while \mathbf{L} is the result of the differentiation $\delta(\mathbf{A}^T\boldsymbol{\sigma})$ with $\boldsymbol{\sigma}$ kept constant.

The definition of the strain vector $\boldsymbol{\varepsilon}$, the vector $\hat{\boldsymbol{\varepsilon}}$ and the matrices \mathbf{A} , \mathbf{G} and \mathbf{L} depend on the strain formulation employed in the development of the finite element. Further information about these quantities is given in the following paragraph for a Timoshenko element with one gauss integration point to avoid shear locking and for a Bernoulli element. Again, the stress integration performed to obtain the stress vector $\boldsymbol{\sigma}$ from the strain vector $\boldsymbol{\varepsilon}$ will be given in Chapter 3.

2.3.3 Strain formulation

An appropriate formulation of the strain vector $\boldsymbol{\varepsilon}$ is necessary to properly account for torsion and warping. Starting from the kinematic model proposed in [75], the local strains at the point $P = [x_1, x_2, x_3]$ of a generic cross-section, as depicted in Figure 2.3, are expressed as

$$\begin{aligned} \varepsilon_x &= u_{1,1} - x_2\vartheta_{3,1} + x_3\vartheta_{2,1} + \frac{1}{2}r^2\vartheta_{1,1}^2 + \bar{\omega}\alpha_{,1} \\ 2\varepsilon_{xy} &= \gamma_{12} + \bar{\omega}_{,2}\alpha - x_3\vartheta_{1,1} \end{aligned} \quad (2.38)$$

$$2\varepsilon_{xz} = \gamma_{13} + \bar{\omega}_{,3}\alpha + x_2\vartheta_{1,1}$$

With

$$\gamma_{12} = u_{2,1} - \vartheta_3, \quad \gamma_{13} = u_{3,1} + \vartheta_2, \quad r^2 = x_2^2 + x_3^2 \quad (2.39)$$

u_1, u_2, u_3 are the local displacements of the centroid G. $\vartheta_1, \vartheta_2, \vartheta_3$ are the local rotations of the cross-section. The warping function $\bar{\omega}$ is defined using the Saint-Venant torsion theory and refers to the centroid G. $\bar{\omega}(x_2, x_3)$ is computed in a separate analysis by using isoparametric quadratic elements with 4 Gauss points each. It can be observed that the only non-linear term in the adopted strain definition is the Wagner term $1/2(r^2\vartheta_{1,1}^2)$. As a matter of fact, the geometrical non-linearities are introduced in the transformation matrices relating global to local quantities and consequently a simple expression of the strains in the local frame can be taken. However, the numerical tests presented in [54] showed that for problems that involve large torsional effects a linear strain definition is inaccurate and that the Wagner term must be added in the strain definition in order to get accurate results. Further simplifications can be introduced when a Bernoulli element is implemented. A detailed description can be found in Paper II [76]. The following quantities are derived from the definition of $\boldsymbol{\varepsilon}$ given in (2.38), for the Timoshenko and the Bernoulli element

Timoshenko	Bernoulli
$\hat{\boldsymbol{\varepsilon}} \ [u_{,11} \ \vartheta_3 \ \vartheta_2 \ \vartheta_{1,1} \ \vartheta_{2,1} \ \vartheta_{3,1} \ \alpha \ \alpha_{,1}]^T$	$[u_{1,1} \ u_{2,11} \ u_{3,11} \ \vartheta_{1,1} \ \vartheta_{1,11}]^T$
$\mathbf{A} \ \begin{bmatrix} 1 & 0 & 0 & r^2\vartheta_{1,1} & x_3 & -x_2 & 0 & \bar{\omega} \\ 0 & -1 & 0 & -x_3 & 0 & 0 & \bar{\omega}_{,2} & 0 \\ 0 & 0 & 1 & x_2 & 0 & 0 & \bar{\omega}_{,3} & 0 \end{bmatrix}$	$\begin{bmatrix} 1 & -x_2 & -x_3 & r^2\vartheta_{1,1} & \bar{\omega} \\ 0 & 0 & 0 & \bar{\omega}_{,2} - x_3 & 0 \\ 0 & 0 & 0 & \bar{\omega}_{,3} + x_2 & 0 \end{bmatrix}$

(2.40)

G Non-zero terms (8x9 matrix)

$$G_{11} = G_{45} = G_{56} = G_{67} = G_{89} = \frac{1}{l_0}$$

$$G_{42} = G_{53} = G_{64} = G_{88} = -\frac{1}{l_0}$$

$$G_{24} = G_{27} = G_{33} = G_{36} = G_{78} = G_{79} = \frac{1}{2}$$

Non-zero terms (5x9 matrix)

$$G_{42} = f_1' \quad G_{52} = f_1''$$

$$G_{48} = f_2'$$

$$G_{24} = G_{58} = -G_{33} = f_2''$$

$$G_{45} = f_3' \quad G_{55} = f_3''$$

$$G_{49} = f_4'$$

$$G_{27} = G_{59} = -G_{36} = f_4''$$

$$G_{11} = f_5'$$

L Only non-zero term (8x8 matrix)

$$L_{44} = r^2 \sigma_{11}$$

Only non-zero term (5x5 matrix)

$$L_{44} = r^2 \sigma_{11}$$

Where in the Bernoulli element the superscript ' indicates a differentiation with respect to the variable x_1 . Hermitian shape functions ($f_1 - f_4$) are used to interpolate u_2, u_3 and ϑ_1 , whereas a linear shape function (f_5) is used for u_1

$$f_1 = 1 - 3\left(\frac{x_1}{l_0}\right)^2 + 2\left(\frac{x_1}{l_0}\right)^3 \tag{2.41}$$

$$f_2 = x\left(1 - \frac{x_1}{l_0}\right)^2 \quad f_3 = 1 - f_1 \quad f_4 = \frac{x_1^2}{l_0}\left(\frac{x_1}{l_0} - 1\right) \quad f_5 = \frac{x_1}{l_0}$$

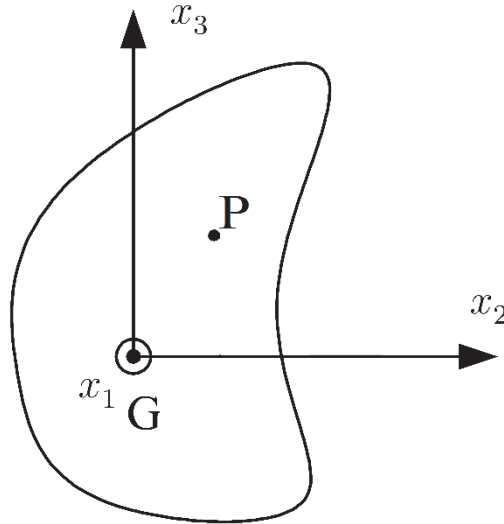


Figure 2.3 Local formulation: generic cross-section.

Chapter 3

Stress integration for steel at elevated temperature

Typically, steel structures in fire have a pronounced nonlinear behaviour. Indeed, steel structural elements at elevated temperatures are subject to thermal expansion and their bearing capacity decreases owing to degradation of mechanical properties. Hence, thermomechanical finite elements require an adequate stress-strain integration procedure that accounts for such effects.

In general, stress-strain curves are defined in a (σ, ε) plane and relate in a uniaxial form one stress to one strain quantity. Though simple, such a description of the material behaviour is inadequate for problems involving more stress and strain components, and the concept of yield surface should be introduced. For ductile materials, and in particular for steel, the yield surface is usually defined according to a Von Mises criterion [77], but many different criteria are available in literature. For instance, a review of different yield surfaces for thin shells was proposed in [78]. In numerical analysis, yield criteria should be combined with iterative integration algorithms to return on the yield surface when stresses are found outside the yield surface. Both explicit and implicit algorithms have been proposed. Among these, the Backward-Euler integration algorithm is reliable and allows for quadratic convergence for the Newton-Raphson iterations at the structural level by generating a consistent tangent operator. Besides, it takes a particularly simple form for the von Mises yield criterion [59].

Several thermomechanical finite elements have been implemented in different finite element software. While most shell elements rely on stress integration procedures based on a Von Mises yield criterion and a Backward Euler algorithm, different formulations, and in turn stress integration procedures, were adopted for 3D beam elements. For instance, SAFIR and OPENSEES provide fiber-elements [11], [79], which imply the adoption of a uniaxial stress-strain relationship. The fiber-element formulation is particularly effective for concrete, but it also enables the implementation of simple uniaxial models for strain reversal in steel structural elements [80]–[82]. In structures in fire, strain reversal is mainly related to the occurrence of large displacements, but also to specific phenomena such as the catenary action or the cooling phase. If strain reversal occurs in sections stressed above the elastic limit, the

effect of permanent strain on the material behaviour should be considered and the stress-strain relationship should be a function of the load history. However, only the axial stress is considered in fiber-elements and, since shear stresses are essential to properly treat torsion, a plane stress approach was preferred.

3.1 European norm provisions

The European design code EN 1993 1-2 [19] deals with the design of steel structures for the accidental situation of fire exposure. In compliance to the norm, the design and analysis of structures should account for the material properties of steel at elevated temperature. Though temperature affects both the thermal and the mechanical properties of steel, only the latter are treated here, as the heat transfer analysis is not considered. More in specific, the thermal elongation and the stress-strain law are directly implied in the mechanical analysis and are described in this paragraph.

According to EN 1993 1-2 [19], thermal elongation of steel should be determined as follows

$$\Delta l/l = 1,2 \times 10^{-5} \theta_a + 0,4 \times 10^{-8} \theta_a^2 - 2,416 \times 10^{-4} \quad 20^\circ\text{C} \leq \theta_a < 750^\circ$$

$$\Delta l/l = 1,1 \times 10^{-2} \quad 750^\circ\text{C} \leq \theta_a \leq 860^\circ \quad (3.1)$$

$$\Delta l/l = 2 \times 10^{-5} \theta_a - 6.2 \times 10^{-3} \quad 860^\circ\text{C} < \theta_a \leq 1200^\circ$$

where l is the length at 20°C, Δl is the temperature induced elongation and θ_a is the steel temperature (in °C).

For heating rates between 2 and 50 K/min, the uniaxial stress-strain relationship for carbon steel at elevated temperature is provided (Figure 3.1).

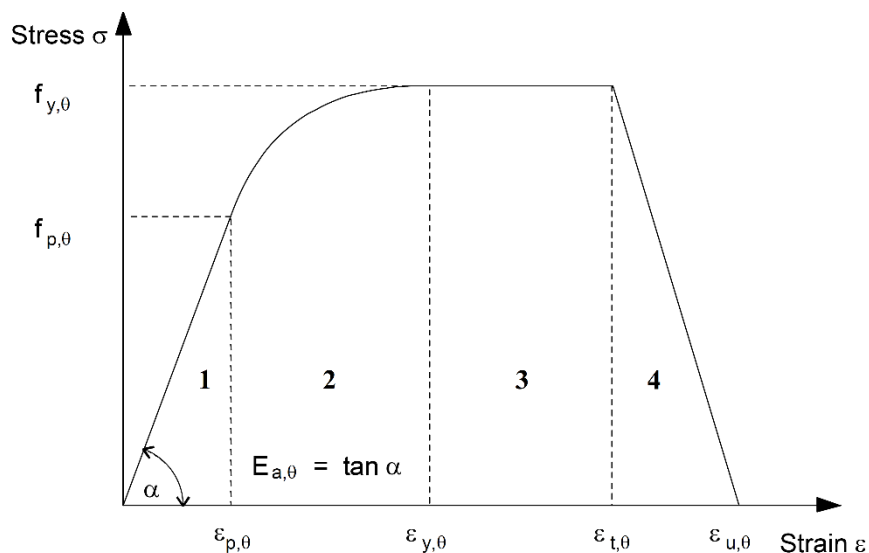


Figure 3.1 Stress-strain relationship for carbon steel at elevated temperatures (EN 1993 1-2 [19]).

where $f_{y,\theta}$ is the effective yield strength, $f_{p,\theta}$ the proportional limit, $E_{a,\theta}$ the slope of the linear elastic range, $\epsilon_{p,\theta} = f_{p,\theta}/E_{a,\theta}$ the strain at the proportional limit, $\epsilon_{y,\theta} = 0.02$ the yield

strain, $\varepsilon_{t,\theta} = 0.15$ the limiting strain for yield strength and $\varepsilon_{u,\theta} = 0.20$ the ultimate strain. In this stress-strain relationship steel has a linear elastic response up to $\varepsilon_{p,\theta}$, followed by a plastic elliptic behaviour. Once the strain exceeds the yield strain $\varepsilon_{y,\theta}$, perfect plasticity occurs up to $\varepsilon_{t,\theta}$. The stresses decrease to zero in the range $\varepsilon_{t,\theta} < \varepsilon \leq \varepsilon_{u,\theta}$. The stress-strain curve is univocally defined by the following equations

Stress σ	Tangent stiffness $E_{t,\theta}$	
$\varepsilon E_{a,\theta}$	$E_{a,\theta}$	$\varepsilon \leq \varepsilon_{p,\theta}$
$f_{p,\theta} - c + \frac{b}{a} \sqrt{a^2 - (\varepsilon_{y,\theta} - \varepsilon)^2}$	$\frac{b(\varepsilon_{y,\theta} - \varepsilon)}{a \sqrt{a^2 - (\varepsilon_{y,\theta} - \varepsilon)^2}}$	$\varepsilon_{p,\theta} < \varepsilon \leq \varepsilon_{y,\theta}$
$f_{y,\theta}$	0	$\varepsilon_{y,\theta} < \varepsilon \leq \varepsilon_{t,\theta}$
$\frac{f_{y,\theta}(\varepsilon_{u,\theta} - \varepsilon)}{(\varepsilon_{u,\theta} - \varepsilon_{t,\theta})}$	$-\frac{f_{y,\theta}}{(\varepsilon_{u,\theta} - \varepsilon_{t,\theta})}$	$\varepsilon_{t,\theta} < \varepsilon \leq \varepsilon_{u,\theta}$

Where the parameters a , b and c are defined as follows

$$a = \sqrt{(\varepsilon_{y,\theta} - \varepsilon_{p,\theta})(\varepsilon_{y,\theta} - \varepsilon_{p,\theta} + c/E_{a,\theta})}$$

$$b = \sqrt{c(\varepsilon_{y,\theta} - \varepsilon_{p,\theta})E_{a,\theta} + c^2}$$

$$c = \frac{(f_{y,\theta} - f_{p,\theta})^2}{(\varepsilon_{y,\theta} - \varepsilon_{p,\theta})E_{a,\theta} - 2(f_{y,\theta} - f_{p,\theta})}$$

The effective yield strength $f_{y,\theta}$, the proportional limit $f_{p,\theta}$ and the slope of the linear elastic range $E_{a,\theta}$ at elevated temperatures should be obtained by multiplying the associated quantities at ambient temperature by the relevant reduction factors, given in Table 3.1.

$$f_{y,\theta} = k_{y,\theta} f_y, \quad f_{p,\theta} = k_{p,\theta} f_p, \quad E_{a,\theta} = k_{E,\theta} E_a \quad (3.4)$$

Table 3.1: Reduction factors for stress-strain law of carbon steel at elevated temperatures

Steel Temperature θ_a [°C]	$k_{y,\theta}$	$k_{p,\theta}$	$k_{E,\theta}$
20	1.000	1.000	1.000
100	1.000	1.000	1.000
200	1.000	0.807	0.900
300	1.000	0.613	0.800
400	1.000	0.420	0.700
500	0.780	0.360	0.600
600	0.470	0.180	0.310
700	0.230	0.075	0.130

800	0.110	0.050	0.090
900	0.060	0.0375	0.0675
1000	0.040	0.0250	0.0450
1100	0.020	0.0125	0.0225
1200	0.000	0.0000	0.0000

Linear interpolation may be used for intermediate values of steel temperatures. The evolution of the reduction factors with temperature is depicted in Figure 3.2.

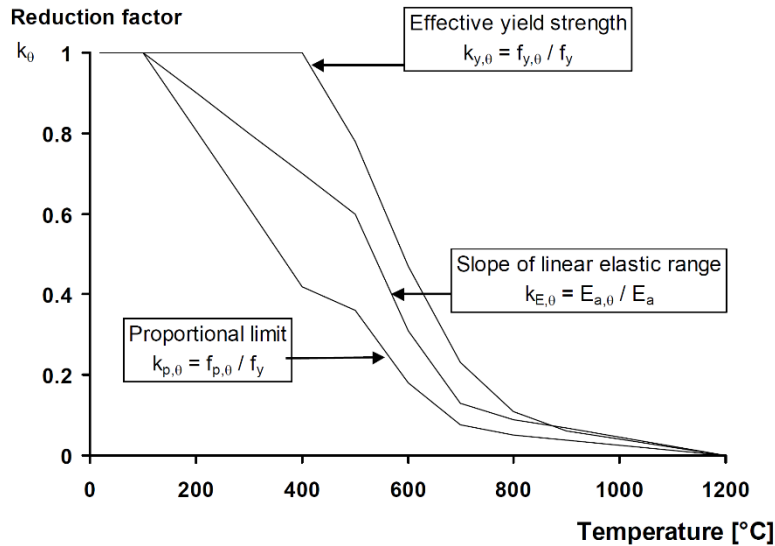


Figure 3.2 Reduction factors for the stress-strain law of carbon steel at elevated temperatures (EN 1993 1-2 [19]).

3.2 2D Stress integration at elevated temperature

Numerical integration over the section of the elements is performed to compute the stress vector σ and the consistent elastoplastic tangent operator C_{ct} from the strain vector ϵ , by using Gauss integration in the cross-section. For the shell elements 7 points in the thickness of the element were found to be sufficient for most of the practical cases. This means, that together with the surface discretisation, each element consists of $3 \times 7 = 21$ Gauss points. Instead, for the 3D beam elements the same cross-section discretisation used in the evaluation of the warping function is adopted, in which each of the employed isoparametric quadratic elements has 4 gauss points. It is worth recalling that in the Timoshenko element only one gauss points in the length is used to avoid shear locking, while the formulation derived for the Bernoulli element is suitable for any number of Gauss points in the length. However, at least 2 gauss points should be used to properly approximate the displacement field. The general framework is valid for both the shell and the 3D beam elements, though different strain and stress components are involved in the computation.

Shell element

$$\epsilon = [\epsilon_x \quad \epsilon_y \quad 2\epsilon_{xy}]^T$$

$$\sigma = [\sigma_x \quad \sigma_y \quad \tau_{xy}]^T$$

3D beam element

$$\epsilon = [\epsilon_x \quad 2\epsilon_{xy} \quad 2\epsilon_{xz}]^T$$

$$\sigma = [\sigma_x \quad \tau_{xy} \quad \tau_{xz}]^T$$

(3.5)

$$\mathbf{C} = \frac{E_{a,\theta}}{(1-\nu^2)} \begin{bmatrix} 1 & \nu & 0 \\ \nu & 1 & 0 \\ 0 & 0 & \frac{(1-\nu)}{2} \end{bmatrix} \quad \mathbf{C} = E_{a,\theta} \begin{bmatrix} 1 & 0 & 0 \\ 0 & \frac{1}{2(1+\nu)} & 0 \\ 0 & 0 & \frac{1}{2(1+\nu)} \end{bmatrix}$$

\mathbf{C} is the elastic tangent operator, which depends on the Young modulus at elevated temperature $E_{a,\theta}$ obtained from (3.4). Since three strains and three stresses are involved, stresses cannot be directly determined from (3.2) and the concept of yield surface should be adopted. A Backward Euler scheme [59] is employed to solve the constitutive equations and obtain the quantities $\boldsymbol{\sigma}$ and \mathbf{C}_{ct} at each Gauss point. Usually, the Backward Euler scheme is implemented in an incremental form. Quantities $\boldsymbol{\sigma}$ and \mathbf{C}_{ct} at step $n+1$ are computed through an iterative procedure starting from the stress vector $\boldsymbol{\sigma}_n$ at step n , and from the strain increment $\Delta\boldsymbol{\varepsilon} = \boldsymbol{\varepsilon}_{n+1} - \boldsymbol{\varepsilon}_n$. Stresses respecting the material behaviour are located inside or lie on the yield surface. In this work, the yield surface of the material is defined according to an isotropic hardening model under plane stress condition and a Von Mises yield criterion and is described by the yield function f

$$f = \sigma_{eq} - \sigma_o(\varepsilon_{pl}) \quad (3.6)$$

The yield stress $\sigma_o(\varepsilon_{pl})$ is obtained from the plastic strain ε_{pl} while the equivalent stress σ_{eq} is determined from the stress vector $\boldsymbol{\sigma}$ (3.5)

Shell element

3D beam element

$$\sigma_{eq} = \sqrt{\sigma_x^2 + \sigma_y^2 + 3\tau_{xy}^2} \quad \sigma_{eq} = \sqrt{\sigma_x^2 + 3\tau_{xy}^2 + 3\tau_{xz}^2} \quad (3.7)$$

Detailed descriptions of the algorithm can be found in [54], [59].

3.2.1 Modified integration scheme

Two modifications are introduced into the classical stress integration procedure to account for the effects of temperature.

First, thermal expansion is considered in the strain vector $\boldsymbol{\varepsilon}$. Indeed, the total strain vector $\boldsymbol{\varepsilon}_{tot}$ of steel at the temperature θ_a consists of two terms

$$\boldsymbol{\varepsilon}_{tot}(\boldsymbol{\sigma}, \theta_a) = \boldsymbol{\varepsilon}_\sigma(\boldsymbol{\sigma}, \theta_a) + \boldsymbol{\varepsilon}_{th}(\theta_a) \quad (3.8)$$

where $\boldsymbol{\varepsilon}_\sigma$ is the stress-related strain and $\boldsymbol{\varepsilon}_{th}$ is the thermal strain vector. A further term due to the contribution of the transient creep strain $\boldsymbol{\varepsilon}_{cr}$ is implicitly considered in $\boldsymbol{\varepsilon}_\sigma(\boldsymbol{\sigma}, \theta_a)$ [83]. The strain $\boldsymbol{\varepsilon}$ associated to the mechanical response of the numerical model corresponds the stress-related strain $\boldsymbol{\varepsilon}_\sigma$, which should be determined from (3.8). The thermal strain $\boldsymbol{\varepsilon}_{th}$ has hydrostatic character and gives no contribution to the transverse strain components. Owing to the different definition of the strain $\boldsymbol{\varepsilon}$ for shell (2.18) and beam elements (2.30), the thermal strain assumes the following forms

Shell element

3D beam element

$$\boldsymbol{\varepsilon}_{th} = \varepsilon_{th}(\theta_a) [1 \ 1 \ 0]^T \quad \boldsymbol{\varepsilon}_{th} = \varepsilon_{th}(\theta_a) [1 \ 0 \ 0]^T \quad \varepsilon_{th}(\theta_a) = \Delta l/l \quad (3.9)$$

where $\varepsilon_{th}(\theta_a)$ is the uniaxial thermal strain, which can be determined from (3.1).

Second, the typical incremental form is not well-suited for stress integration at elevated temperature, especially if temperature varies during the analysis. In fact, as depicted in Figure 3.3a for a uniaxial stress-strain law, the converged stress σ_n has no physical meaning in respect to the stress-strain law associated to the temperature $\theta_{a,n+1}$ and thus, cannot be the starting point of stress integration at step $n + 1$. Consequently, an additional assumption is introduced. Let us define the plastic strain $\varepsilon_{pl,n}$ as the residual strain obtained when the stress σ_n is elastically unloaded to zero (Figure 3.3). According to [81], it can be assumed that the plastic strain remains unaffected during a change of temperature $\varepsilon_{pl,n+1} \approx \varepsilon_{pl,n}$. Thus, the stress σ_{n+1} at the step $n + 1$, lying on the stress-strain curve associated to the temperature $\theta_{a,n+1}$, can be evaluated from the plastic strain $\varepsilon_{pl,n}$ and from the strain ε_{n+1} . Once the stress $\sigma_{n+1} = \sigma_{n+1}(\varepsilon_{pl,n}, \varepsilon_{n+1})$ is determined, the plastic strain is updated for the new step with the actual plastic strain $\varepsilon_{pl,n+1}$.

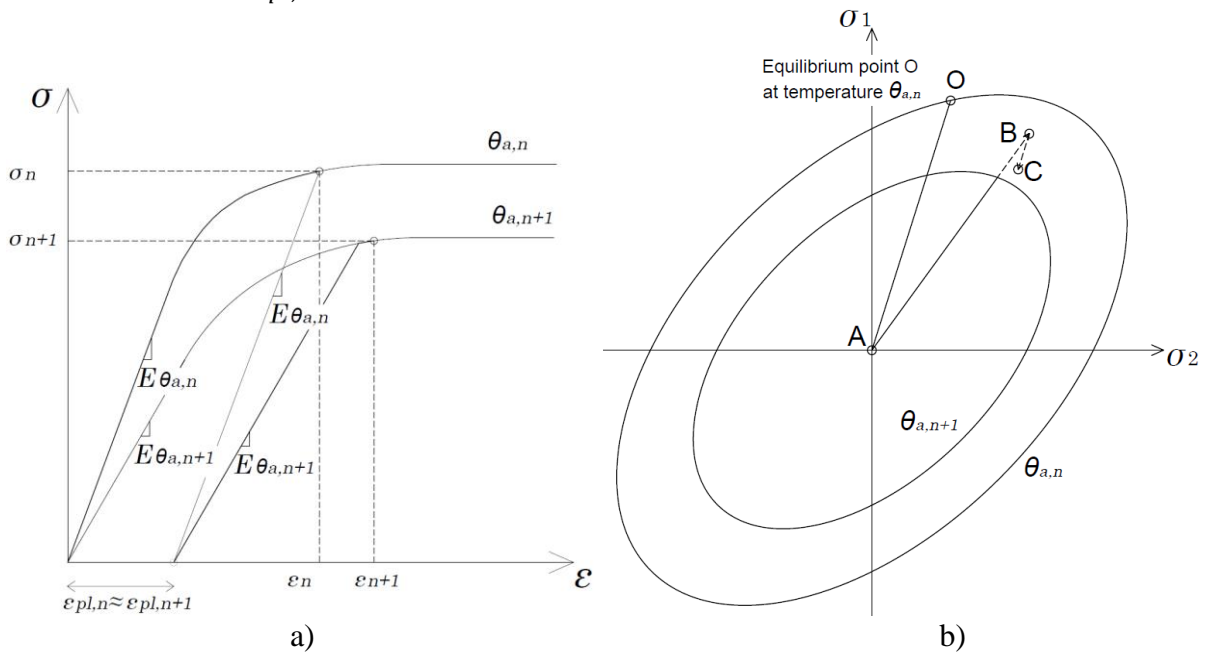


Figure 3.3 a) Uniaxial stress-strain law for temperatures $\theta_{a,n}$ and $\theta_{a,n+1}$ b) Modified Backward-Euler scheme

With the same perspective, the Backward Euler scheme is modified to calculate σ_{n+1} from the plastic strain $\varepsilon_{pl,n}$. Figure 3.3b shows the implemented procedure in the plane of principal stresses (σ_1, σ_2) , which can be obtained from the components of the stress vector σ (3.5). In detail, before a new step $n + 1$ is introduced, the converged stress configuration at the previous step (O) is unloaded to the point A. The residual plastic strain associated to configuration A is assumed to be unaffected by thermal increment from $\theta_{a,n}$ to $\theta_{a,n+1}$ and is used to determine the yield surface according to (3.6) and the uniaxial stress-strain relationship. The step $n + 1$ is then initialised introducing an elastic predictor (B). Backward-Euler iterations (C and further iterations) are applied until a new converged stress configuration and the associated $\varepsilon_{pl,n+1}$ are obtained. Further information about the implemented algorithm can be found in Paper I [76], [84].

3.2.2 Yield surface definition

In order to define the yield surface in the modified Backward-Euler scheme, the yield stress $\sigma_o(\varepsilon_{pl})$ in (3.6) should be defined explicitly and account for effects of temperature θ . The stress-strain relationship in (3.2) is rearranged and expressed as a function of ε_{pl} to directly compute the yield stress $\sigma_o(\varepsilon_{pl}, \theta)$ from the plastic strain ε_{pl} (Figure 3.4).

Stress $\sigma_o(\varepsilon_{pl}, \theta)$	Tangent stiffness $E_{t,\theta}$	
$f_{p,\theta}$	$E_{a,\theta}$	$\varepsilon_{pl} = 0$
$\left[Y + \sqrt{Y^2 - XZ} \right] / X$	$\frac{Y'}{X} + \frac{2YY' - XZ'}{2X\sqrt{Y^2 - XZ}}$	$0 < \varepsilon_{pl} \leq \varepsilon_{y,\theta} - \frac{f_{y,\theta}}{E_{a,\theta}}$
$f_{y,\theta}$	0	$\varepsilon_{y,\theta} - \frac{f_{y,\theta}}{E_{a,\theta}} < \varepsilon_{pl} \leq \varepsilon_{t,\theta} - \frac{f_{y,\theta}}{E_{a,\theta}}$ (3.10)
$\frac{f_{y,\theta}(\varepsilon_{u,\theta} - \varepsilon_{pl})}{\left(\varepsilon_{u,\theta} - \varepsilon_{t,\theta} + \frac{f_{y,\theta}}{E_{a,\theta}} \right)}$	$-\frac{f_{y,\theta}}{\left(\varepsilon_{u,\theta} - \varepsilon_{t,\theta} + \frac{f_{y,\theta}}{E_{a,\theta}} \right)}$	$\varepsilon_{t,\theta} - \frac{f_{y,\theta}}{E_{a,\theta}} < \varepsilon_{pl} \leq \varepsilon_{u,\theta}$

With

$$X = 1 + \frac{b^2}{a^2 E_{a,\theta}^2}$$

$$Y = f_{p,\theta} - c + \frac{b^2}{a^2 E_{a,\theta}} (\varepsilon_{y,\theta} - \varepsilon_{pl}) \quad Y' = -\frac{b^2}{a^2 E_{a,\theta}} \quad (3.11)$$

$$Z = (f_{p,\theta} - c)^2 - b^2 + \frac{b^2}{a^2} (\varepsilon_{y,\theta} - \varepsilon_{pl})^2 \quad Z' = -2 \frac{b^2}{a^2} (\varepsilon_{y,\theta} - \varepsilon_{pl})$$

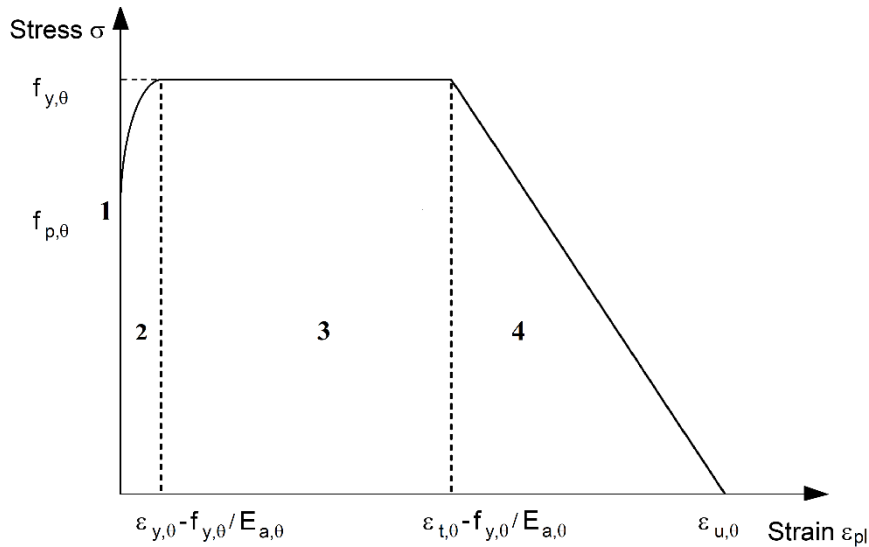


Figure 3.4 Reduction factors for the stress-strain law of carbon steel at elevated temperatures.

Chapter 4

Numerical simulation of steel structures in fire

Finite elements described in the previous chapters, as well as elements implemented in commercial software, have been employed in the investigation of several aspects of the behaviour of structures in fire. A detailed description of the principal outcomes of the research work is summarised in this chapter. In Paper I the derivation and the application of the shell finite element is presented and a branch-switching procedure for analysis at elevated temperature is provided. The buckling of compressed steel plates and steel columns is studied. Paper II focuses on the development and validation of the 3D beam finite element conceived for the analysis of steel members subject to torsional actions at elevated temperature. This element, as well as the shell element, are employed in a parametric analysis in Paper III, in which the torsional and flexural-torsional buckling of compressed built-up sections are investigated. Paper IV shows the context in which the thermomechanical finite elements are employed in the design of steel structures in accordance with Fire Safety Engineering principles.

4.1 Buckling of compressed steel plates and steel columns at elevated temperature (Paper I)

Numerical investigation of local or global buckling in thin-walled steel members is usually performed introducing perturbative forces or initial imperfections. In general, initial imperfections based on a preliminary linear buckling analysis provide accurate results at ambient temperature. However, in fire analyses the introduction of appropriate imperfection shape and amplitude may not be trivial owing to the effects of temperature. Indeed, when the temperature of a steel member increases the material mechanical properties degrade, and redistribution of the load may also occur. Thus, the buckling mode at elevated temperature may differ from the one at ambient temperature. Observations about the influence of different initial imperfection on single plates and on typical H steel columns at elevated temperature are presented based on numerical simulation. In addition, numerical analyses by means of an

alternative procedure, namely “Branch-switching”, are performed with the purpose of gaining a physical insight about the phenomenon of buckling of thin-walled steel members in fire.

The branch-switching procedure applies on perfect structures and thus, enables the numerical simulation of structural problems without the introduction of initial imperfections. Its application to elasto-plastic instability problems was proposed in [58]. The complete description of the physical behaviour of the structure is provided by detecting bifurcation points along the fundamental equilibrium path and then switching to the secondary path. The bifurcation point is detected by analysing the lowest eigenvalues w of the global stiffness matrix of the structure \mathbf{K}_g calculated at each converged solution. If one eigenvalue is negative it means that a critical point has been detected. One can find in the literature numerical procedures to determine whether the detected critical point is a bifurcation or a limit point. In practice, by looking at the displacement charts as function of temperature, it is easy to discriminate between a bifurcation and a limit point. The buckling mode of the structure associated to the bifurcation point is obtained as the eigenvector \mathbf{v} associated to the negative eigenvalue. In the new step of analysis $n + 1$, the first equilibrium point on the secondary path is searched according to the minimisation procedure developed by Petryk [85]. The procedure lies upon the fact that along a stable deformational path, the displacement vector of the structure \mathbf{d} corresponds to an absolute minimum of the functional J , where

$$J = \frac{1}{2} \mathbf{d}^T \mathbf{K}_g \mathbf{d} - \mathbf{d}^T \mathbf{f}_{ex} \quad (4.1)$$

\mathbf{f}_{ex} is the vector of external loads of the structure. In order to ensure that the minimisation procedure will not terminate on the fundamental path, a small perturbation vector is added to the usual predictor \mathbf{d}_{n+1} and a new predictor $\mathbf{d}_{n+1,BS}$ is defined

$$\mathbf{d}_{n+1,BS} = \mathbf{d}_{n+1} + \frac{\|\mathbf{d}_{n+1}\|}{100} \frac{\mathbf{v}}{\|\mathbf{v}\|} \quad (4.2)$$

The minimisation procedure consists then in solving at each iteration k the following nonlinear system

$$(\mathbf{K}_g^{(k)} + \beta \mathbf{I}) \Delta \mathbf{d} = -\mathbf{r}^{(k)} \quad (4.3)$$

$\mathbf{r}^{(k)}$ is the residual vector at iteration k and \mathbf{I} is the identity matrix, while $\Delta \mathbf{d}$ is the displacement increment obtained from previous iteration ($\Delta \mathbf{d} = \mathbf{d}_{n+1,BS}$ for $k=1$). β is a coefficient taken as 0 if $\mathbf{K}_g^{(k)}$ is definite positive and as $1.1 \min(w)$ otherwise, where w is the lowest eigenvalue of $\mathbf{K}_g^{(k)}$.

Elastic buckling of uniformly compressed simply supported plates at ambient temperature can be univocally determined in terms of both buckling load and buckling mode from the length-to-width ratio a/b of the plate. Figure 4.1 depicts the solution of the differential equations that govern the behaviour of plates that are simply supported on four sides. For instance, the expected buckling mode of a plate with $a=2250\text{mm}$ and $b=450\text{mm}$ ($a/b=5$) is characterised by 5 halfwaves ($n=1$; $m=5$). The initial geometrical imperfection based on the buckling mode and the elastic buckling load can be defined as follows

$$w(x, y) = w_o \sin\left(\frac{m\pi x}{a}\right) \sin\left(\frac{n\pi y}{b}\right) = w_o \sin\left(\frac{5\pi x}{a}\right) \sin\left(\frac{\pi y}{b}\right) \quad (4.4)$$

$$P_{buck,el} = k \frac{\pi^2 E}{12(1-\nu^2)} \left(\frac{t}{b}\right)^2 A = \frac{\pi^2 E}{3(1-\nu^2)} \left(\frac{t}{b}\right)^2 A \quad (4.5)$$

Where t is the thickness of the plate and $A = bt$ is the area of the cross-section of the plate. w_o is the imperfection amplitude, and k the parameter that determines the elastic buckling load magnitude. For $a/b=5$, k is equal to 4 (Figure 4.1).

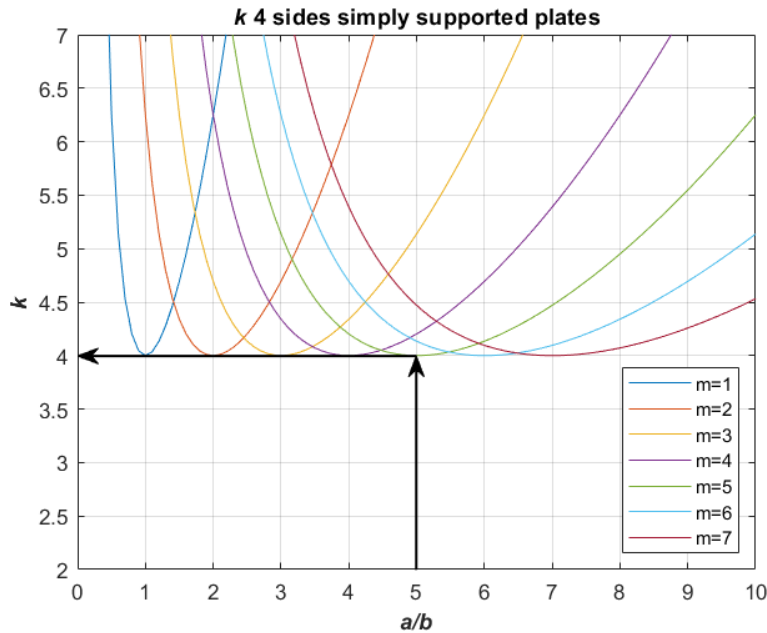


Figure 4.1 Buckling load factor k in respect to a/b and the buckling mode shape.

In principle, the buckling of the same plate uniformly heated at temperature θ_a should occur at $P_{buck,el}(\theta_a) = P_{buck,el}(E(\theta_a))$, in which the Young modulus E is reduced according to (3.4). This is confirmed by numerical analysis performed with shell models when the buckling of a perfect plate occurs in elasticity as shown in Figure 4.2. Indeed, the buckling mode associated to the first identified bifurcation point corresponds to the theoretical one, i.e. 5 halfwaves ($n=1$; $m=5$), as depicted in Figure 4.2a. In the shown case study, the thickness t is set to 8.5 mm and a uniform temperature of 200°C affects the plate in order to have buckling in elasticity. However, for $t=11\text{mm}$ and $\theta_a=500^\circ\text{C}$ the plate buckles in the plastic range and the numerical buckling mode at elevated temperature ($m=7$ in Figure 4.3a) is different from the expected one. In both case studies, the Young modulus of steel is defined as $E=210\text{GPa}$. Further interesting observations can be made by performing classical analyses with initial imperfections. For a very small imperfection amplitude ($w_o = 1e^{-3}\text{mm}$), the lowest maximum load P_{max} of the first plate is found for imperfections with the same number of half-waves as the one of the numerical buckling mode. However, for amplitudes of practical interest ($w_o=0.1t$; $w_o=b/200$) the lowest maximum load P_{max} is obtained for a number of halfwaves different from the expected one ($m=5$), as plasticity significantly affects the plate before buckling. In Figure 4.2b results of analyses with imperfections with a number of halfwaves m from 1 to 8 are presented, as well as the maximum load found in the analysis of the perfect structure with the branch-switching procedure. For the second plate, the number of halfwaves obtained from elastic theory ($m=5$) never gives the lowest buckling load, which is attained instead with 6 or 7 halfwaves (Figure 4.3b). It seems clear that the choice of an appropriate imperfection shape is not straightforward.

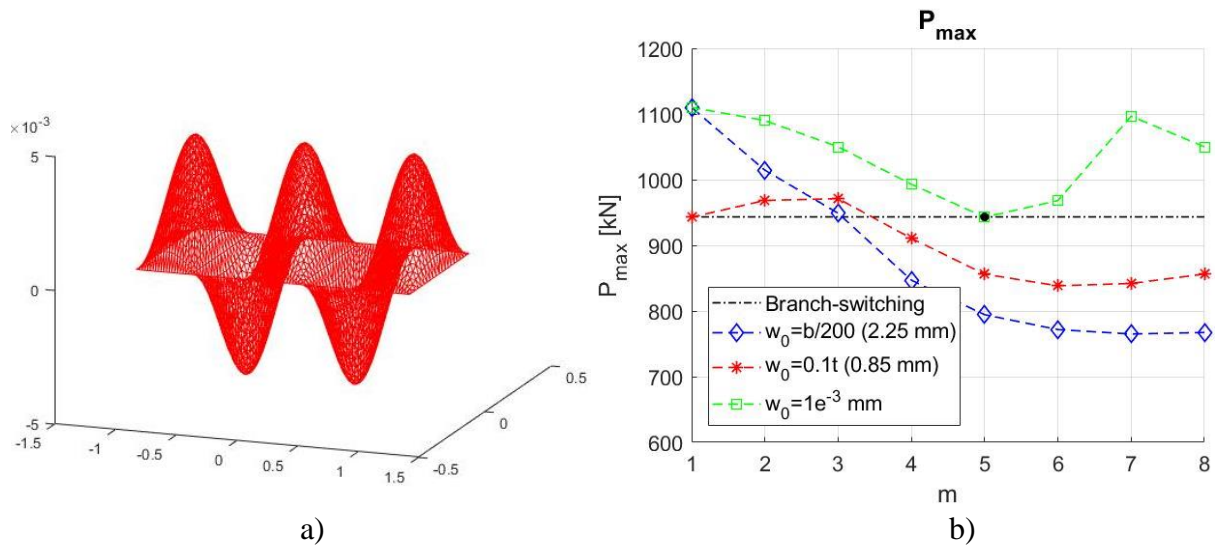


Figure 4.2 Plate buckling in elasticity a) Buckling mode b) Buckling and maximum loads

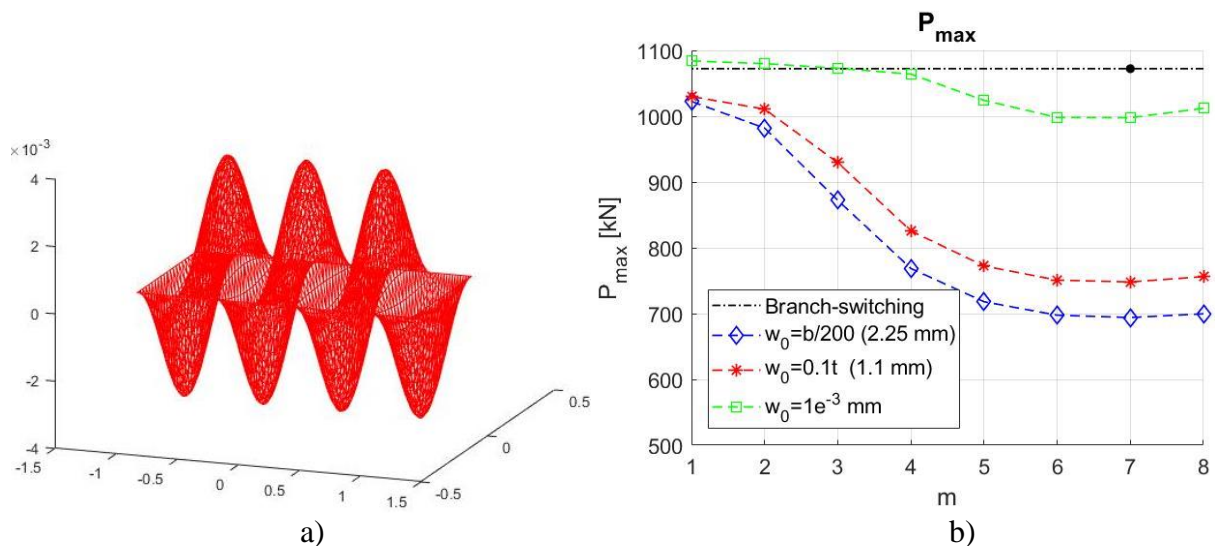


Figure 4.3 Plate buckling in plasticity a) Buckling mode b) Buckling and maximum loads

A typical approach to the investigation of structures in fire considers the structures subjected to constant loading, while the temperature inside the members increases. As a consequence, the investigation of columns subjected to a constant load, but increasing temperature may provide meaningful information. For unprotected columns, a uniform temperature distribution in the cross-section and along the column may be assumed. Branch-switching analysis of such columns might reveal that the buckling load at ambient temperature differs from the one obtained by checking the tangent stiffness at elevated temperature. Indeed, even if the member is uniformly heated, when plasticity occurs, the buckling mode at ambient temperature may be different from that at elevated temperature, due to the complexity of the tangent operator C_{ct} . As a matter of fact, the way in which components of C_{ct} degrade with temperature cannot be attributed only to the variation of the tangent modulus $E_{t,\theta}$. This is the case of the column depicted in Figure 4.4. The column consists of an HEA300 profile of 7m of length, loaded with a constant axial load of 1000kN. Figure 4.4a corresponds to the buckling mode obtained by means of a linear buckling analysis, while in Figure 4.4b is shown the buckling mode associated to the critical point found by increasing the temperature, identified at 594°C. It is interesting to note that conservative predictions are obtained

4.1 Buckling of compressed steel plates and steel columns at elevated temperature (Paper I)

introducing imperfections based on the buckling mode at elevated temperature (hot imperfection), as shown in Figure 4.5. In this figure, the evolution of the lateral displacement with temperature is depicted for analyses with the “hot” (Figure 4.4a) and the “cold” (Figure 4.4b) imperfection. Besides, the results indicate that small imperfections based on the buckling mode at ambient temperature (cold imperfection) might induce a different behaviour compared to the one obtained for perfect columns with the branch-switching analysis, possibly due to convergence problems in the numerical analyses.

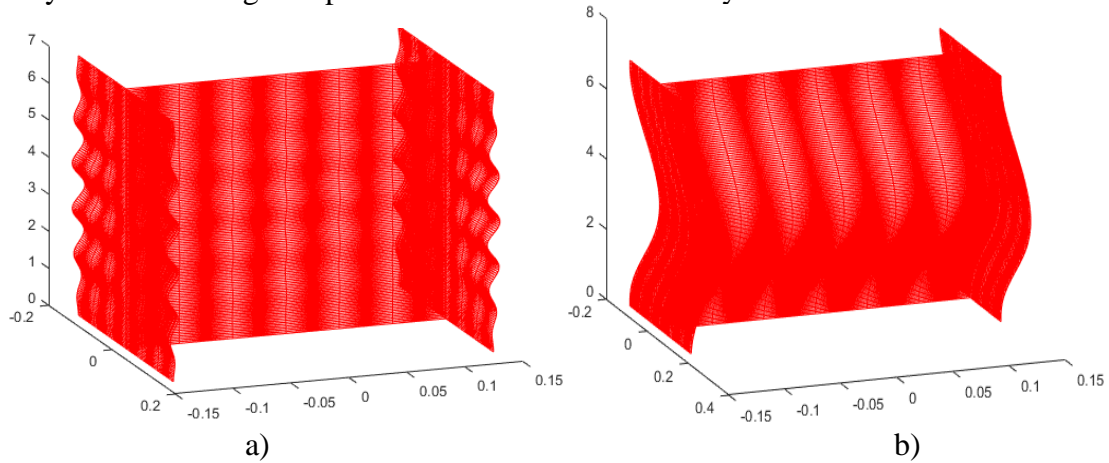


Figure 4.4 Buckling mode of a HEA300 column a) at ambient temperature b) at elevated temperature (594°C)

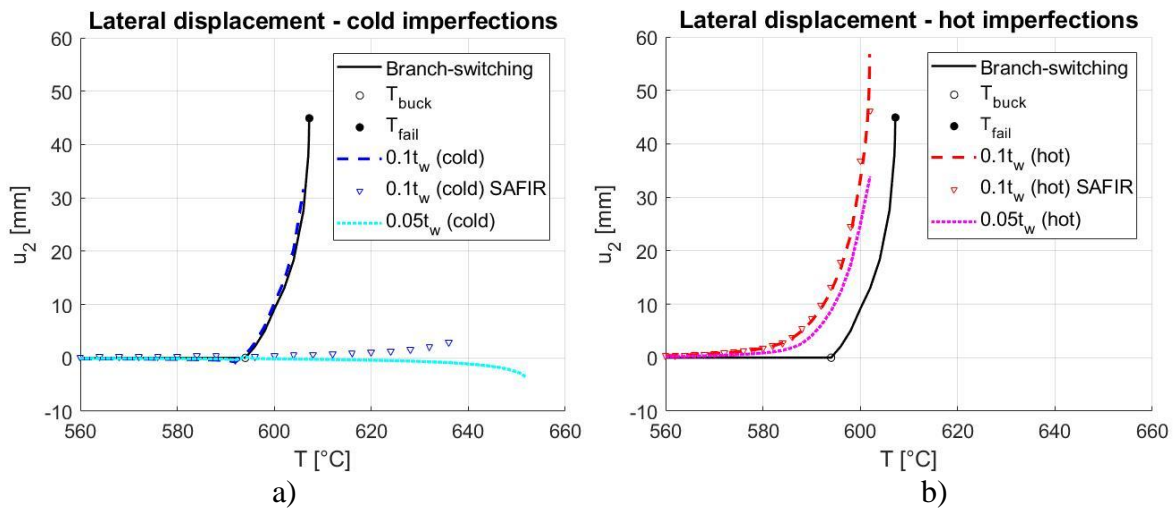


Figure 4.5 Lateral displacement vs. Temperature of a HEA300 column a) cold imperfections b) hot imperfections

In conclusion, the definition of the shape and the amplitude of initial geometrical imperfections for steel structures subjected to fire is not trivial. The branch-switching procedure provides an alternative to perform preliminary instability analyses and get important insight into the post-buckling behaviour. Since the perfect structure is studied, uncertainties related to the initial imperfections are removed.

4.2 Steel members subject to torsion at elevated temperature (Paper II)

Despite torsional effects are typically not predominant in steel structures in fire, some of the instability phenomena in steelworks are related to the torsional behaviour. For instance, in portal frames of industrial halls lateral-torsional buckling may occur in the steel rafters between discrete intermediate restraints. Torsion and lateral-torsional buckling should be carefully considered in industrial halls with inclined roof when the profiled steel roof cladding does not provide enough lateral and torsional restraint to the purlins, or when travelling cranes are present and the runaway beams are subjected to eccentric vertical and lateral horizontal actions relative to the shear centre.

Since for the solution of large structural problems shell elements entail a high computational demand, 3D beam elements should be preferred. Thermomechanical beam elements are implemented in several software: among the others, SAFIR [11], VULCAN [12], [13], ABAQUS [14], ANSYS [15] and DIANA [17] should be mentioned. However, often warping effects are not included or are not properly considered in the formulations of the implemented beam elements.

The 3D beam element proposed in Chapter 2 gives improved results compared to the ones from the 3D beam elements of two commercial software taken as reference, namely SAFIR and ABAQUS. In fact, the developed element is capable of better representing the behaviour of steel elements in fire subjected to torsional stresses. As warping is accounted in the formulation, the element is well-suited for the analysis of steel members with thin-walled open cross-sections. An extract of the validation of the element against shell analyses is proposed here, as well as a comparison of the performance of a Timoshenko and a Bernoulli formulation.

A cantilever steel beam subjected to significant torsional actions is depicted in Figure 4.6. The cantilever beam is subjected to a uniform increasing temperature and a constant load. As shown in Figure 4.7a, results from the developed corotational 3D beam element with a Timoshenko formulation (COR BEAM TIM) are in excellent agreement with the reference solution obtained by means of the corotational shell element (COR SHELL) described in Chapter 2. Instead, the 3D beam elements from the two commercial software do not give accurate results. The analysis performed employing the SAFIR 3D beam element (SAF BEAM) overestimates the failure temperature of about 105°C as the software SAFIR is not capable of updating the torsional stiffness with temperature. Nevertheless, also by reducing fictitiously the initial torsional stiffness (SAF BEAM_{RED}) as suggest by the software developer, the behaviour of the cantilever beam is not properly caught, though a better estimate of the failure temperature is obtained. The ABAQUS 3D beam element (ABQ BEAM) gives results that are close to the SAFIR element, but the analysis does not converge anymore at about 470°C. Timoshenko and Bernoulli formulations are compared in Figure 4.7b. Two integration points are employed in the Bernoulli formulation, while a one-point integration rule defines the Timoshenko element. Sufficiently accurate solutions were obtained with 10 elements. With only 5 elements the Bernoulli beam element provided a better solution, though not accurate enough yet, compared to the Timoshenko one. Nevertheless, the Timoshenko beam element requires less computational time because of the simpler integration rule, and its use should be preferred.

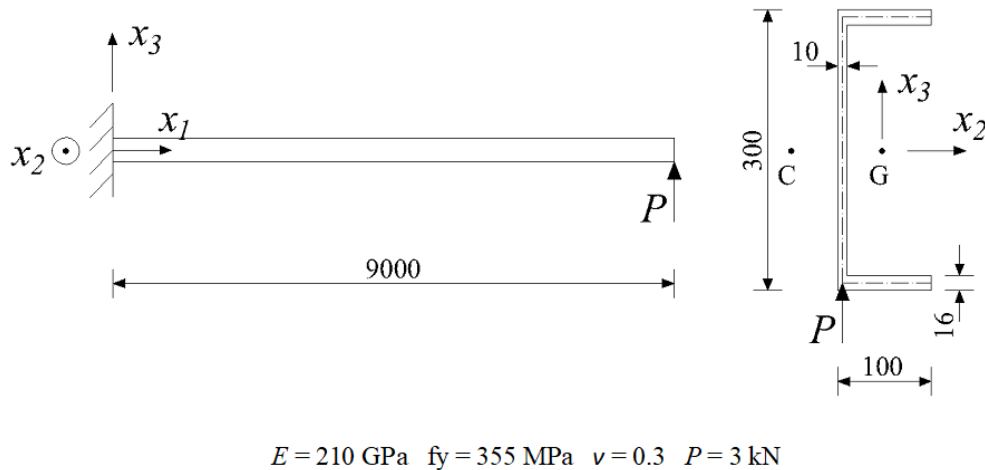


Figure 4.6 Cantilever beam with C-shaped cross-section. Dimensions in mm

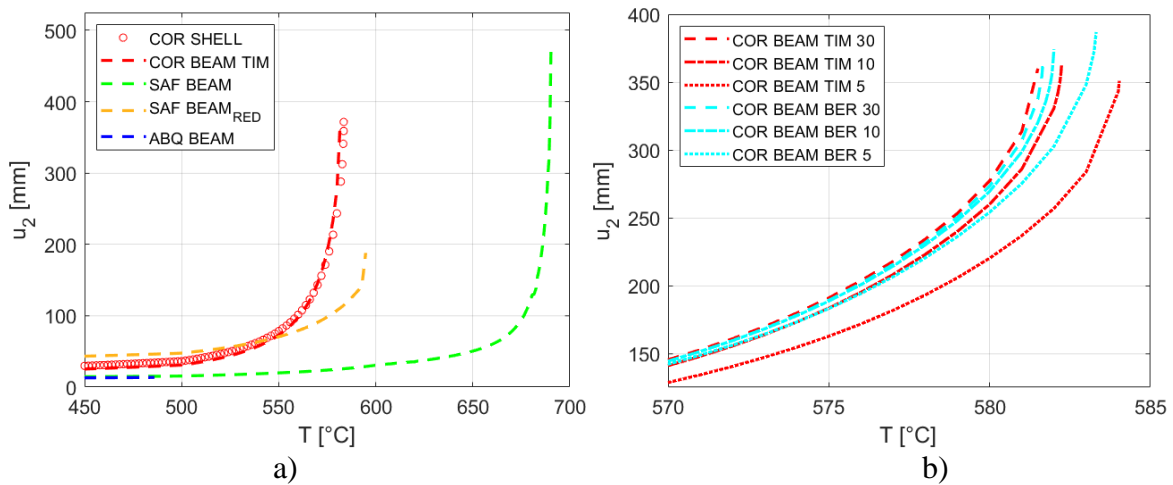


Figure 4.7 Cantilever beam - Lateral displacements a) 3D beam elements b) Timoshenko and Bernoulli formulations

The L-frame depicted in Figure 4.8 consisting of two I-shaped clamped steel members, is a good example for testing the numerical response of the 3D beam element for jointed structural members. In the proposed analysis, a vertical and an axial load are applied at the midspan of the horizontal member and are kept constant, while temperature is uniformly increased with linear heating rate equal to 2°C/min. To consider the continuity of the framing structure the out-of-plane displacement of the node at the intersection between beam and column is prevented in the beam model. Similarly, in the reference shell model the out-of-plane displacement at the intersection of the cross-section centroidal lines of the beam and the column is also prevented. In order to ensure consistency between the behaviour of the shell and the beam models, a complete and direct transmission of warping is obtained introducing a diagonal stiffener in the design of the structural joint (Figure 4.8). It follows that, the warping degree of freedom α (see (2.22)) has the same value in the two members at the common node ($\alpha_{Col} = \alpha_{Beam}$). Figure 4.9 shows that in the reference model lateral-torsional buckling affects the horizontal beam and that collapse occurs at 592°C. The beam element predictions (COR BEAM TIM) attain the reference solution (COR SHELL) with good precision, whereas both ABAQUS and SAFIR do not provide accurate predictions and the failure temperature is overestimated of about 25 °C (Figure 4.9b). Again, by reducing fictitiously the initial torsional stiffness (SAF BEAM_{RED}), a better estimate of the failure temperature is obtained,

but lateral displacement is significantly overestimated up to 580°C, since buckling occurs for a much lower temperature.

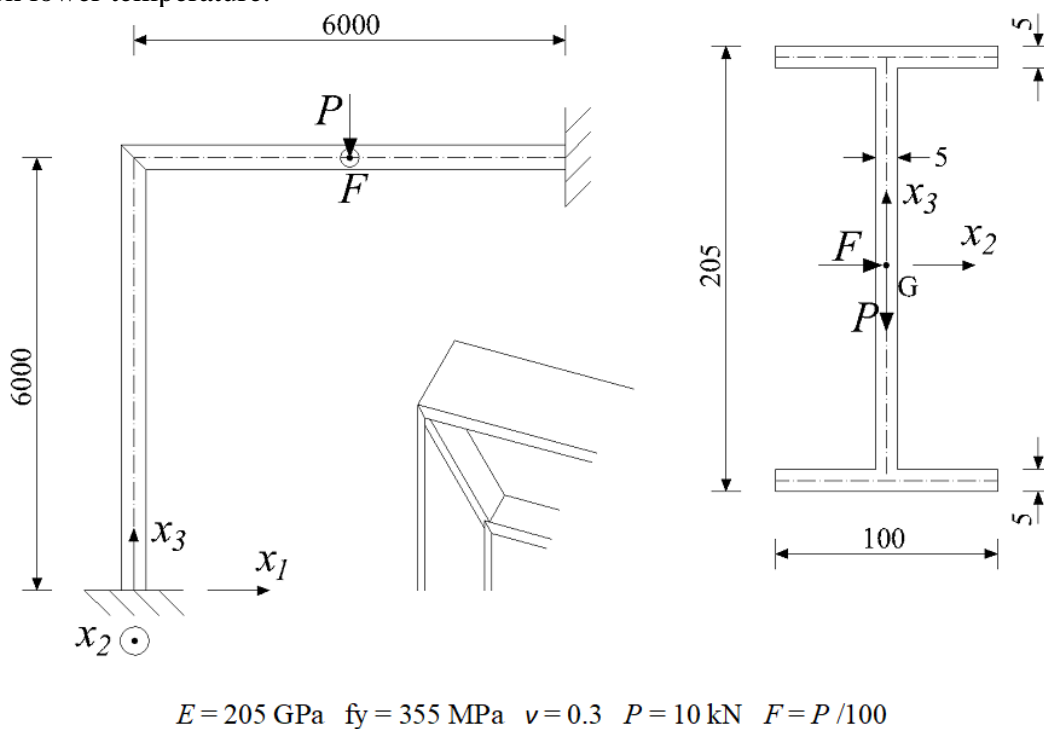


Figure 4.8 L-frame with I-shaped cross-section. Dimensions in mm

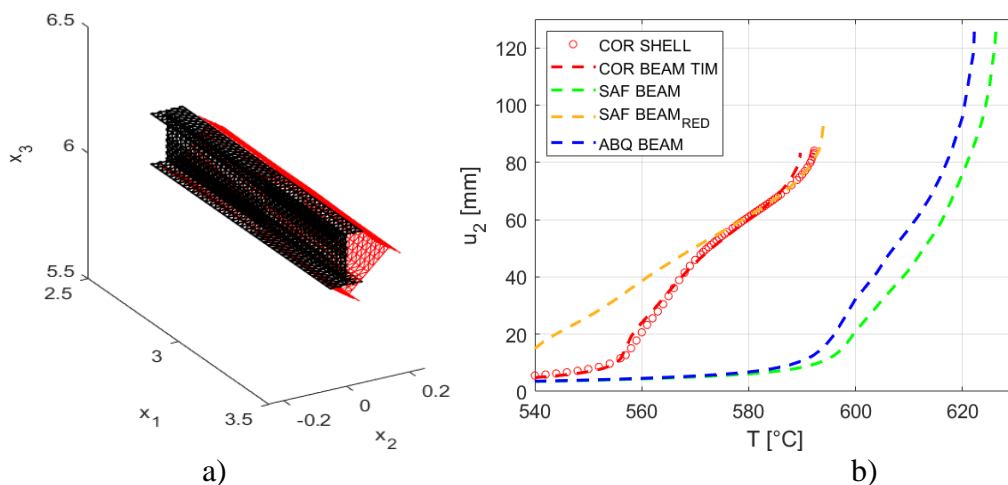


Figure 4.9 L-frame - a) Deformed shape of the loaded area at 592 °C: COR SHELL element – dimensions in [m] b) Lateral displacements

It turns out that an inconsistent formulation for torsion may lead to significant underestimation of the failure temperature also in typical steel structures, in which steel members are subjected only to vertical and lateral actions. This is the case of the steel structure depicted in Figure 4.10, in which the loads are constant, while the temperature in the central span of the continuous beam increases uniformly. The continuous beam belongs to the second floor of an eight-storey structure tested in Cardington (UK) in the mid '90s. Vertical loads are obtained for the critical combination at the Ultimate Limit State from [86], whereas lateral loads are determined as a fraction of the vertical ones. Since loads are transmitted from the centroid of the secondary beams (IPE360) to the primary beams and the secondary and primary beams have aligned top flanges, loads P and F are applied with an eccentricity of

+0.12m with respect to the centroid of the primary beam. Predictions from the developed and the SAFIR 3D beam elements differ of about 45°C, since SAFIR underestimates the torsional effects in the final part of the analysis for lateral forces F defined as either 10% or 1% of the vertical loads P (Figure 4.11). Again, after a while ABAQUS analyses are not able to converge and hence, they are not shown in Figure 4.11.

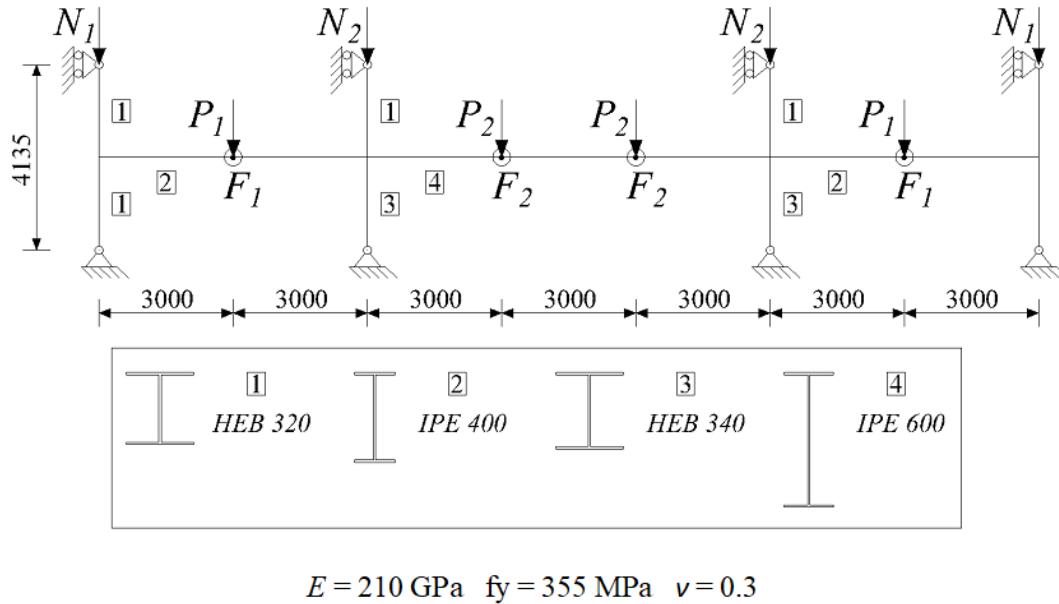


Figure 4.10 Cardington continuous beam. Dimensions in mm

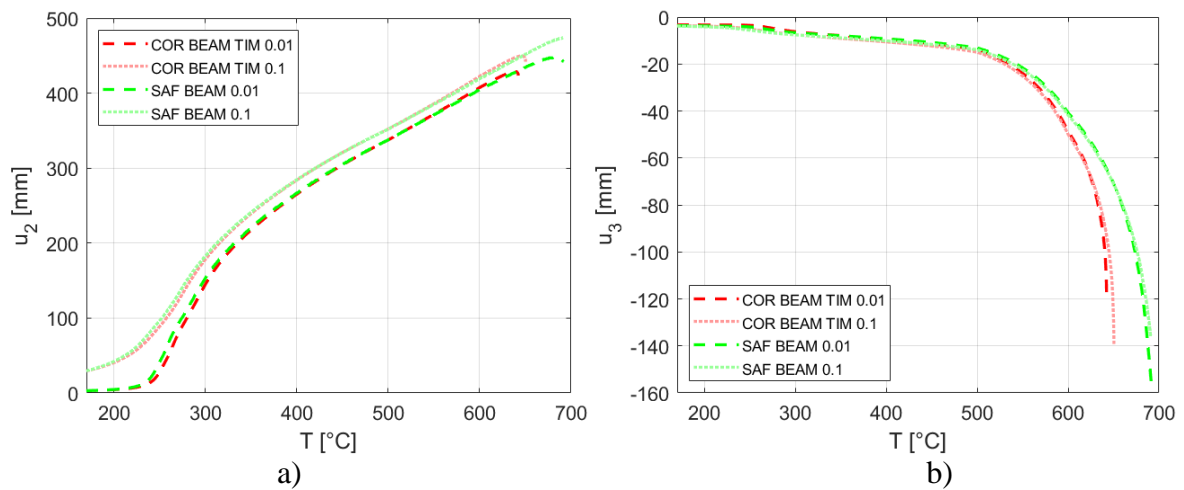


Figure 4.11 Cardington continuous beam - Comparison between 3D beam elements a) lateral displacements b) vertical displacements

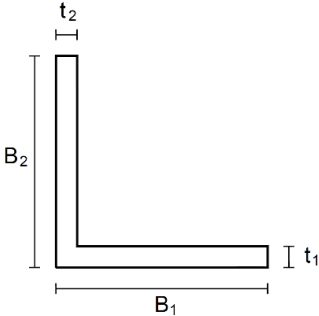
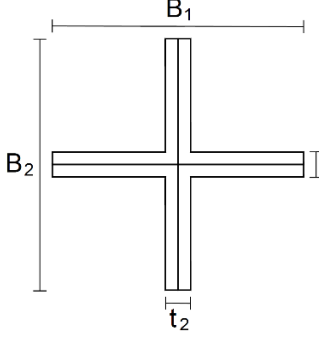
It should be mentioned, that if normal stresses contribute considerably to the element collapse, better predictions may be obtained by means of the commercial software. Nevertheless, in the presented case studies, in which torsional effects are predominant, commercial software do not provide reasonable estimate of the failure temperature.

4.3 Torsional and flexural-torsional buckling of steel members in fire (Paper III)

Torsional and flexural-torsional buckling of compressed steel members are relevant phenomena for mono-symmetric or cruciform cross-sections. Though these sections are frequently employed in bracing systems or in truss structures, there is a lack of knowledge about their behaviour in fire situation. In particular, no provisions are given in EN 1993-1-2 [19] about the torsional and flexural-torsional buckling behaviour of steel members in compression at elevated temperature. Furthermore, torsional and flexural-torsional buckling have mainly attracted the interest when the behaviour of cold-formed steel profiles at both ambient and elevated temperatures was concerned [40], [42]–[46], while hot rolled cross-sections were investigated only at ambient temperature [47], [87]–[90]. Hence, there is a paucity of studies about the torsional and flexural-torsional buckling at elevated temperatures of hot-rolled and welded steel sections.

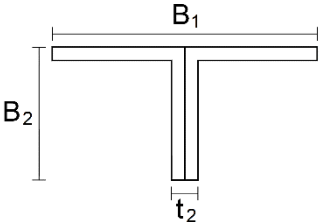
Numerical simulation by means of Finite Element Analysis (FEA) is a valid and reliable option to investigate the resistance of concentrically compressed members subjected to fire sensitive to torsional or flexural-torsional buckling. Results of a parametric study, consisting in more than 23500 geometrically and materially imperfect nonlinear analyses (GMNIA) carried out on concentrically compressed steel members are presented in this work. Either 3D beam or shell element models are employed in the analyses. The compressive resistance of Angle (L), Tee (T) and Cruciform (X) sections with different lengths is studied for Class 1 to Class 3 profiles. The class in fire situation is defined according to EN 1993-1-2 [19] and is provided for each investigated cross-section in Table 4.1-Table 4.3. T and X cross sections are obtained by coupling two or four L sections respectively. These sections are conservatively classified based on the classification of the single angular of which they are composed, since closely built-up sections are usually connected at discrete points along the member length. Single angles with equal legs in pure compression are essentially either of Class 1 or of Class 4. Class 4 cross-sections are not considered as they are affected by local buckling before the attainment of the yield stress [91] and a separate investigation is necessary. In order to present more comprehensive results, T section composed of both equal and unequal leg L sections are considered. The members are subjected to five uniform temperature distributions from 400°C to 800°C (400°C, 500°C, 600°C, 700°C, 800°C), since similarly to columns that buckle flexurally [20], this is the most relevant temperature range for practical cases. Steel with three different grades (S235, S275, S355) are employed in the analyses, while residual stresses are deemed negligible at elevated temperature, as assumed in many relevant publications about the resistance of steel members in fire [20], [27], [33], [44], [92]. To induce buckling, initial imperfections based on the relevant buckling mode obtained from linear buckling analyses are introduced with an amplitude of 1/1000 of the length of the columns.

Table 4.1: List of the cross-section dimensions for L and X profiles

Section	L section			X section			S235	S275	S355
	B ₁ (=B ₂) [m]	t ₁ (=t ₂) [m]	B ₁ /t ₁	B ₁ (=B ₂) [m]	t ₁ (=t ₂) [m]	B ₁ /t ₁			
	0.050	0.009	5.56	0.100	0.018	5.56		+	* ¹
	0.090	0.016	5.63	0.180	0.032	5.63	□ ¹	+	* ¹
	0.065	0.011	5.91	0.130	0.022	5.91			* ¹
	0.060	0.010	6.00	0.120	0.020	6.00		+	* ¹
	0.100	0.016	6.25	0.200	0.032	6.25	□ ¹	+	* ¹
	0.045	0.007	6.43	0.090	0.014	6.43		+	* ¹
	0.065	0.010	6.50	0.130	0.020	6.50		+	* ¹
	0.100	0.015	6.67	0.200	0.030	6.67	□ ¹	+	* ¹
	0.200	0.028	7.14	0.400	0.056	7.14		+	* ¹
	0.250	0.034	7.35	0.500	0.068	7.35		+	* ¹
	0.150	0.020	7.50	0.300	0.040	7.50	□ ¹		* ¹
	0.250	0.033	7.58	0.500	0.066	7.58		+	* ¹
	0.200	0.026	7.69	0.400	0.052	7.69	□ ¹	+	* ¹
	0.070	0.009	7.78	0.140	0.018	7.78		+	* ¹
	0.250	0.032	7.81	0.500	0.064	7.81			* ¹
	0.120	0.015	8.00	0.240	0.030	8.00	□ ¹	+	
	0.150	0.018	8.33	0.300	0.036	8.33	□ ¹	+	
	0.140	0.016	8.75	0.280	0.032	8.75	□ ¹	+	
	0.300	0.033	9.09	0.600	0.066	9.09	□ ¹		
	0.110	0.012	9.17	0.220	0.024	9.17	□ ¹		
	0.120	0.013	9.23	0.240	0.026	9.23	□ ¹		
	0.250	0.027	9.26	0.500	0.054	9.26	□ ¹		
	0.140	0.015	9.33	0.280	0.030	9.33			
	0.300	0.032	9.38	0.600	0.064	9.38	□ ²		
	0.160	0.017	9.41	0.320	0.034	9.41	□ ¹		
0.180	0.019	9.47	0.360	0.038	9.47	□ ¹			

Superscript = Class at elevated temperature [19]

Table 4.2: List of the cross-section dimensions for T profiles (coupled equal leg L profiles)

Section	B ₁ [m]	B ₂ [m]	t ₁ [m]	t ₂ [m]	B ₁ /t ₁	B ₂ /t ₂	S235	S275	S355
	0.100	0.050	0.009	0.018	11.11	2.78		+	* ¹
	0.180	0.090	0.016	0.032	11.25	2.81	□ ¹	+	* ¹
	0.130	0.065	0.011	0.022	11.82	2.95			* ¹
	0.120	0.060	0.010	0.020	12.00	3.00		+	* ¹
	0.200	0.100	0.016	0.032	12.50	3.13	□ ¹	+	* ¹

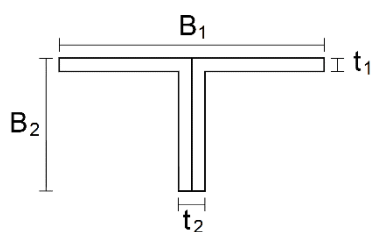
0.090	0.045	0.007	0.014	12.86	3.21		+ ¹	*1
0.130	0.065	0.010	0.020	13.00	3.25		+ ¹	*1
0.200	0.100	0.015	0.030	13.33	3.33	□ ¹	+ ¹	*1
0.400	0.200	0.028	0.056	14.29	3.57		+ ¹	*1
0.500	0.250	0.034	0.068	14.71	3.68		+ ¹	*1
0.300	0.150	0.020	0.040	15.00	3.75	□ ¹		*1
0.500	0.250	0.033	0.066	15.15	3.79		+ ¹	*1
0.400	0.200	0.026	0.052	15.38	3.85	□ ¹	+ ¹	*1
0.140	0.070	0.009	0.018	15.56	3.89		+ ¹	*1
0.500	0.250	0.032	0.064	15.63	3.91			*1
0.240	0.120	0.015	0.030	16.00	4.00	□ ¹	+ ¹	
0.300	0.150	0.018	0.036	16.67	4.17	□ ¹	+ ¹	
0.280	0.140	0.016	0.032	17.50	4.38	□ ¹	+ ¹	
0.600	0.300	0.033	0.066	18.18	4.55	□ ¹		
0.220	0.110	0.012	0.024	18.33	4.58	□ ¹		
0.240	0.120	0.013	0.026	18.46	4.62	□ ¹		
0.500	0.250	0.027	0.054	18.52	4.63	□ ¹		
0.280	0.140	0.015	0.030	18.67	4.67			
0.600	0.300	0.032	0.064	18.75	4.69	□ ²		
0.320	0.160	0.017	0.034	18.82	4.71	□ ¹		
0.360	0.180	0.019	0.038	18.95	4.74	□ ¹		

Superscript = Class at elevated temperature [19]

Table 4.3: List of the cross-section dimensions for T profiles (coupled unequal leg L profiles)

Section	B ₁ [m]	B ₂ [m]	t ₁ [m]	t ₂ [m]	B ₁ /t ₁	B ₂ /t ₂	S 235	S 275	S 355
	0.100	0.130	0.009	0.018	11.11	7.22	□ ³		
	0.100	0.130	0.010	0.020	10.00	6.50	□ ²	+ ³	
	0.100	0.130	0.012	0.024	8.33	5.42	□ ¹	+ ¹	*2
	0.110	0.140	0.010	0.020	11.00	7.00	□ ³	+ ³	
	0.110	0.140	0.012	0.024	9.17	5.83	□ ¹	+ ²	*3
	0.120	0.160	0.012	0.024	10.00	6.67	□ ²	+ ³	
	0.130	0.180	0.012	0.024	10.83	7.50	□ ³		
	0.130	0.180	0.014	0.028	9.29	6.43	□ ¹	+ ²	*3
	0.140	0.180	0.012	0.024	11.67	7.50	□ ³		
	0.140	0.180	0.014	0.028	10.00	6.43	□ ²	+ ³	
	0.150	0.200	0.014	0.028	10.71	7.14	□ ³	+ ³	
	0.200	0.200	0.016	0.032	12.50	6.25	□ ³		

Superscript = Class at elevated temperature [19]



In order to provide meaningful observations, results are presented in the form of the buckling coefficient in the fire design situation χ_{fi} , which is obtained as the ratio between the failure load and the yielding load at elevated temperature $\chi_{fi} = N/N_{yield}$. Numerical outcomes are compared with the prediction from the actual design curve of EN 1993-1-2 [19] and with the ones obtained for a new proposed buckling curve, as shown for L sections with a steel grade of 235MPa in Figure 4.12a. Detailed information about the definition of the actual design curve and the proposed one can be found in Paper III [93]. For sake of clarity, it is sufficient to remark that the results and predictions of the buckling coefficient χ_{fi} are expressed in respect to the slenderness at elevated temperature of the columns $\bar{\lambda}_\theta = \bar{\lambda}[k_{y,\theta}/k_{E,\theta}]^{0.5}$, where $k_{y,\theta}$ and $k_{E,\theta}$ are the reduction factors for the yield strength and Young's modulus at temperature θ_a and $\bar{\lambda}$ is the slenderness at ambient temperature, in turn defined as

$$\bar{\lambda} = \bar{\lambda}_{cr} = \sqrt{\frac{Af_y}{N_{cr}}} \quad (4.6)$$

With A the area of the section and f_y the yield stress at ambient temperature. N_{cr} should be the lowest elastic critical load at ambient temperature, which may be associated to a torsional, flexural-torsional or flexural buckling mode. However, it was found that an improved buckling curve can be obtained by replacing the critical buckling load N_{cr} in (4.6) with the lowest elastic flexural buckling load $\min(N_{cr,y}, N_{cr,z})$. Indeed, since the length of the column l is not well represented by the non-dimensional slenderness $\bar{\lambda}$ associated to the relevant buckling mode, a better representation of the length range is obtained referring to the non-dimensional flexural slenderness of the column. The proposed buckling curve is based on the same framework of [19] and [91], but differs in the definition of the generalised imperfection factor η .

$$\chi_{fi} = 1 \quad \bar{\lambda}_\theta \leq \bar{\lambda}_0$$

$$\chi_{fi} = \frac{1}{\varphi_\theta + \sqrt{\varphi_\theta^2 - \bar{\lambda}_\theta^2}} \quad \bar{\lambda}_\theta > \bar{\lambda}_0 \quad (4.7)$$

$$\varphi_\theta = \frac{1}{2} \left[1 + \eta + \bar{\lambda}_\theta^2 \right] \quad \text{with } \eta = \eta_{PROP} = \frac{\alpha}{\bar{\lambda}_\theta^\gamma} \left(\bar{\lambda}_\theta - \frac{\bar{\lambda}_0^2}{\bar{\lambda}_\theta} \right)$$

According to [19], the imperfection factor α is defined as follows

$$\alpha = \beta \sqrt{235/f_y}; \quad \beta = 0.65 \quad (4.8)$$

The calibration of the buckling curve is based on the numerical results. The selected values for the parameters β , γ and $\bar{\lambda}_0$ are reported in Table 4.4.

Table 4.4: Parameter values for the proposed buckling curve

	L	T	T (unequal)	X
β	1.00	1.25	1.10	0.85
γ	0.50	0.80	0.50	0.35
$\bar{\lambda}_0$	0.15	0.22	0.20	0.20

Safer predictions are obtained with the proposed buckling curve, as shown for the L section and all the investigated steel grades in Figure 4.12b.

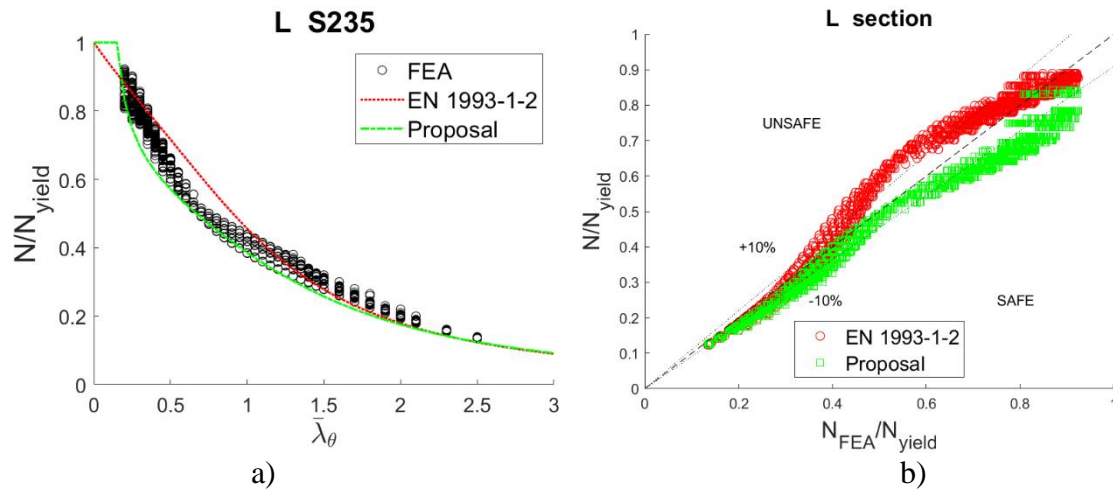


Figure 4.12 L sections a) Buckling curves for S235 b) Numerical vs. design resistance

The definition of the generalised imperfection factor η plays a key role in the derivation of the buckling curve. The effectiveness of the chosen formulation can be highlighted by comparing η_{PROP} and $\eta_{EN\ 1993\ 1-2} = \alpha \bar{\lambda}_\theta$ with an equivalent generalised imperfection factor obtained for numerical results η_{NUM} . The latter can be defined observing that the framework given in (4.7) comes from the following equation

$$\chi_{fi} + \eta \frac{\chi_{fi}}{1 - \chi_{fi} \bar{\lambda}_\theta^2} = 1 \quad (4.9)$$

Substituting the reduction factor at elevated temperature χ_{fi} with the one obtained from finite element analysis $\chi_{fi,FEA} = N_{FEA}/N_{yield}$, the imperfection factor η_{NUM} is obtained as

$$\eta_{NUM} = \left(\frac{1}{\chi_{fi,FEA}} - 1 \right) \left(1 - \chi_{fi,FEA} \bar{\lambda}_\theta^2 \right) \quad (4.10)$$

Comparison is proposed in Figure 4.13 for L sections with a steel grade of 235MPa. Conservatively, η_{NUM} was calculated for the lower boundary of FEA. The lower boundary was determined from the envelope of the finite element outcomes in Figure 4.12a. The proposed generalised imperfection factor reproduces with good accuracy the numerical one for slenderness up to $\bar{\lambda}_\theta = 1$. Though for $\bar{\lambda}_\theta > 1$ the numerical imperfection factor is overestimated by the proposal, the estimate of the buckling coefficient χ_{fi} is still good, as shown in Figure 4.13. Indeed, the higher the slenderness, the more the term $\bar{\lambda}_\theta^2$ becomes predominant in the definition of φ_θ in (4.7) and the contribution of η to χ_{fi} is less important.

The numerical results and the design curve predictions are compared for all the section types in Figure 4.14a. A Statistical investigation assuming a normal distribution for the predictions is depicted in Figure 4.14b. Considering safe the predictions for which $N/N_{FEA} \leq 1$, the proposed buckling curve attains a 97% probability of safe results.

Statistical investigation performed separately on each cross-section type can be found in Paper III [93]. The probability of non-exceedance of the safe-unsafe limit for L, T and X sections is reported in brief in Figure 4.15.

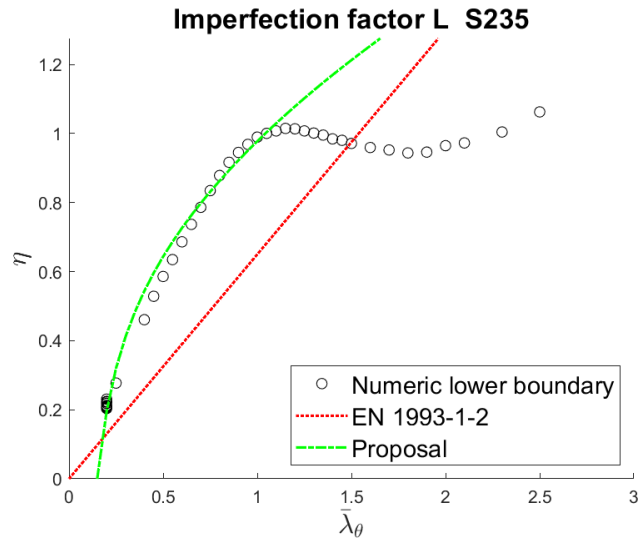


Figure 4.13 Generalised imperfection factors comparison

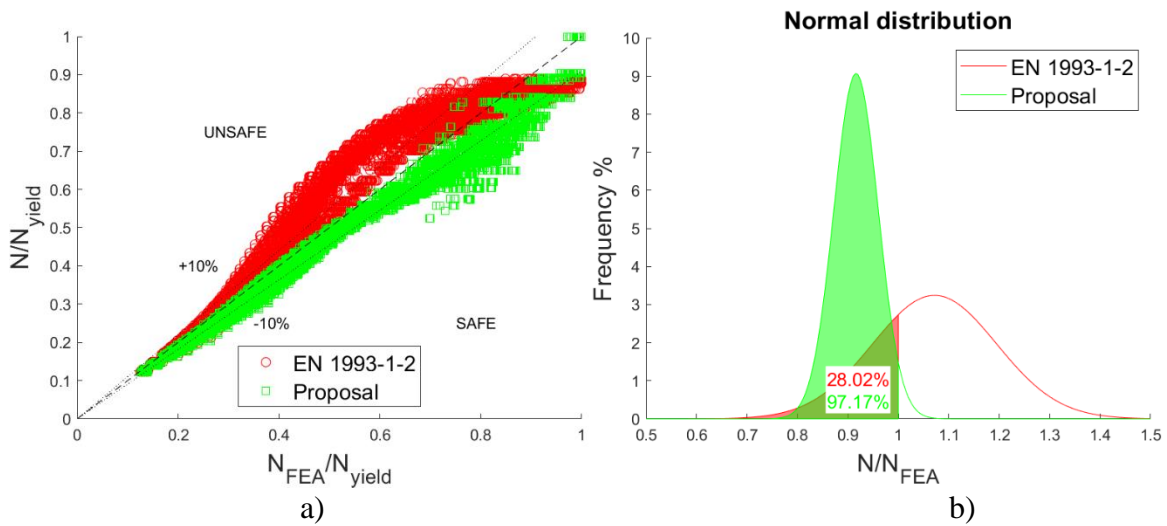


Figure 4.14 a) Numerical vs. design resistance b) Statistical investigation

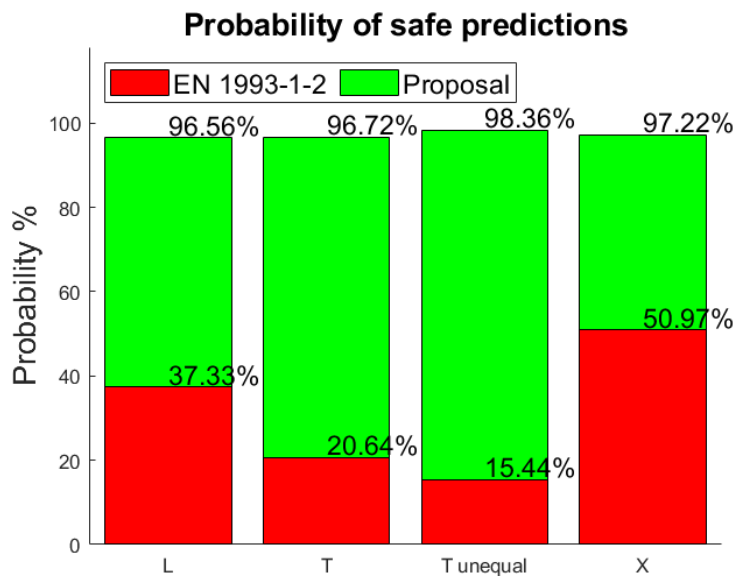


Figure 4.15 Probability of safe predictions

4.4 Fire Safety Engineering principles applied on a multi-storey steel building (Paper IV)

To better understand the relevance of the developed finite elements, it is necessary to look at the bigger picture and show the context in which thermomechanical finite elements may be employed in the design practice. Therefore, the application of Fire Safety Engineering principles to a building is proposed here.

Unwanted fire spread inside buildings may have catastrophic consequences both in terms of casualties and economical losses. Fire safety is paramount as a fundamental requirement of design, construction and operation. As an alternative to the prescriptive approach, Fire safety requirements may be satisfied with the Performance-Based Fire Engineering approach, also known as Fire Safety Engineering (FSE). An exhaustive application of FSE principles on the design of a building requires the investigation of the performance of a structure in a range of various fire scenarios. Since the number of possible fire scenarios may be very large, relevant fire scenarios may be identified through risk-ranking process performing a quantitative Fire Risk Assessment with an event tree analysis.

A floor of a typical steel-framed 15 storey office building is analysed (Figure 4.16). The steel moment resisting frame was designed in Japan and is outlined in ISO/TR 24679-4 [94]. The floor consists of two office rooms (XX01 and XX02), separated by a partition wall that is not fire-rated, whilst in order to prevent fire spread the offices are separated from the corridor by an EI 60 fire-rated partition.

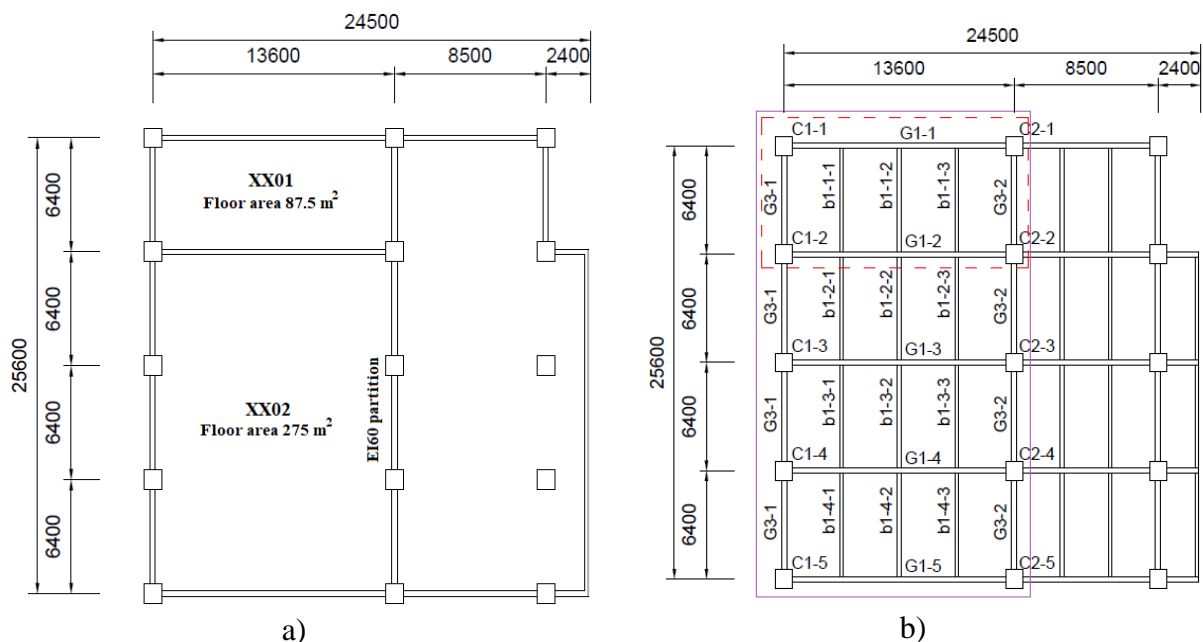


Figure 4.16 a) Typical floor b) Steelwork layout

Two relevant fire scenarios, i.e. SS7a and SS7b, that are also severe for the structures, are identified according to the event tree analysis in Figure 4.17. The two scenarios with the highest risk (R), defined as the product between probability of occurrence (P) and consequences (C), were selected. The probability of occurrence is estimated according to data found in literature [95]. The consequences are defined following the German guidelines "Leitfaden Ingenieurmethoden des Brandschutzes" [96] that suggest to estimate the damaged

4.4 Fire Safety Engineering principles applied on a multi-storey steel building (Paper IV)

area based on a quantitative analysis, i.e. dividing the expected damaged area by the total area of the building. The SS7a scenario considers the fire only in the XX01 compartment by assuming that the wall between compartment XX01 and XX02, even though not fire resistant, provides a barrier. A fire on the XX01+XX02 surface is considered in the SS7b scenario, assuming that the wall between the two compartments does not provide an effective fire barrier.

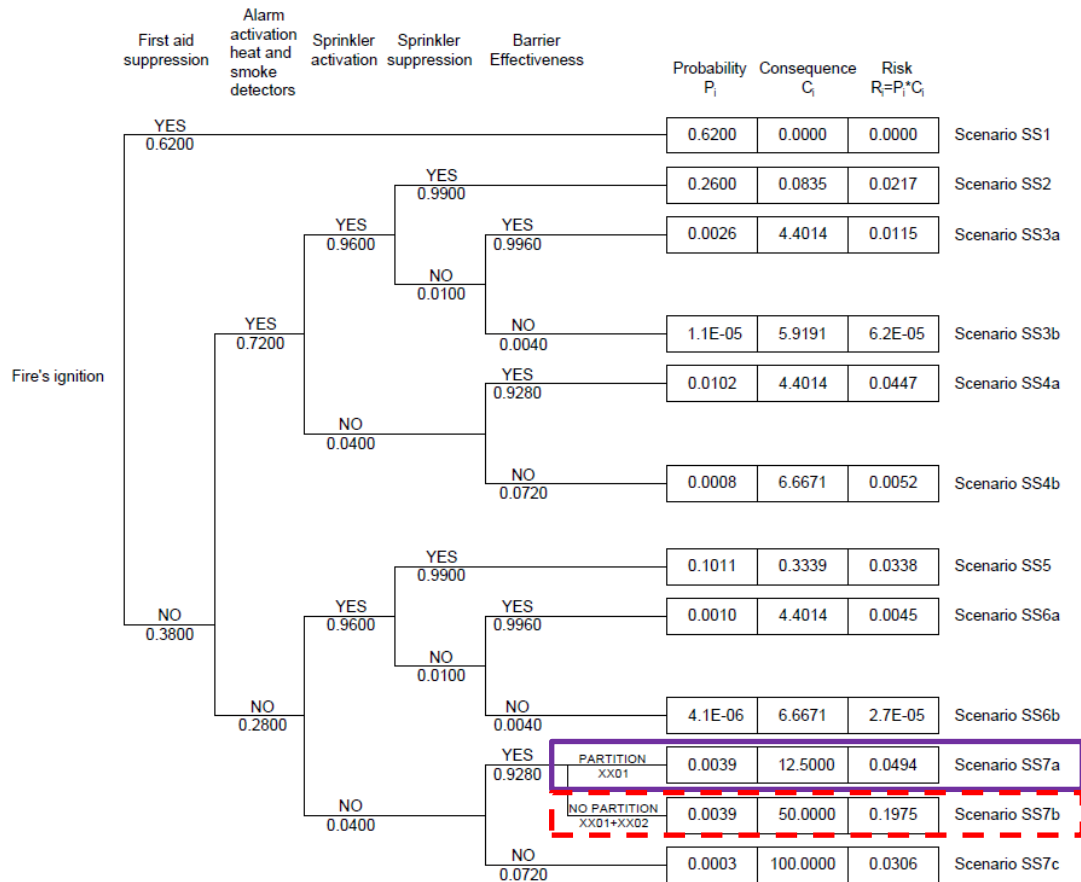


Figure 4.17 Event tree analysis

The fire development is modelled with different methods and software and is characterised by two rate of heat release (RHR) for an office occupancy and a fire distributed in the whole compartment. Zone models, namely Ozone v3.0.3 [97] and CFAST [98], and the computational fluid dynamics (CFD) software Fire Dynamics Simulator (FDS) v7 [99] are employed. OZone provides only one mean temperature of the gas in the hot zone. In the CFAST analysis, the fire drives combustion products from the lower to the upper layer via the plume. The temperature within each layer is uniform and a variation of temperature is found only in the height of the compartment. FDS simulation allow for recording temperatures at different locations inside the compartment. Indeed, by means of Adiabatic Surface Temperatures (AST) devices, significant temperature variations are registered in all the directions. The AST devices provide the maximum achievable solid surface temperature at the given location and can be directly used as boundary condition to perform the thermal analysis. For explicative purpose, the temperature distribution after 50 min at the ceiling level is depicted in Figure 4.18 for the SS7b fire scenario.

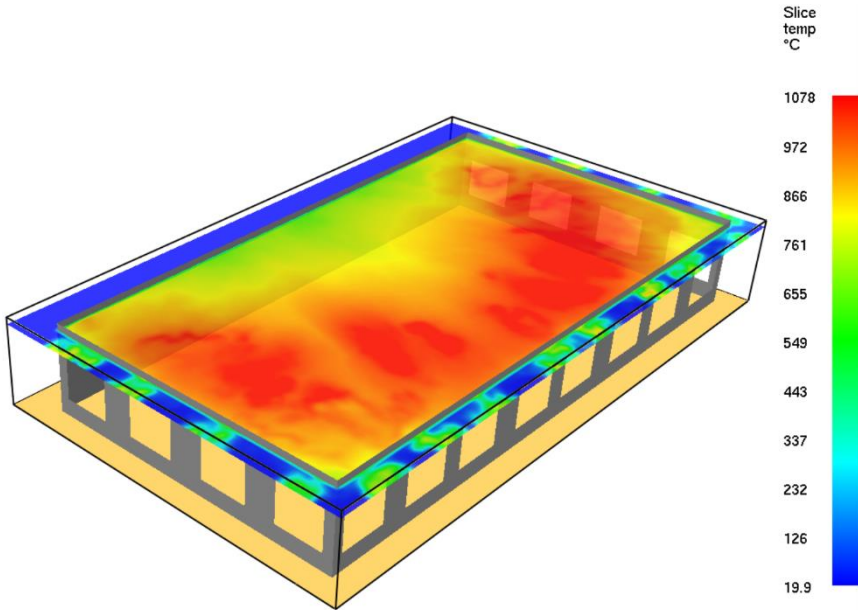


Figure 4.18 Temperature distribution at the ceiling level in scenario SS7b scenario after 50 min

A comparison of the gas temperatures from the different fire development analyses is proposed in Figure 4.19. The temperature evolution according to the nominal fire curve ISO834 is given as well. Both average (CFAST AVG) and peak temperatures (CFAST MAX) are registered in the CFAST analyses. Good agreement is found between the analyses based on the zone models and FDS for both peak and average gas temperatures.

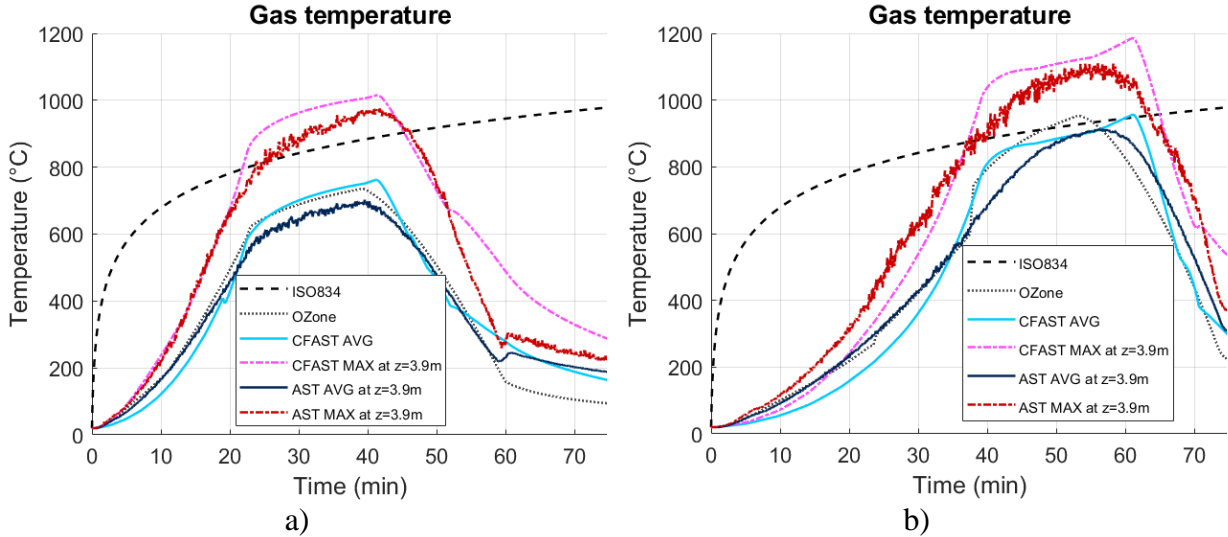


Figure 4.19 Gas temperature comparison: a) SS7a scenario b) SS7b scenario

The gas temperatures obtained from the fire development analyses are employed as boundary conditions in thermal analyses. Such analyses give the temperatures inside the structural elements, i.e. steel columns, beams and concrete slabs, and are modelled in the software SAFIR [11]. Once the thermal response of the structure is obtained, a thermomechanical analysis is performed by means of the same software. The simulation process is outlined in Figure 4.20.

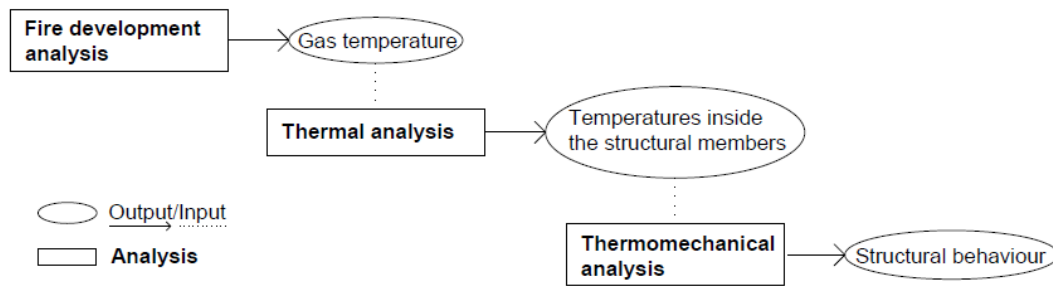


Figure 4.20 Numerical simulation process

In conclusion, the following thermomechanical analyses are performed and compared:

1. Compartment subjected to the ISO 834.
2. Compartment subjected to the temperatures obtained in Ozone
3. Compartment subjected to the average temperatures of the hot zone obtained in CFAST (CFAST AVG)
4. Compartment subjected to the maximum temperatures at the ceiling level obtained in CFAST (CFAST MAX)
5. Compartment subjected to the temperatures obtained from the AST in FDS

For each of the 1-4 analyses, only one temperature evolution is applied as boundary condition to all the structural elements. Instead, in the analysis 5 the temperatures registered by 45 and 180 AST devices are employed for the SS7a and SS7b scenarios respectively. The failure times of the different analyses are summarised in Table 4.5. Though not considered in Paper IV, the results obtained based on the gas temperatures from the nominal curve ISO834 are presented as well in Table 4.5. A more comprehensive discussion of the numerical models and the structural behaviour can be found in the same paper.

Table 4.5: Failure time

Failure time t_{fail}					
	ISO834	OZone	CFAST AVG	CFAST MAX	AST
SS7a	52 min	60 min	59 min	38 min	63 min
SS7b	19 min	44 min	44 min	39 min	44 min

Failure always occurs in the steel beams. Indeed, columns are not critical because designed to withstand seismic actions and temperature variations in the cross-sections are not as important as in beams. Hence, as partial or total collapse is generally triggered by column failure, the consequence estimates of 12.5% and 50% assigned to the selected fire scenarios might be overestimated. The employment of AST as boundary condition for the thermal analysis of the structural elements provides sound results, but the process is particularly time consuming. Comparable failure times are found when the AST temperatures and both the OZone and the CFAST average temperatures of the hot zone are employed. Moreover, these analyses exhibit an almost identical structural behaviour. On the contrary, the CFAST maximum temperatures at the ceiling level, as well as the ISO834 gas temperature lead to overconservative results and are thus not recommended. As a final remark, depending on the scope of the numerical investigation, natural fire scenarios might provide sufficiently accurate predictions, whilst the use of CFD models would be rather beneficial for the analysis of the effect on structures of fires in large compartments, e.g. localised fires.

Chapter 5

Conclusions and further research

In this Chapter, the main conclusions of the research work are summarised and some indications for future research are outlined.

5.1 Conclusions

This thesis presents the derivation and the application of thermomechanical finite elements for the analysis of steel structures in fire. The first part of the research work has been devoted to the development of a shell and a 3D beam finite element. Practical applications of these elements have been studied, paying particular attention to the buckling of steel members. All the conclusions are based on numerical simulation, performed mainly by means of the following numerical findings, developed in the context of the research work:

- A thermomechanical shell finite element suitable for the analysis of steel structures in fire (Chapter 2 and Chapter 3 – Paper I).
- A thermomechanical 3D beam finite element that properly accounts for torsion and warping in steel members at elevated temperatures (Chapter 2 and Chapter 3 – Paper II).
- A branch-switching procedure to perform preliminary instability analyses and get important insight into the post-buckling behaviour of steel structures subjected to fire (Chapter 4 - Paper I).

The main conclusions from the 4 papers are listed hereafter.

Paper I

- Buckling modes at elevated temperature cannot be determined by a linear elastic buckling analysis at ambient temperature.

- For single plates, the evaluation of the maximum load P_{max} and the overall physical behaviour are affected by the choice of the number of half-waves of the initial imperfection. The definition of the shape and the amplitude for the imperfections is not trivial.
- The branch-switching procedure can be employed to perform preliminary instability analyses and to get important insight into the post-buckling behaviour of steel structures subjected to fire. The uncertainties related to the shape and amplitudes of the imperfections are removed by studying the perfect structure.
- It may happen that with very small imperfections the post-buckling is not detected, and inaccurate results are obtained. Such inaccurate results can easily be identified performing a branch-switching analysis on the perfect structure.

Paper II

- Extensive numerical validation showed that the developed corotational 3D beam element allows for improved predictions compared to beam elements from two commercial software, namely ABAQUS and SAFIR, when steel structures subjected to significant torsional actions at elevated temperature are studied. The formulation is suitable for members with open-cross section and properly accounts for warping and degradation of torsional strength and stiffness with temperature.
- The Bernoulli assumption applies to problems in which the shear deformations are negligible. The displacement field is defined by a higher order polynomial and thus a converged solution is obtained with less elements compared to the Timoshenko formulation. However, the Timoshenko beam element requires less computational time because of a simpler definition of the displacement field. Consequently, the use of the Timoshenko element is suggested even in the case of negligible shear deformations.
- In cases where torsional effects contribute considerably to the element collapse, commercial programmes do not provide reasonable estimate of the failure temperature. Better predictions may be obtained if normal stresses, for instance owing to flexure, have also an important role. Therefore, special attention should be paid to: (1) structural elements that are particularly sensitive to torsional and lateral-torsional buckling phenomena, e.g., high beams with I-cross-sections loaded on the top of the compression flange and channel sections; and (2) structural elements that are subjected to torsion.

Paper III

- Though compressed steel L profiles or closely spaced built-up members are widely used in the design practice, the EN 1993-1-2 provisions do not provide dedicated guidance for the evaluation of their resistance to compression at elevated temperature. Such members require special attention as usually torsional or flexural-torsional buckling is the relevant buckling mode. It turns out that the EN 1993-1-2 provisions can lead to both conservative and unconservative predictions depending on the slenderness at elevated temperature $\bar{\lambda}_\theta$.
- The proposed formulation for a buckling curve allows for improved predictions of the resistance to compression of Class 1 to Class 3 L, T or X steel members. Statistical investigation proves the proposal to be reliable and safe. In general, better statistical correlation is found between numerical results and the proposed buckling curve rather than the EN 1993-1-2 buckling curve.

- The proposed buckling curve gives better predictions if the lowest flexural buckling mode is used in the definition of the slenderness at elevated temperature $\bar{\lambda}_\theta$, instead of the lowest buckling mode, i.e. torsional or flexural-torsional. This is due to the fact that the flexural slenderness better represents the length of the column.

Paper IV

Conclusions from Paper IV are relative to the investigated case study but could be extended to structures that present similar features, i.e. regular structure, office building, regular opening distribution and assuming a natural fire uniformly distributed on the compartment surface. It should be noted that the following conclusions do not apply to fires in large compartments, e.g. localised fires, for which zone models do not seem appropriate and the use of CFD models would be more beneficial.

- A satisfactory approximation of the temperature inside the compartment can be reached with simplified models. Indeed, in the investigated case study, the average gas temperature obtained with zone models (Ozone and CFAST) and with more exhaustive CFD analysis (FDS) are in good agreement. Also, the evolution of the peak temperatures from CFAST and FDS exhibit a very similar behaviour.
- Comparable failure time are found employing temperatures from CFD and zone models, but only if mean temperatures are taken from the latter (OZONE and CFAST AVG). In fact, the application of peak temperatures from CFAST (CFAST MAX) leads to an early collapse of the structure.
- The consequence evaluation in the risk-ranking process may be revised. Indeed, columns are not critical in the proposed case study because designed to withstand large seismic actions and they are only partially heated. Hence, as partial or total collapse is generally triggered by column failure, the consequence estimations of 12.5% and 50% respectively assigned to both the scenarios were likely to be overestimated.

5.2 Further research

Some suggestions are provided to improve and extend the work presented in this thesis:

Computational improvements

The main framework of the developed finite elements is versatile and may be adapted for several purposes. For instance, a 2D heat transfer analyses could be implemented to obtain temperatures inside the elements. In the current analysis procedure, temperature distributions induced by the fire exposure are obtained from thermal analysis performed with existing software such as SAFIR. The output temperatures at the nodes of the discretised thermal problem are then processed (by interpolation or extrapolation) to obtain the temperature at the Gauss points later employed in the mechanical analysis. It would be beneficial to perform thermal analysis that give temperatures at the exact Gauss points used in the mechanical analyses, especially for complex temperature distributions. For this purpose, starting from a 2D discretisation of the section of the elements as the one used to compute the geometrical properties in the 3D beam element, a thermal analysis could be implemented to obtain temperatures directly at the gauss points used in the mechanical problem.

A further improvement could be introduced by considering residual stresses. Residual stresses are the stresses that remain inside a steel profile after the fabrication process ends and the profile is free from any external loading or thermal gradient. An initial stress configuration as such might affect the mechanical behaviour of steel elements and should be considered in numerical simulation. In the proposed thermomechanical elements, initial residual stresses could be easily taken into account at the gauss point level, according to [100]. Some tests were performed by the author and, as stated in several research works [20], [28], [33], [34], [92], it was found that in most of the relevant applications to steel structures at elevated temperature, residual stresses may be neglected since a relaxation of initial residual stresses is likely to occur owing to the temperature increase. Nevertheless, residual stresses might still have a relevant role when combined with geometrical imperfections and high steel grades or at low temperatures, i.e. less than 400°C [24], [26]–[28], [101].

Effects of geometrical imperfections on the buckling of single steel members and steel frames

Single imperfections or a combination of them (see Annex C of [102]) should be introduced in numerical models to properly capture the behaviour steel structures. The shape of these imperfections should be accurately selected in order to obtain conservative results. When steel members in fire are studied this is not an easy task, as also shown by the author in [84]. Indeed, though at ambient temperature a linear buckling analysis may be sufficient to determine appropriate imperfections, this might not be the case at elevated temperature, especially for non-uniform temperature distribution. Besides, the choice of the imperfection amplitude can also determine which imperfection shape gives the most conservative results. Hence, the influence of geometrical imperfection on the buckling resistance of steel members at elevated temperatures deserves a deeper investigation. A promising alternative consists in checking the tangent stiffness of perfect structures, as in the branch-switching procedure. The eigenmode relative to the first critical point associated to buckling can be used to define the shape of the initial imperfection. This procedure might be particularly effective for non-uniform temperature distributions. Nevertheless, in order to identify eigenmodes associated to buckling phenomena, only symmetric configuration should be studied, and the temperature distribution should not compromise the symmetry of the problem.

Analogous considerations could be taken for the buckling of steel frames in fire situation. Again, the choice of the shape of the initial geometrical imperfection determines the behaviour and the load-carrying capacity of the structure. The definition of an appropriate imperfection might not be straightforward, in particular in fire situation. For steel frames at ambient temperature, Shayan et al. [103] proposed an interesting procedure which considers the introduction of a combination of several eigenmodes. A similar solution could be adopted for steel frames at elevated temperatures. Starting from portals uniformly heated on all the structural members, a procedure adaptable to frames with a more complex temperature distribution could be studied.

Refined models and experimental campaign for built-up members

Connections between the single profiles composing the built-up T and X sections, were not considered in the numerical models presented in Paper III [93]. Indeed, closely built-up members, consisting of single sections connected through packing plates or star-battened angles, may be checked for buckling as single integral members if the spacing of the connections is short enough [91]. Nevertheless, further investigations could be performed by employing more refined models to account for the influence of connecting plates or battens.

Finally, since no experimental tests on the investigated profiles are available in literature, future experimental campaign would be beneficial to confirm the numerical results.

Fire Safety Engineering investigations with direct coupling between fire development (FDS) and thermal analysis (SAFIR)

Integrated modelling methodologies applied to compartment fires rely on the coupling between Computational Fluid Dynamics (CFD) and finite element (FE) software. At the present, in the common coupling strategy, temperatures obtained from the CFD simulation are employed as boundary condition in heat transfer analyses, that may be directly performed with FE software involved in the structural analysis, e.g. SAFIR. Devices may be defined in CFD analyses to record temperatures in different positions inside a compartment. In order to obtain a temperature value that can be used as boundary conditions for the thermal analysis, adiabatic surface temperature devices may be used and provide the maximum achievable solid surface temperature at the given location. The described procedure is time consuming and the temperature of each device should be carefully coupled to the associated structural element. Tondini et al. proposed in [104] an alternative strategy to directly couple the CFD software FDS with SAFIR. In this procedure, a single transfer file obtained from FDS contains all the information required to obtain the thermal response of the structure. Moreover, radiant intensities are also considered in the heat transfer analyses. It would be interesting to provide considerations about the application of this procedure in future investigations. Results with different coupling solutions and fire development models could be compared.

Bibliography

- [1] Y. Wang, I. Burgess, F. Wald, and M. Gillie, *Performance-Based Fire Engineering of Structures*. London: CRC Press, 2013.
- [2] Y. C. Wang, *Steel and Composite Structures: Behaviour and design for fire safety*, 1st ed. London; New York: Spoon Press, 2002.
- [3] International Organization for Standardization (ISO), *ISO 16733-1. Fire safety engineering - selection of design fire scenarios and design fires - part 1: Selection of design fire scenarios*. Standard. Geneva, Switzerland, 2015.
- [4] International Organization for Standardization (ISO), *ISO 16732-1. Fire safety engineering - fire risk assessment - part 1: General*. Standard. Geneva, Switzerland, 2012.
- [5] K. Bergmeister, P. Brunello, M. Pachera, F. Pesavento, and B. A. Schrefler, 'Simulation of fire and structural response in the Brenner Base Tunnel by means of a combined approach: A case study', *Eng. Struct.*, vol. 211, 2020, doi: <https://doi.org/10.1016/j.engstruct.2020.110319>.
- [6] T. Gernay and N. E. Khorasani, 'Recommendations for performance-based fire design of composite steel buildings using computational analysis', *J. Constr. Steel Res.*, vol. 166, 2020, doi: <https://doi.org/10.1016/j.jcsr.2019.105906>.
- [7] E. Rackauskaite, P. Kotsovinos, and G. Rein, 'Structural response of a steel-frame building to horizontal and vertical travelling fires in multiple floors', *Fire Saf. J.*, vol. 91, pp. 542–552, 2017, doi: <http://dx.doi.org/10.1016/j.firesaf.2017.04.018>.
- [8] T. Gernay, N. E. Khorasani, and M. Garlock, 'Fire fragility curves for steel buildings in a community context : A methodology', *Eng Struct*, vol. 113, pp. 259–276, 2016.
- [9] D. Lange, S. Devaney, and A. Usmani, 'An application of the PEER PBEE framework to structures in fire.', vol. *Engineering Structures*, no. 66, pp. 110–115, 2014, doi: <https://doi.org/10.1016/j.engstruct.2014.01.052>.
- [10] E. Nigro, A. Bilotta, D. Asprone, F. Jalaver, A. Prota, and G. Manfredi, 'Probabilistic approach for failure assessment of steel structures in fire by means of plastic limit analysis', *Fire Saf. J.*, vol. 68, pp. 16–29, 2014.
- [11] J.-M. Franssen and T. Gernay, 'Modeling structures in fire with SAFIR®: Theoretical background and capabilities', *J. Struct. Fire Eng.*, vol. 8, no. 3, pp. 300–323, 2017.
- [12] C. G. Bailey, 'Development of computer software to simulate the structure behaviour of steel-framed buildings in fire', *Comput. Struct.*, vol. 67, pp. 421–438, 1998.
- [13] S. R. Najjar and I. W. Burgess, 'A nonlinear analysis for three-dimensional steel frames in fire conditions', *Eng. Struct.*, vol. 18, no. 77–89, 1992.

- [14] Dassault Systèmes, *ABAQUS Version 6.14, User's Manual*. 2014.
- [15] ANSYS Inc., *ANSYS Version 17.0, User's Manual*. 2016.
- [16] S. Mazzoni, F. McKenna, M. H. Scott, and G. L. Fenves, *OpenSees Command Language Manual*. University of California, Berkeley, 2006.
- [17] DIANA FEA BV, *DIANA Version 10.1, User's Manual*. 2016.
- [18] Z. F. Huang and K. H. Tan, 'FE Simulation of space steel frames in fire with warping effect', *Adv. Steel Constr.*, vol. 3, no. 3, pp. 652–667, 2007.
- [19] CEN (European Committee for Standardisation), *Eurocode 3 Design of steel structures - Part 1-2: General rules - Structural fire design*. 2005.
- [20] J.-M. Franssen, J.-B. Schleich, and L.-G. Cajot, 'A simple model for the fire resistance of axially-loaded members according to eurocode 3', *J. Constr. Steel Res.*, vol. 35, no. 1, pp. 49–69, Jan. 1995, doi: 10.1016/0143-974X(94)00042-D.
- [21] J.-M. Franssen, J.-B. Schleich, L.-G. Cajot, and W. Azpiazu, 'A simple model for the fire resistance of axially-loaded members - comparison with experimental results', *J. Constr. Steel Res.*, vol. 37, no. 3, pp. 175–204, May 1996, doi: 10.1016/0143-974X(96)00008-9.
- [22] C. G. Bailey, I. W. Burgess, and R. J. Plank, 'The Lateral-torsional Buckling of Unrestrained Steel Beams in Fire', *J. Constr. Steel Res.*, vol. 36, no. 2, pp. 101–119, 1996.
- [23] P. Vila Real and J.-M. Franssen, 'Lateral Torsional Buckling of Steel -Beams in Case of Fire – Numerical Modelling', presented at the First International Workshop Structures in Fire, Copenhagen, 2000.
- [24] P. Vila Real and J.-M. Franssen, 'Numerical modelling of lateral buckling of steel I beams under fire conditions—comparison with Eurocode 3', *J. Fire Prot. Eng.*, vol. 11, no. 2, pp. 112–128, 2001.
- [25] P. Vila Real, P. Piloto, and J.-M. Franssen, 'A new proposal of a simple model for the lateral-torsional buckling of unrestrained steel I-beams in case of fire: experimental and numerical validation', *J. Constr. Steel Res.*, vol. 59, no. 2, pp. 179–199, 2003.
- [26] P. Vila Real, N. Lopes, L. Simões da Silva, and J.-M. Franssen, 'Parametric analysis of the lateral–torsional buckling resistance of steel beams in case of fire', *Fire Saf. J.*, vol. 42, no. 6–7, pp. 416–424, Sep. 2007, doi: 10.1016/j.firesaf.2006.11.010.
- [27] P. Vila Real, N. Lopes, L. S. da Silva, and J.-M. Franssen, 'Lateral-torsional buckling of unrestrained steel beams under fire conditions: improvement of EC3 proposal', *Comput. Struct.*, vol. 82, no. 20, pp. 1737–1744, 2004.
- [28] P. M. M. Vila Real, R. Cazeli, L. Simões da Silva, A. Santiago, and P. Piloto, 'The effect of residual stresses in the lateral-torsional buckling of steel I-beams at elevated temperature', *J. Constr. Steel Res.*, vol. 60, no. 3–5, pp. 783–793, Mar. 2004, doi: 10.1016/S0143-974X(03)00143-3.
- [29] C. Couto, P. Vila Real, N. Lopes, and B. Zhao, 'Numerical investigation of the lateral–torsional buckling of beams with slender cross sections for the case of fire', *Eng. Struct.*, vol. 106, pp. 410–421, Jan. 2016, doi: 10.1016/j.engstruct.2015.10.045.
- [30] C. Couto, P. Vila Real, N. Lopes, and B. Zhao, 'Local buckling in laterally restrained steel beam-columns in case of fire', *J. Constr. Steel Res.*, vol. 122, pp. 543–556, Jul. 2016, doi: 10.1016/j.jcsr.2016.04.012.

- [31] C. Couto, É. Maia, P. Vila Real, and N. Lopes, 'The effect of non-uniform bending on the lateral stability of steel beams with slender cross-section at elevated temperatures', *Eng. Struct.*, vol. 163, pp. 153–166, May 2018, doi: 10.1016/j.engstruct.2018.02.033.
- [32] J.-M. Franssen, F. Morente, P. Vila Real, F. Wald, A. Sanzel, and B. Zhao, 'Fire Design of Steel Members with Welded or Hot-rolled Class 4 Cross-sections (FIDESC4)', 2016.
- [33] C. Couto, P. Vila Real, N. Lopes, and B. Zhao, 'Resistance of steel cross-sections with local buckling at elevated temperatures', *J. Constr. Steel Res.*, vol. 109, pp. 101–114, Jun. 2015, doi: 10.1016/j.jcsr.2015.03.005.
- [34] C. Couto, P. Vila Real, N. Lopes, and B. Zhao, 'Effective width method to account for the local buckling of steel thin plates at elevated temperatures', *Thin-Walled Struct.*, vol. 84, pp. 134–149, Nov. 2014, doi: 10.1016/j.tws.2014.06.003.
- [35] O. Kaitila, 'Imperfection sensitivity analysis of lipped channel columns at high temperatures', *J. Constr. Steel Res.*, vol. 58, no. 3, pp. 333–351, 2002.
- [36] M. Feng, Y. C. Wang, and J. M. Davies, 'Structural behaviour of cold-formed thin-walled short steel channel columns at elevated temperatures. Part 1: experiments', *Thin-Walled Struct.*, vol. 41, no. 6, pp. 543–570, Jun. 2003, doi: 10.1016/S0263-8231(03)00002-8.
- [37] M. Feng, Y. C. Wang, and J. M. Davies, 'Structural behaviour of cold-formed thin-walled short steel channel columns at elevated temperatures. Part 2: Design calculations and numerical analysis', *Thin-Walled Struct.*, vol. 41, no. 6, pp. 571–594, Jun. 2003, doi: 10.1016/S0263-8231(03)00003-X.
- [38] M. Feng, Y. C. Wang, and J. M. Davies, 'Axial strength of cold-formed thin-walled steel channels under non-uniform temperatures in fire', *Fire Saf. J.*, vol. 38, no. 8, pp. 679–707, Dec. 2003, doi: 10.1016/S0379-7112(03)00070-5.
- [39] J. Chen and B. Young, 'Cold-formed steel lipped channel columns at elevated temperatures', *Eng. Struct.*, vol. 29, no. 10, pp. 2445–2456, Oct. 2007, doi: 10.1016/j.engstruct.2006.12.004.
- [40] N. Silvestre, P. B. Dinis, and D. Camotim, 'Developments on the Design of Cold-Formed Steel Angles', *J. Struct. Eng.*, vol. 139, no. 5, pp. 680–694, May 2013, doi: 10.1061/(ASCE)ST.1943-541X.0000670.
- [41] B. W. Schafer, 'Review: The Direct Strength Method of cold-formed steel member design', *J. Constr. Steel Res.*, vol. 64, no. 7–8, pp. 766–778, Jul. 2008, doi: 10.1016/j.jcsr.2008.01.022.
- [42] G. M. De Barros Chodraui, Y. Shifferaw, M. Malite, and B. W. Schafer, 'On the stability of cold-formed steel angles under compression', *Rev. Esc. Minas*, vol. 60, no. 2, pp. 355–363, 2007.
- [43] D. Popovic, G. J. Hancock, and K. J. R. Rasmussen, 'Compression tests on cold-formed angles loaded parallel with a leg', *J. Struct. Steel Res.*, vol. 127, no. 6, pp. 600–607, 2001.
- [44] T. Ranawaka and M. Mahendran, 'Numerical modelling of light gauge cold-formed steel compression members subjected to distortional buckling at elevated temperatures', *Thin-Walled Struct.*, vol. 48, no. 4, pp. 334–344, Apr. 2010, doi: 10.1016/j.tws.2009.11.004.

- [45] L. Laím and J. P. C. Rodrigues, 'Fire design methodologies for cold-formed steel beams made with open and closed cross-sections', *Eng. Struct.*, vol. 171, pp. 759–778, Sep. 2018, doi: 10.1016/j.engstruct.2018.06.030.
- [46] H. D. Craveiro, J. Henriques, A. Santiago, and L. Laím, 'Numerical investigation on thin-walled CFS columns in fire', in *Proceedings of the International Colloquia on Stability and Ductility of Steel Structures*, 2019, pp. 286–294.
- [47] P. B. Dinis, D. Camotim, and N. Silvestre, 'On the local and global buckling behaviour of angle, T-section and cruciform thin-walled members', *Thin-Walled Struct.*, vol. 48, no. 10–11, pp. 786–797, Oct. 2010, doi: 10.1016/j.tws.2010.04.012.
- [48] Chrysanthos Maraveas, Thomas Gernay, and Jean-Marc Franssen, 'Buckling of steel plates at elevated temperatures: theory of perfect plates vs finite element analysis', presented at the CONFAB 2017, London, UK, 2017.
- [49] C. Maraveas, T. Gernay, and J. M. Franssen, 'Sensitivity of elevated temperature load carrying capacity of thin-walled steel members to local imperfections', p. 11.
- [50] J. A. Purkiss, *Fire safety engineering design of structures*, 2nd ed. Amsterdam ; Boston: Elsevier/Butterworth-Heinemann, 2007.
- [51] R. Alsafadie, J.-M. Battini, H. Somja, and M. Hjiqj, 'Local formulation for elasto-plastic corotational thin-walled beams based on higher-order curvature terms', *Finite Elem. Anal. Des.*, vol. 47, no. 2, pp. 119–128, Feb. 2011, doi: 10.1016/j.finel.2010.08.006.
- [52] J.-M. Battini, 'A non-linear corotational 4-node plane element', *Mech. Res. Commun.*, vol. 35, no. 6, pp. 408–413, Sep. 2008, doi: 10.1016/j.mechrescom.2008.03.002.
- [53] J.-M. Battini, 'A modified corotational framework for triangular shell elements', *Comput. Methods Appl. Mech. Eng.*, vol. 196, no. 13–16, pp. 1905–1914, Mar. 2007, doi: 10.1016/j.cma.2006.10.006.
- [54] J.-M. Battini, 'Co-Rotational Beam Elements in Instability Problems', KTH, Royal Institute of Technology, Stockholm, 2002.
- [55] J.-M. Battini, 'Co-rotational beam elements with warping effects in instability problems', *Comput. Methods Appl. Mech. Eng.*, vol. 191, no. 17–18, pp. 1755–1789, 2002.
- [56] J.-M. Battini and C. Pacoste, 'On the choice of the linear element for corotational triangular shells', *Comput. Methods Appl. Mech. Eng.*, vol. 195, no. 44–47, pp. 6362–6377, Sep. 2006, doi: 10.1016/j.cma.2006.01.007.
- [57] J.-M. Battini and C. Pacoste, 'On the choice of local element frame for corotational triangular shell elements', *Commun. Numer. Methods Eng.*, vol. 20, no. 10, pp. 819–825, 2004.
- [58] J.-M. Battini and C. Pacoste, 'Plastic instability of beam structures using co-rotational elements', *Comput. Methods Appl. Mech. Eng.*, vol. 191, no. 51, pp. 5811–5831, Dec. 2002, doi: 10.1016/S0045-7825(02)00498-X.
- [59] M. A. Crisfield, *Non-linear finite element analysis of solids and structures*. Chichester ; New York: Wiley, 1991.
- [60] A. Eriksson, 'Element formulation and numerical techniques for stability problems in shells', *Comput. Methods Appl. Mech. Eng.*, vol. 191, no. 35, pp. 3775–3810, 2002.

- [61] C. A. Felippa, 'A study of optimal membrane triangles with drilling freedoms', *Comput. Methods Appl. Mech. Eng.*, vol. 192, no. 16, pp. 2125–2168, Apr. 2003, doi: 10.1016/S0045-7825(03)00253-6.
- [62] C. A. Felippa and B. Haugen, 'A unified formulation of small-strain corotational finite elements: I. Theory', *Comput. Methods Appl. Mech. Eng.*, vol. 194, no. 21–24, pp. 2285–2335, Jun. 2005, doi: 10.1016/j.cma.2004.07.035.
- [63] K. M. Hsiao and W. J. Lin, 'A co-rotational finite element formulation for buckling and postbuckling analyses', *Comput Methods Appl Mech Engrg*, vol. 188, pp. 567–594, 2000.
- [64] Z. Li, Y. Xiang, B. A. Izzuddin, L. Vu-Quoc, X. Zhuo, and C. Zhang, 'A 6-node co-rotational triangular elasto-plastic shell element', *Comput. Mech.*, vol. 55, no. 5, pp. 837–859, May 2015, doi: 10.1007/s00466-015-1138-1.
- [65] Z. X. Li, X. Zhuo, L. Vu-Quoc, B. A. Izzuddin, and H. Y. Wei, 'A four-node corotational quadrilateral elastoplastic shell element using vectorial rotational variables: FOUR-NODE COROTATIONAL QUADRILATERAL ELASTOPLASTIC SHELL ELEMENT', *Int. J. Numer. Methods Eng.*, vol. 95, no. 3, pp. 181–211, Jul. 2013, doi: 10.1002/nme.4471.
- [66] Z. X. Li, B. A. Izzuddin, and L. Vu-Quoc, 'A 9-node co-rotational quadrilateral shell element', *Comput. Mech.*, vol. 42, no. 6, pp. 873–884, Nov. 2008, doi: 10.1007/s00466-008-0289-8.
- [67] Z. Li and L. Vu-Quoc, 'An efficient co-rotational formulation for curved triangular shell element', *Int. J. Numer. Methods Eng.*, vol. 72, no. 9, pp. 1029–1062, Nov. 2007, doi: 10.1002/nme.2064.
- [68] C. Pacoste, 'Co-rotational flat facet triangular elements for shell instability analyses', *Comput. Methods Appl. Mech. Eng.*, vol. 156, no. 1, pp. 75–110, Apr. 1998, doi: 10.1016/S0045-7825(98)80004-2.
- [69] C. Pacoste and A. Eriksson, 'Beam elements in instability problems', *Comput. Methods Appl. Mech. Eng.*, vol. 144, no. 1–2, pp. 163–197, 1997.
- [70] C. C. Rankin and B. Nour-Omid, 'Finite rotation analysis and consistent linearization using projectors', *Comput Methods Appl Mech Engrg*, vol. 93, pp. 353–384, 1991.
- [71] C. C. Rankin and B. Nour-Omid, 'The use of projectors to improve finite element performance', *Comput. Struct.*, vol. 30, pp. 257–267, 1988.
- [72] D. Talamona, 'A Quadrangular Shell Finite Element for Concrete and Steel Structures Subjected to Fire', *J. Fire Prot. Eng.*, vol. 15, no. 4, pp. 237–264, Nov. 2005, doi: 10.1177/1042391505052769.
- [73] J.-M. Franssen, 'Contributions a la modelisation des incendies et de leurs effets sur les batiments', KTH, Royal Institute of Technology, Liege, Belgium, 1997.
- [74] C. Jeyachandrabose, J. Kirkhope, and C. R. Babu, 'An alternative explicit formulation for the DKT plate-bending element', *Int. J. Numer. Methods Eng.*, vol. 21, no. 7, pp. 1289–1293, Jul. 1985, doi: 10.1002/nme.1620210709.
- [75] R. Gruttmann, R. Sauer, and W. Wagner, 'Theory and numerics of three-dimensional beams with elastoplastic behaviour', *Int. J. Numer. Methods Eng.*, vol. 48, pp. 1675–1702, 2000.

- [76] L. Possidente, N. Tondini, and J.-M. Battini, '3D Beam Element for the Analysis of Torsional Problems of Steel-Structures in Fire', *J. Struct. Eng.*, vol. 146, no. 7, p. 04020125, Jul. 2020, doi: 10.1061/(ASCE)ST.1943-541X.0002665.
- [77] R. Von Mises, 'Mechanik der festen Körper im plastisch deformablen Zustand', *Gotting Nachr Math Phys*, vol. K1, pp. 582–592, 1913.
- [78] M. Robinson, 'A comparison of yield surfaces for thin shells', *Int J Mech Sci*, vol. 13, pp. 345–354, 1971.
- [79] N. Elhami Khorasani, M. E. M. Garlock, and S. E. Quiel, 'Modeling steel structures in OpenSees: Enhancements for fire and multi-hazard probabilistic analyses', *Comput. Struct.*, vol. 157, pp. 218–231, Sep. 2015, doi: 10.1016/j.compstruc.2015.05.025.
- [80] A. El-Rimawi, I. W. Burgess, and R. J. Plank, 'The treatment of strain reversal in structural members during the cooling phase of fire', *J Constr Steel Res*, vol. 37, no. 2, pp. 115–135, 1996.
- [81] J.-M. Franssen, 'The unloading of building materials submitted to fire', *Fire Saf. J.*, vol. 16, no. 3, pp. 213–227, 1990.
- [82] S. E. Quiel and M. E. M. Garlock, 'A closed-form analysis of perimeter member behavior in a steel building frame subject to fire', *Eng. Struct.*, vol. 30, no. 11, pp. 3276–3284, Nov. 2008, doi: 10.1016/j.engstruct.2008.05.006.
- [83] CEN (European Committee for Standardisation), 'Eurocode 3 Design of steel structures - Part 1-2: General rules - Structural fire design'. 2005.
- [84] L. Possidente, N. Tondini, and J.-M. Battini, 'Branch-switching procedure for post-buckling analysis of thin-walled steel members at elevated temperature', *Thin-Walled Struct.*, vol. 136, pp. 90–98, Mar. 2019, doi: 10.1016/j.tws.2018.12.012.
- [85] H. Petryk and K. Thermann, 'On discretized plasticity problems with bifurcations', *Int. J. Solids Struct.*, vol. 29, no. 6, pp. 745–765, Jan. 1992, doi: 10.1016/0020-7683(92)90125-D.
- [86] M. Veljkovic et al., 'Eurocodes: Background & Applications. Design of Steel Buildings. Worked examples'. Joint Research Center, Brussels, 2015.
- [87] G. Chen and N. S. Trahair, 'Inelastic torsional buckling strengths of cruciform columns', *Eng. Struct.*, vol. 16, no. 2, pp. 83–90, 2006.
- [88] R. Dabrowski, 'On Torsional Stability of Cruciform Columns', *J Constr Steel Res*, vol. 9, pp. 51–59, 1988.
- [89] A. Taras and R. Greiner, 'Torsional and flexural torsional buckling — A study on laterally restrained I-sections', *J. Constr. Steel Res.*, vol. 64, no. 7–8, pp. 725–731, Jul. 2008, doi: 10.1016/j.jcsr.2008.01.019.
- [90] N. S. Trahair, 'Strength design of cruciform steel columns', *Eng. Struct.*, vol. 35, pp. 307–313, Feb. 2012, doi: 10.1016/j.engstruct.2011.11.026.
- [91] CEN (European Committee for Standardisation), *Eurocode 3 Design of steel structures - Part 1-1: General rules and rules for building*. 2005.
- [92] S. E. Quiel and M. E. M. Garlock, 'Calculating the buckling strength of steel plates exposed to fire', *Thin-Walled Struct.*, vol. 48, no. 9, pp. 684–695, Sep. 2010, doi: 10.1016/j.tws.2010.04.001.

- [93] L. Possidente, N. Tondini, and J.-M. Battini, 'Torsional and flexural-torsional buckling of compressed steel members in fire', *J. Constr. Steel Res.*, vol. 171, p. 106130, Aug. 2020, doi: 10.1016/j.jcsr.2020.106130.
- [94] Standard, International Organization for Standardization (ISO), 'Fire safety engineering - performance of structures in fire - part 4: Example of a fifteen-storey steel-framed office building.', Geneva, Switzerland, 2017.
- [95] I. Del Prete, G. Cefarelli, and E. Nigro, 'Application of criteria for selecting fire scenarios for structures within fire safety engineering approach', *J. Build. Eng.*, vol. 8, pp. 208–217, 2016.
- [96] D. Hossler, 'Leitfaden Ingenieurmethoden des Brandschutzes, Technischer Bericht vfdB TB 04-01, 3', Auflage Altenberge, Braunschweig, Germany, 2013.
- [97] J.-F. Cadorin, 'Compartment Fire Models for Structural Engineering. PhD thesis, Faculte des Sciences appliquées', Faculte des Sciences appliquées, Université de Liege, Liege, Belgium, 2003.
- [98] NIST, *Consolidated Fire and Smoke Transport, Technical Reference Guide, Special Publication 1018-1, Sixth Edition.* 2017.
- [99] NIST, *Fire Dynamics Simulator, Technical Reference Guide, NIST Technical Note 1889v1.* 2019.
- [100] J.-M. Franssen, 'Residual stresses in steel profiles submitted to the fire : an analogy', in *Proc. 3rd CIB/W14 FSF workshop on modelling, Rijswijk, Netherland, 1996*, vol. 96-CVB-R0365, pp. 103–112.
- [101] M. Kucukler, 'Lateral instability of steel beams in fire: Behaviour, numerical modelling and design', *J. Constr. Steel Res.*, vol. 170, p. 106095, Jul. 2020, doi: 10.1016/j.jcsr.2020.106095.
- [102] CEN (European Committee for Standardisation), *Eurocode 3 Design of steel structures - Part 1-5: Plated structural elements.* 2007.
- [103] S. Shayan, K. J. R. Rasmussen, and H. Zhang, 'On the modelling of initial geometric imperfections of steel frames in advanced analysis', *J. Constr. Steel Res.*, vol. 98, pp. 167–177, Jul. 2014, doi: 10.1016/j.jcsr.2014.02.016.
- [104] N. Tondini, O. Vassart, and J.-M. Franssen, 'DEVELOPMENT OF AN INTERFACE BETWEEN CFD AND FE SOFTWARE', Zurich, Switzerland, 2012, p. 11.

Appendix A

Paper I

Appendix B

Paper II

Appendix C

Paper III

Appendix D

Paper IV

List of Bulletins from the previous Department of Structural Engineering,
currently Division of Concrete Structures and Division of Structural Design and Bridges
at
KTH Royal Institute of Technology, Stockholm, Sweden

TRITA-BKN. Bulletin

is from February 2018 replaced by the common publication series of
the School of Architecture and the Built Environment (ABE)

TRITA-ABE-DLT-YYX

Pacoste, C., On the Application of Catastrophe Theory to Stability Analyses of Elastic Structures.
Doctoral Thesis, 1993. Bulletin 1.

Stenmark, A-K., Dämpning av 13 m lång stål balk – "Ullevibalken". Utprovning av dämpmassor och fastsättning
av motbalk samt experimentell bestämning av modformer och förlustfaktorer. Vibration tests of full-scale steel
girders to determine optimum passive control.
Licentiatavhandling, 1993. Bulletin 2.

Silfwerbrand, J., Renovering av asfaltgolv med cementbundna plastmodifierade avjämningsmassor.
1993. Bulletin 3.

Norlin, B., Two-Layered Composite Beams with Nonlinear Connectors and Geometry – Tests and Theory.
Doctoral Thesis, 1993. Bulletin 4.

Habtezion, T., On the Behaviour of Equilibrium Near Critical States.
Licentiate Thesis, 1993. Bulletin 5.

Krus, J., Hållfasthet hos frostnedbruten betong.
Licentiatavhandling, 1993. Bulletin 6.

Wiberg, U., Material Characterization and Defect Detection by Quantitative Ultrasonics.
Doctoral Thesis, 1993. Bulletin 7.

Lidström, T., Finite Element Modelling Supported by Object Oriented Methods.
Licentiate Thesis, 1993. Bulletin 8.

Hallgren, M., Flexural and Shear Capacity of Reinforced High Strength Concrete Beams without Stirrups.
Licentiate Thesis, 1994. Bulletin 9.

Krus, J., Betongbalkars lastkapacitet efter miljöbelastning.
1994. Bulletin 10.

Sandahl, P., Analysis Sensitivity for Wind-related Fatigue in Lattice Structures.
Licentiate Thesis, 1994. Bulletin 11.

Sanne, L., Information Transfer Analysis and Modelling of the Structural Steel Construction Process.
Licentiate Thesis, 1994. Bulletin 12.

Zhitao, H., Influence of Web Buckling on Fatigue Life of Thin-Walled Columns.
Doctoral Thesis, 1994. Bulletin 13.

Kjörling, M., Dynamic response of railway track components. Measurements during train passage and dynamic laboratory loading.

Licentiate Thesis, 1995. Bulletin 14.

Yang, L., On Analysis Methods for Reinforced Concrete Structures.

Doctoral Thesis, 1995. Bulletin 15.

Petersson, Ö., Svensk metod för dimensionering av betongvägar.

Licentiatavhandling, 1996. Bulletin 16.

Lidström, T., Computational Methods for Finite Element Instability Analyses.

Doctoral Thesis, 1996. Bulletin 17.

Krus, J., Environment- and Function-induced Degradation of Concrete Structures.

Doctoral Thesis, 1996. Bulletin 18.

Editor, Silfwerbrand, J., Structural Loadings in the 21st Century.

Sven Sahlin Workshop, June 1996. Proceedings. Bulletin 19.

Ansell, A., Frequency Dependent Matrices for Dynamic Analysis of Frame Type Structures.

Licentiate Thesis, 1996. Bulletin 20.

Troive, S., Optimering av åtgärder för ökad livslängd hos infrastrukturkonstruktioner. Licentiatavhandling, 1996.

Bulletin 21.

Karoumi, R., Dynamic Response of Cable-Stayed Bridges Subjected to Moving Vehicles.

Licentiate Thesis, 1996. Bulletin 22.

Hallgren, M., Punching Shear Capacity of Reinforced High Strength Concrete Slabs.

Doctoral Thesis, 1996. Bulletin 23.

Hellgren, M., Strength of Bolt-Channel and Screw-Groove Joints in Aluminium Extrusions.

Licentiate Thesis, 1996. Bulletin 24.

Yagi, T., Wind-induced Instabilities of Structures.

Doctoral Thesis, 1997. Bulletin 25.

Eriksson, A., and Sandberg, G., (editors), Engineering Structures and Extreme Events – proceedings from a symposium, May 1997. Bulletin 26.

Paulsson, J., Effects of Repairs on the Remaining Life of Concrete Bridge Decks.

Licentiate Thesis, 1997. Bulletin 27.

Olsson, A., Object-oriented finite element algorithms.

Licentiate Thesis, 1997. Bulletin 28.

Yunhua, L., On Shear Locking in Finite Elements.

Licentiate Thesis, 1997. Bulletin 29.

Ekman, M., Sprickor i betongkonstruktioner och dess inverkan på beständigheten.

Licentiate Thesis, 1997. Bulletin 30.

Karawajczyk, E., Finite Element Approach to the Mechanics of Track-Deck Systems.

Licentiate Thesis, 1997. Bulletin 31.

Fransson, H., Rotation Capacity of Reinforced High Strength Concrete Beams.

Licentiate Thesis, 1997. Bulletin 32.

Edlund, S., Arbitrary Thin-Walled Cross Sections. Theory and Computer Implementation. Licentiate Thesis, 1997. Bulletin 33.

Forsell, K., Dynamic analyses of static instability phenomena. Licentiate Thesis, 1997. Bulletin 34.

Ikäheimonen, J., Construction Loads on Shores and Stability of Horizontal Formworks. Doctoral Thesis, 1997. Bulletin 35.

Racutanu, G., Konstbyggnaders reella livslängd. Licentiatavhandling, 1997. Bulletin 36.

Appelqvist, I., Sammanbyggnad. Datastrukturer och utveckling av ett IT-stöd för byggprocessen. Licentiatavhandling, 1997. Bulletin 37.

Alavizadeh-Farhang, A., Plain and Steel Fibre Reinforced Concrete Beams Subjected to Combined Mechanical and Thermal Loading. Licentiate Thesis, 1998. Bulletin 38.

Eriksson, A. and Pacoste, C., (editors), Proceedings of the NSCM-11: Nordic Seminar on Computational Mechanics, October 1998. Bulletin 39.

Luo, Y., On some Finite Element Formulations in Structural Mechanics. Doctoral Thesis, 1998. Bulletin 40.

Troive, S., Structural LCC Design of Concrete Bridges. Doctoral Thesis, 1998. Bulletin 41.

Tärno, I., Effects of Contour Ellipticity upon Structural Behaviour of Hyparform Suspended Roofs. Licentiate Thesis, 1998. Bulletin 42.

Hassanzadeh, G., Betongplattor på pelare. Förstärkningsmetoder och dimensioneringsmetoder för plattor med icke vidhäftande spännarmering. Licentiatavhandling, 1998. Bulletin 43.

Karoumi, R., Response of Cable-Stayed and Suspension Bridges to Moving Vehicles. Analysis methods and practical modeling techniques. Doctoral Thesis, 1998. Bulletin 44.

Johnson, R., Progression of the Dynamic Properties of Large Suspension Bridges during Construction – A Case Study of the Höga Kusten Bridge. Licentiate Thesis, 1999. Bulletin 45.

Tibert, G., Numerical Analyses of Cable Roof Structures. Licentiate Thesis, 1999. Bulletin 46.

Ahlenius, E., Explosionslaster och infrastrukturkonstruktioner - Risker, värderingar och kostnader. Licentiatavhandling, 1999. Bulletin 47.

Battini, J-M., Plastic instability of plane frames using a co-rotational approach. Licentiate Thesis, 1999. Bulletin 48.

Ay, L., Using Steel Fiber Reinforced High Performance Concrete in the Industrialization of Bridge Structures. Licentiate Thesis, 1999. Bulletin 49.

Paulsson-Tralla, J., Service Life of Repaired Concrete Bridge Decks. Doctoral Thesis, 1999. Bulletin 50.

Billberg, P., Some rheology aspects on fine mortar part of concrete.
Licentiate Thesis, 1999. Bulletin 51.

Ansell, A., Dynamically Loaded Rock Reinforcement.
Doctoral Thesis, 1999. Bulletin 52.

Forsell, K., Instability analyses of structures under dynamic loads.
Doctoral Thesis, 2000. Bulletin 53.

Edlund, S., Buckling of T-Section Beam-Columns in Aluminium with or without Transverse Welds. Doctoral Thesis, 2000. Bulletin 54.

Löfsjögård, M., Functional Properties of Concrete Roads – General Interrelationships and Studies on Pavement Brightness and Sawcutting Times for Joints.
Licentiate Thesis, 2000. Bulletin 55.

Nilsson, U., Load bearing capacity of steel fibre reinforced shotcrete linings.
Licentiate Thesis, 2000. Bulletin 56.

Silfwerbrand, J. and Hassanzadeh, G., (editors), International Workshop on Punching Shear Capacity of RC Slabs – Proceedings. Dedicated to Professor Sven Kinnunen. Stockholm June 7-9, 2000. Bulletin 57.

Wiberg, A., Strengthening and repair of structural concrete with advanced, cementitious composites. Licentiate Thesis, 2000. Bulletin 58.

Racutanu, G., The Real Service Life of Swedish Road Bridges - A case study.
Doctoral Thesis, 2000. Bulletin 59.

Alavizadeh-Farhang, A., Concrete Structures Subjected to Combined Mechanical and Thermal Loading. Doctoral Thesis, 2000. Bulletin 60.

Wäppling, M., Behaviour of Concrete Block Pavements - Field Tests and Surveys.
Licentiate Thesis, 2000. Bulletin 61.

Getachew, A., Trafiklaster på broar. Analys av insamlade och Monte Carlo genererade fordonsdata.
Licentiatavhandling, 2000. Bulletin 62.

James, G., Raising Allowable Axle Loads on Railway Bridges using Simulation and Field Data.
Licentiate Thesis, 2001. Bulletin 63.

Karawajczyk, E., Finite Elements Simulations of Integral Bridge Behaviour.
Doctoral Thesis, 2001. Bulletin 64.

Thöyrä, T., Strength of Slotted Steel Studs.
Licentiate Thesis, 2001. Bulletin 65.

Tranvik, P., Dynamic Behaviour under Wind Loading of a 90 m Steel Chimney.
Licentiate Thesis, 2001. Bulletin 66.

Ullman, R., Buckling of Aluminium Girders with Corrugated Webs.
Licentiate Thesis, 2002. Bulletin 67.

Getachew, A., Traffic Load Effects on Bridges. Statistical Analysis of Collected and Monte Carlo Simulated Vehicle Data.
Doctoral Thesis, 2003. Bulletin 68.

Quilligan, M., Bridge Weigh-in-Motion. Development of a 2-D Multi-Vehicle Algorithm.
Licentiate Thesis, 2003. Bulletin 69.

James, G., Analysis of Traffic Load Effects on Railway Bridges.
Doctoral Thesis 2003. Bulletin 70.

Nilsson, U., Structural behaviour of fibre reinforced sprayed concrete anchored in rock.
Doctoral Thesis 2003. Bulletin 71.

Wiberg, A., Strengthening of Concrete Beams Using Cementitious Carbon Fibre Composites.
Doctoral Thesis 2003. Bulletin 72.

Löfsjögård, M., Functional Properties of Concrete Roads – Development of an Optimisation Model and Studies on Road Lighting Design and Joint Performance.
Doctoral Thesis 2003. Bulletin 73.

Bayoglu-Flener, E., Soil-Structure Interaction for Integral Bridges and Culverts.
Licentiate Thesis 2004. Bulletin 74.

Lutfi, A., Steel Fibrous Cement Based Composites. Part one: Material and mechanical properties.
Part two: Behaviour in the anchorage zones of prestressed bridges.
Doctoral Thesis 2004. Bulletin 75.

Johansson, U., Fatigue Tests and Analysis of Reinforced Concrete Bridge Deck Models.
Licentiate Thesis 2004. Bulletin 76.

Roth, T., Langzeitverhalten von Spannstählen in Betonkonstruktionen.
Licentiate Thesis 2004. Bulletin 77.

Hedebratt, J., Integrerad projektering och produktion av industrigolv – Metoder för att förbättra kvaliteten.
Licentiatavhandling, 2004. Bulletin 78.

Österberg, E., Revealing of age-related deterioration of prestressed reinforced concrete containments in nuclear power plants – Requirements and NDT methods.
Licentiate Thesis 2004. Bulletin 79.

Broms, C.E., Concrete flat slabs and footings New design method for punching and detailing for ductility.
Doctoral Thesis 2005. Bulletin 80.

Wiberg, J., Bridge Monitoring to Allow for Reliable Dynamic FE Modelling - A Case Study of the New Årsta Railway Bridge.
Licentiate Thesis 2006. Bulletin 81.

Mattsson, H-Å., Funktionsentreprenad Brounderhåll – En pilotstudie i Uppsala län.
Licentiate Thesis 2006. Bulletin 82.

Masanja, D. P, Foam concrete as a structural material.
Doctoral Thesis 2006. Bulletin 83.

Johansson, A., Impregnation of Concrete Structures – Transportation and Fixation of Moisture in Water Repellent Treated Concrete.
Licentiate Thesis 2006. Bulletin 84.

Billberg, P., Form Pressure Generated by Self-Compacting Concrete – Influence of Thixotropy and Structural Behaviour at Rest.

Doctoral Thesis 2006. Bulletin 85.

Enckell, M., Structural Health Monitoring using Modern Sensor Technology – Long-term Monitoring of the New Årsta Railway Bridge.

Licentiate Thesis 2006. Bulletin 86.

Söderqvist, J., Design of Concrete Pavements – Design Criteria for Plain and Lean Concrete.

Licentiate Thesis 2006. Bulletin 87.

Malm, R., Shear cracks in concrete structures subjected to in-plane stresses.

Licentiate Thesis 2006. Bulletin 88.

Skoglund, P., Chloride Transport and Reinforcement Corrosion in the Vicinity of the Transition Zone between Substrate and Repair Concrete.

Licentiate Thesis 2006. Bulletin 89.

Liljencrantz, A., Monitoring railway traffic loads using Bridge Weight-in-Motion.

Licentiate Thesis 2007. Bulletin 90.

Stenbeck, T., Promoting Innovation in Transportation Infrastructure Maintenance – Incentives, Contracting and Performance-Based Specifications.

Doctoral Thesis 2007. Bulletin 91.

Magnusson, J., Structural Concrete Elements Subjected to Air Blast Loading.

Licentiate Thesis 2007. Bulletin 92.

Pettersson, L., G., Full Scale Tests and Structural Evaluation of Soil Steel Flexible Culverts with low Height of Cover.

Doctoral Thesis 2007. Bulletin 93

Westerberg, B., Time-dependent effects in the analysis and design of slender concrete compression members.

Doctoral Thesis 2008. Bulletin 94

Mattsson, H-Å, Integrated Bridge Maintenance. Evaluation of a pilot project and future perspectives.

Doctoral Thesis 2008. Bulletin 95

Andersson, A., Utmattningsanalys av järnvägsbroar. En fallstudie av stålbroarna mellan Stockholm Central och Söder Målarstrand, baserat på teoretiska analyser och töjningsmätningar.

Licentiate Thesis 2009. Bulletin 96

Malm, R., Predicting shear type crack initiation and growth in concrete with non-linear finite element method.

Doctoral Thesis 2009. Bulletin 97

Bayoglu Flener, E., Static and dynamic behavior of soil-steel composite bridges obtained by field testing.

Doctoral Thesis 2009. Bulletin 98

Gram, A., Numerical Modelling of Self-Compacting Concrete Flow

Licentiate Thesis 2009. Bulletin 99

Wiberg, J., Railway bridge response to passing trains. Measurements and FE model updating.

Doctoral Thesis 2009. Bulletin 100

Athuman M.K. Ngoma, Characterisation and Consolidation of Historical Lime Mortars in Cultural Heritage Buildings and Associated Structures in East Africa.

Doctoral Thesis 2009. Bulletin 101

Ülker-Kaustell, M., Some aspects of the dynamic soil-structure interaction of a portal frame railway bridge.

Licentiate Thesis 2009. Bulletin 102

Vogt, C., Ultrafine particles in concrete
Doctoral Thesis 2010. Bulletin 103

Selander, A., Hydrophobic Impregnation of Concrete Structures
Doctoral Thesis 2010. Bulletin 104

Ilina, E., Understanding the application of knowledge management to safety critical facilities
Doctoral Thesis 2010. Bulletin 105

Leander, J., Improving a bridge fatigue life prediction by monitoring
Licentiate Thesis 2010. Bulletin 106

Andersson, A., Capacity assessment of arch bridges with backfill – Case of the old Årsta railway bridge
Doctoral Thesis 2011. Bulletin 107

Enckell, M., Lessons Learned in Structural Health Monitoring of Bridges Using Advanced Sensor Technology
Doctoral Thesis 2011. Bulletin 108

Hansson, H., Warhead penetration in concrete protective structures
Licentiate Thesis 2011. Bulletin 109

Gonzalez Silva, I., Study and Application of Modern Bridge Monitoring Technique
Licentiate Thesis 2011. Bulletin 110

Safi, M., LCC Applications for Bridges and Integration with BMS
Licentiate Thesis 2012. Bulletin 111

Guangli, D., Towards sustainable construction, life cycle assessment of railway bridges
Licentiate Thesis 2012. Bulletin 112

Hedebratt, J., Industrial Fibre Concrete Slabs – Experiences and Tests on Pile-Supported Slab
Doctoral Thesis 2012. Bulletin 113

Ahmed, L., Models for analysis of shotcrete on rock exposed to blasting
Licentiate Thesis 2012. Bulletin 114

Le, T., N., Corotational formulation for nonlinear dynamic analysis of flexible beam structures
Licentiate Thesis 2012. Bulletin 115

Johansson, C., Simplified dynamic analysis of railway bridges under high-speed trains
Licentiate Thesis 2013. Bulletin 116

Jansson, R., Fire Spalling of Concrete – Theoretical and Experimental Studies
Doctoral Thesis 2013. Bulletin 117

Leander, J., Refining the fatigue assessment procedure of existing steel bridges
Doctoral Thesis 2013. Bulletin 118

Le, T., N., Nonlinear dynamics of flexible structures using corotational beam elements
Doctoral Thesis 2013. Bulletin 119

Ülker-Kaustell, M., Essential modelling details in dynamic FE-analyses of railway bridges
Doctoral Thesis 2013. Bulletin 120

Safi, M., Life-Cycle Costing. Applications and Implementations in Bridge Investment and Management
Doctoral Thesis 2013. Bulletin 121

Arvidsson, T., Train-Bridge Interaction: Literature Review and Parameter Screening
Licentiate Thesis 2014. Bulletin 122

Rydell, C., Seismic high-frequency content loads on structures and components within nuclear facilities
Licentiate Thesis 2014. Bulletin 123

Bryne, L. E., Time dependent material properties of shotcrete for hard rock tunnelling
Doctoral Thesis 2014. Bulletin 124

Wennström, J., Life Cycle Costing in Road Planning and Management: A Case Study on Collisionfree Roads
Licentiate Thesis 2014. Bulletin 125

Gonzalez Silva, I., Application of monitoring to dynamic characterization and damage detection in bridges
Doctoral Thesis 2014. Bulletin 126

Sangiorgio, F., Safety Format for Non-linear Analysis of RC Structures Subjected to Multiple Failure Modes
Doctoral Thesis 2015. Bulletin 127

Gram, A., Modelling of Cementitious Suspensial Flow – Influence of Viscosity and Aggregate Properties
Doctoral Thesis 2015. Bulletin 128

Du, G., Life Cycle Assessment of bridges, model development and Case Studies
Doctoral Thesis 2015. Bulletin 129

Zhu, J., Towards a Viscoelastic Model for Phase Separation in Polymer Modified Bitumen
Licentiate Thesis 2015. Bulletin 130

Chen, F., The Future of Smart Road Infrastructure. A Case Study for the eRoad.
Licentiate Thesis 2015. Bulletin 131

Ahmed, L., Models for analysis of young cast and sprayed concrete subjected to impact-type loads
Doctoral Thesis 2015. Bulletin 132

Albrektsson, J., Durability of Fire Exposed Concrete – Experimental Studies Focusing on Stiffness & Transport Properties
Licentiate Thesis 2015. Bulletin 133

Wallin, J., Systematic planning and execution of finite element model updating
Licentiate Thesis 2015. Bulletin 134

Wadi, A., Flexible Culverts in Sloping Terrain
Licentiate Thesis 2015. Bulletin 135

McCarthy, R., Self-Compacting Concrete for Improved Construction Technology
Licentiate Thesis 2015. Bulletin 136

Veganzones Munõs, J.J., Bridge Edge Beams: LCCA and Structural Analysis for the Evaluation of New Concepts
Licentiate Thesis 2016. Bulletin 137

Abbasiverki, R., Analysis of underground concrete pipelines subjected to seismic high-frequency loads
Licentiate Thesis 2016. Bulletin 138

Gasch, T., Concrete as a multi-physical material with applications to hydro power facilities

Licentiate Thesis 2016. Bulletin 139

Ali, M., M., Use of Macro Basalt Fibre Concrete for Marine Applications
Licentiate Thesis 2016. Bulletin 140

Döse, M., Ionizing Radiation in Concrete and Concrete Buildings – Empirical Assessment
Licentiate Thesis 2016. Bulletin 141

Khan, A., Fundamental investigation to improve the quality of cold mix asphalt
Licentiate Thesis 2016. Bulletin 142

Zhu, J., Storage Stability and Phase Separation Behaviour of Polymer-Modified Bitumen
Doctoral Thesis 2016. Bulletin 143

Chen, F., Sustainable Implementation of Electrified Roads
Doctoral Thesis 2016. Bulletin 144

Svedholm, C., Efficient modelling techniques for vibration analyses of railway bridges
Doctoral Thesis 2017. Bulletin 145

Solat Yavari, M., Slab Frame Bridges, Structural Optimization Considering Investment Cost and Environmental Impacts
Licentiate Thesis 2017. Bulletin 146

Tell, S., Vibration mitigation of high-speed railway bridges, Application of fluid viscous dampers
Licentiate Thesis 2017. Bulletin 147

Elgazzar, H., End-Shield Bridges for Highspeed Railway – Full scale dynamic testing and numerical simulations
Licentiate Thesis 2017. Bulletin 148

Sousa Neves, A. C., Structural Health Monitoring of Bridges: Model-free damage detection method using Machine Learning
Licentiate Thesis 2017. Bulletin 149

Sjölander, A., Analyses of shotcrete stress states due to varying lining thickness and irregular rock surfaces
Licentiate Thesis 2017. Bulletin 150

Heng, P., Simplified Mechanical Models for the Nonlinear Dynamic Analysis of Elasto-plastic Steel Structures Impacted by a Rigid Body
Doctoral Thesis 2017. Bulletin 151

Mohammadi Mohaghegh, A., Structural Properties of High-Performance Macro Basalt Fibre Concrete; Flexure, Shear, Punching Shear and Fire Spalling
Doctoral Thesis 2018. Bulletin 152

Zangeneh Kamali, A., Dynamic Soil-Structure Interaction of Railway Bridges: Numerical and Experimental results
Licentiate Thesis 2018. ABE-DLT-182

Zäll, E., Footbridge Dynamics – Human-Structure Interaction
Licentiate Thesis 2018. ABE-DLT-183

Liu, F., Dynamic analysis of hollow core concrete floors
Licentiate Thesis 2018. ABE-DLT-184

Eriksson, D., Numerical models for degradation of concrete in hydraulic structure due to long-term contact with water

Licentiate Thesis 2018. ABE-DLT-185

Arvidsson, T., Train - Track - Bridge Interaction for the Analysis of Railway Bridges and Train Running Safety

Doctoral Thesis 2018. ABE-DLT-186

Chhang, S., Energy-momentum conserving time-stepping algorithms for nonlinear dynamics of planar and spatial Euler-Bernoulli/Timoshenko beams

Doctoral Thesis 2018. ABE-DLT-1836

Wadi, A. H. H., Soil-Steel Composite Bridges: Research advances and application

Doctoral Thesis 2018. ABE-DLT-1842

Khouri Chalouhi, E., Optimal design solutions of concrete bridges considering environmental impact and investment cost

Licentiate Thesis 2019. ABE-DLT-194

Gasch, T., Multiphysical analysis methods to predict the ageing and durability of concrete

Doctoral Thesis 2019. ABE-DLT-1910

Magnusson, J., Shear in Concrete Structural Elements Subjected to Dynamic Loads

Doctoral Thesis 2019. ABE-DLT-1916

Skoglund, O., Innovative structural details using high strength steel for steel bridges

Licentiate Thesis 2019. ABE-DLT-1933

Hellgren, R., Condition assessment of concrete dams in cold climate

Licentiate Thesis 2019. ABE-DLT-1934

Liu, F., Experimental and numerical analyses of the dynamic behaviour of hollow-core concrete floors

Doctoral Thesis 2020. ABE-DLT-207

Sjölander, A., Structural behaviour of shotcrete in hard rock tunnels

Doctoral Thesis 2020. ABE-DLT-209

Lind Östlund, J., Dynamic soil-structure interaction of simply supported high-speed railway bridges

Licentiate Thesis 2020. ABE-DLT-2025

Sousa Neves, A. C., Structural Health Monitoring of Bridges: Data-driven damage detection method using Machine Learning

Doctoral Thesis 2020. ABE-DLT-2027

Schönbeck, P., Use of configuration information in construction projects to ensure high performance of healthcare facilities

Licentiate Thesis 2020. ABE-DLT-2029

Wang, R., Reliability-based fatigue assessment of existing steel bridges

Licentiate Thesis 2020. ABE-DLT-2031

Veganzones Muñoz, J. J., Bridge Edge Beams - LCCA and Structural Analysis for the Evaluation of New Concepts

Doctoral Thesis 2020. ABE-DLT-2037

Tell, S., Vibrationsdämpning av broar med viskösa dämpare

Doctoral Thesis 2020. ABE-DLT-2046

The Divisions also publish other series. For full information, please see our website: www.byv.kth.se.